# REPUBLIC OF TURKEY YILDIZ TECHNICAL UNIVERSITY GRADUATE SCHOOL OF NATURAL AND APPLIED SCIENCES

# PERFORMANCE ANALYSIS OF GENERALIZED-K FADING CHANNELS IN VEHICULAR COMMUNICATIONS

#### Kardeş ASLAN

DOCTOR OF PHILOSOPHY THESIS

Department of Electronics and Communication Engineering

Communications Program

Advisor

Assoc. Prof. Dr. Tansal GÜÇLÜOĞLU

# REPUBLIC OF TURKEY YILDIZ TECHNICAL UNIVERSITY GRADUATE SCHOOL OF NATURAL AND APPLIED SCIENCES

### PERFORMANCE ANALYSIS OF GENERALIZED-K FADING CHANNELS IN VEHICULAR COMMUNICATIONS

A thesis submitted by Kardeş ASLAN in partial fulfillment of the requirements for the degree of **DOCTOR OF PHILOSOPHY** is approved by the committee on 09.07.2021 in Department of Electronics and Communication Engineering, Communications Program .

Assoc. Prof. Dr. Tansal GÜÇLÜOĞLU Yildiz Technical University Advisor

**Approved By the Examining Committee** 

# Assoc. Prof. Dr. Tansal GÜÇLÜOĞLU, Advisor Yildiz Technical University Assoc. Prof. Dr. Hacı İLHAN, Member Yildiz Technical University Dr. Gökalp TULUM, Member Istanbul Arel University Assoc. Prof. Dr. Hamid TORPİ, Member Yildiz Technical University Assoc. Prof. Dr. Eylem ERDOĞAN, Member İstanbul Medeniyet University

I hereby declare that I have obtained the required legal permissions during data collection and exploitation procedures, that I have made the in-text citations and cited the references properly, that I haven't falsified and/or fabricated research data and results of the study and that I have abided by the principles of the scientific research and ethics during my Thesis Study under the title of Performance Analysis of Generalized-k Fading Channels in Vehicular Communications supervised by my supervisor, Assoc. Prof. Dr. Tansal GÜÇLÜOĞLU. In the case of a discovery of false statement, I am to acknowledge any legal consequence.

Kardeş ASLAN

Signature



#### **ACKNOWLEDGEMENTS**

First of all, I'd like to give my sincere thanks to my honorific supervisor, Prof. Dr. Tansal GÜÇLÜOĞLU, who accepted me as his Ph.D. student. Thereafter, he offered me so much advice, patiently supervising me, and always guiding me in the right direction. I've learned a lot from him, without his help I could not have finished my dissertation successfully.

I would like to thank my thesis monitor committee members, Assoc. Prof. Dr. Hacı İLHAN, and Assoc. Prof. Dr. Gökalp TULUM, for their encouragement, motivation, and constructive feedback on this dissertation. I also wish to sincerely thank the magnificent support of Turkish Scholarship, Council of Higher Education (YOK), and Yildiz Technical University.

I hope that this thesis would be helpful to researchers working on generalized-k channel and NOMA in VANETs.

Kardeş ASLAN

#### TABLE OF CONTENTS

LI	ST O	F SYMBOLS	viii
LI	ST O	F ABBREVIATIONS	ix
LI	ST O	F FIGURES	xii
Αŀ	3STR	ACT	xiv
Ö	ZET		xvi
1	INT	RODUCTION	1
	1.1	Literature Review	1
		1.1.1 Characteristic of Vehicular Channels	2
		1.1.2 Modeling of Vehicular Channels	4
	1.2	Objective of the Thesis	8
	1.3	Hypothesis	9
2	BAC	CKGROUND	11
	2.1	Generalized-k Fading Channels	11
	2.2	Derivation of Generalized-K Probability Density Function	13
	2.3	NOMA	15
	2.4	Performance Evaluation Tools	16
		2.4.1 Outage Probability	16
		2.4.2 Outage Capacity	16
		2.4.3 Average Channel Capacity	16
		2.4.4 Symbol Error Rate	17
		2.4.5 Asymptotic Analysis, Diversity and Array Gain	17
3	PER	FORMANCE OF MAXIMAL RATIO TRANSMISSION OVER	
	GEN	IERALIZED-K FADING CHANNELS	18
	3.1	Introduction	18
	3.2	System Description	19
	3.3	Performance Analysis	21
		3.3.1 Outage Probability	22

		3.3.2 Channel Capacity	24		
		3.3.3 Symbol Error Rate	25		
		3.3.4 Diversity and Coding Gain	26		
		3.3.5 Impact of Channel Estimation Errors	26		
	3.4	Simulation Results	27		
	3.5	Chapter Summary	31		
4	PER	FORMANCE ANALYSIS OF DOWNLINK-NOMA OVER GENERALIZED-			
	K FA	ADING CHANNELS	33		
	4.1	Introduction	33		
	4.2	System Description	34		
	4.3	Performance Analysis	36		
		4.3.1 Outage Probability	36		
		4.3.2 Average Channel Capacity	39		
		4.3.3 Asymptotic AVC	41		
		4.3.4 Symbol Error Rate	41		
		4.3.5 Diversity and Coding Gains	43		
		4.3.6 Performance Analysis of Downlink-NOMA over $K_G$ Fading			
		Channels Using Mixture-Gamma Function	44		
		4.3.7 Performance of OMA over Generalized-K Fading Channels	46		
	4.4	Simulation Results	47		
	4.5	Chapter Summary	53		
5	PERFORMANCE ANALYSIS OF NOMA UPLINK OVER GENERALIZED-K				
	FAD	ING CHANNELS	55		
	5.1	Introduction	55		
	5.2	System Description	56		
	5.3	Performance Analysis	59		
		5.3.1 Outage Probability	59		
		5.3.2 Average Channel Capacity	62		
		5.3.3 Symbol Error Rate	64		
	5.4	Simulation Results	66		
	5.5	Chapter Summary	68		
6	RESULTS AND DISCUSSION				
	6.1	Conclusions	69		
	6.2	Future Works	70		
RE	FERI	ENCES	71		
Α	DER	RIVATIONS OF (3.11) AND (3.12)	82		

В	DERIVATION OF (3.24)	85
C	DERIVATION OF (4.5)	87
D	<b>DERIVATIONS OF (4.13) AND (4.14)</b>	89
E	DERIVATION OF (5.8)	91
PU	BLICATIONS FROM THE THESIS	95

#### LIST OF SYMBOLS

$Pr(\cdot)$	Probability of A Random Variable
$f_X(\cdot)$	Probability Density Function
$F_X(\cdot)$	Cumulative Distribution Function
$\mathbb{E}(\cdot)$	Expectation of Random Variable
$G^{m,n}_{p,q}(\cdot)$	Meijer-G Function
$\Gamma(\cdot)$	Gamma Function
$  \cdot  $	Frobenius Norm
$erfc(\cdot)$	Complementary Error Eunction
$K_{k-m}(\cdot)$	Modified Bessel Function of Second Kind
$M(\cdot)$	Moment Generating Function
$W(\cdot)$	Whittaker Function

#### LIST OF ABBREVIATIONS

ACF Auto Correlation Function

AF Amplify-and-Forward

AFD Average Fade Duration

AoA Angle-of-Arrival

AoD Angle-of-Departure

AVC Average Channel Capacity

AWGN Additive Gaussian White Noise

BER Bit Error Rate

BPSK Binary Phase Shift Keying

BS Base Station

CCF Channel Correlation Function

CDF Cumulative Distribution Function

CEE Channel Estimation Error

CIR Channel Impulse Response

DF Decode-and-Forward

EGC Equal Gain Combining

FDMA Frequency Division Multiple Access

FSO Free-Space Optics

GG Gamma-Gamma

GPS Global Positioning System

IoT Internet of Things

ITS Intelligent Transportation Systems

I2V Infrastructure-to-Vehicle

LCR Level Crossing Rate

LOS Line-of-Sight

LS Least Square

LSF Local Scattering Function

MG Mixture gamma

MGF Moment Generating Function

MIMO Multiple-Input-Multiple-Output

MPCs Multipath Components

MRC Maximum Ratio Combining

MRT Maximum Ratio Transmission

NL Nakagami-Lognormal (NL)

NOMA Non-Orthogonal Multiple Access

OMA Orthogonal Multiple Access

OP Outage Probability

PDF Probability Density Function

PDP power Delay Profile

PDS Power Doppler Spectra

QPSK Quadrature Phase-Shift Keying

RL Rayleigh-Lognormal

RSUs Roadside Units

SC Superposition Coding

SER Symbol Error Rate

SIC Successive Interference Cancellation

SINR Signal-to-Interference-Plus-Noise Ratio

SNR Signal-to-Noise Ratio

STBC Space-Time Block Code

STC Space Time Codes

STCF Spatial Time Correlation Function

SWIPT Simultaneous Wireless Information and Power Transfer

TDMA Time Division Multiple Access

UAV Unmanned Aerial Vehicle

VANET Vehicular ad-hoc Network

V2I Vehicle to Infrastructure

V2V Vehicle-to-Vehicle

WSS Wide-Sense Stationary

WSSUS WSS Uncorrelated Scatterering

#### LIST OF FIGURES

Figure 1.1	Vehicle-to-vehicle communication	2
Figure 1.2	Relationship among different channel functions	4
Figure 2.1	Pathloss, Shadowing and Multipath Fadings. [37, Fig. 4.3]	12
Figure 3.1	Block diagram of the maximum-ratio transmission over	
	generalized-K channel	20
Figure 3.2	Histogram and analytical plots PDF of the SNR	23
Figure 3.3	Simulation and analytical plots of CDF of the SNR	23
Figure 3.4	Symbol error rate for different number of transmit antennas	28
Figure 3.5	Outage probability of MRT over $K_G$ channels	29
Figure 3.6	Channel capacity of the system	29
Figure 3.7	Asymptotic SER of BPSK for MRT over $K_G$ channel	30
Figure 3.8	Asymptotic outage probability	30
Figure 3.9	SER when imperfect channel estimation is used	31
Figure 4.1	Block Diagram of Downlink-NOMA System with M Users	34
Figure 4.2	Histogram and theoretical PDF of SINR of downlink-NOMA over $K_G$	
	channel	48
Figure 4.3	CDF of SINR for downlink-NOMA over $K_G$ channel from simulation	
	and derivation	48
Figure 4.4	OPs of first users in all systems	48
Figure 4.5	OPs of first user in system with two users for different multipath	
	and shadowing parameters	49
Figure 4.6	AVCs of first users in all systems	50
Figure 4.7	AVC of first user in system with three users	51
Figure 4.8	SERs of first users in all systems	51
Figure 4.9	SERs of first user in system with five users for different multipath	
	and shadowing parameters	52
Figure 4.10	SERs of all users in the nearest user	53
Figure 5.1	System Model	57
Figure 5.2	Simulation and Theoretic PDF of SNR of Downlink-NOMA over $K_G$	
	channel	62

Figure 5.3	Simulation and Theoretic CDFs of SNR of Downlink-NOMA over $K_G$	
	channel	62
Figure 5.4	Outage Probabilities of all users for Uplink-NOMA over $K_G$ channels.	66
Figure 5.5	Average Channel Capacities of each user in Uplink-NOMA over $K_G$	
	channels	67
Figure 5.6	SER of all users for Uplink-NOMA over $K_G$ channels	68

#### Performance Analysis of Generalized-k Fading Channels in Vehicular Communications

Kardes ASLAN

Department of Electronics and Communication Engineering
Doctor of Philosophy Thesis

Advisor: Assoc. Prof. Dr. Tansal GÜÇLÜOĞLU

Releasing autonomous vehicles in the near future; communication of vehicles with each other to circumvent traffic congestion, road safety, fuel-saving, efficient transportation, road tolls, their connecting over the internet and storing of data of vehicles on cloud and fog enforce research of vehicular communication systems. In the first chapter of this dissertation, non-wide sense stationary (WSS) vehicular channels having various issues are addressed. Then, the literature about vehicular channels are presented.

Although shadowing effects are mostly neglected in the literature, it is known that it is available in the most wireless communication environment. Hence, a channel model like generalized-k ( $K_G$ ) including shadowing is a realistic one. Therefore,  $K_G$  fading channels are described in the second chapter of this dissertation because the selected channel for each different topic addressed in this dissertation is the  $K_G$  fading channel.

In wireless communication, applying diversity techniques such as multiple-input-multiple-output (MIMO), maximum ratio combining (MRC), antenna selection, equal gain combining (EGC), beamforming is important in order to increase communication quality. One of them is the maximum ratio transmission (MRT) technique with low receiver complexity can make ultra reliable vehicular feasible in practice. In the third chapter of this dissertation, performance improvement with MRT over  $K_G$  channels is investigated by considering error rates and outage probability (OP).

In recent years, non-orthogonal multiple access (NOMA) has drawn a lot of attention due to serving multiple users in the same resource blocks (i.e., the same time-slots and frequency bands). It accomplishes that by multiplexing multiple users in the power domain with superposition coding (SC) at the transmitter and by using successive interference cancellation (SIC) at the receiver. Thus, it considerably reduces frequency scarcity and latency compared to orthogonal multiple access (OMA) techniques used in previous communication generations. Therefore, in the fourth chapter of this dissertation, the performance of downlink-non-orthogonal multiple access (NOMA) which provides a noticeable gain in the frequency spectrum, quite decreases latency, and is provisioned to be used in the fifth generation, is researched in  $K_G$  vehicular fading channels.

In the fifth chapter of this dissertation, the performance of uplink-NOMA over  $K_G$  vehicular channels is studied. Frequency scarcity and latency leads inherently to a bigger problems in vehicular channels due to the requirement of fast and reliable. Therefore, NOMA is more important for vehicular channels than other channels. To this end, performance metrics such as OP, average channel capacity (AVC), and symbol error probability (SER) are mathematically analyzed for the considered system.

**Keywords:** Vehicular channels, generalized-k channels, maximum ratio transmission, NOMA

YILDIZ TECHNICAL UNIVERSITY
GRADUATE SCHOOL OF SCIENCE AND ENGINEERING

#### Araçlar Arası Haberleşmede Genelleştirilmiş-k Sönümleme Kanallarının Performans Analizi

Kardeş ASLAN

Elektronik ve Haberleşme Mühendisliği Anabilim Dalı Doktora Tezi

Danışman: Doç. Dr. Tansal GÜÇLÜOĞLU

Yakın gelecekte sürücüsüz araçların yaygın bir şekilde piyasaya girecek olması, trafikteki tıkanıklığın giderilmesi, güvenli yolculuk, yakıt tasarrufu, yol geçiş ücretleri ve trafik yönetimi için araçların kendi aralarında haberleşmesi ve internete bağlanması, araç verilerinin internet üzerinden bulut ve sis'te depolanma gereksinimi araçlar arası kanalların araştırılmasını elzem kılmıştır. Bu tezin ilk bölümünde geniş anlamda durağan telsiz haberleşmede karşılaşılan sorunlara başka sorunların da eklendiği geniş anlamda durağan olmayan araçlar arası haberleşme kanalları hakkında genel bir bilgi verilmiş olup daha sonra bu konuda yapılmış literatür çalışmaları ele alınmıştır.

Literatürde çoğu kez gölgelemenin etkileri çok yollu sönümlemeye dahil edilmemesine rağmen bir çok haberleşme ortamında gölgelemenin mevcut olduğunu dolaysıyla gölgelemenin dahil edildiği bir kanal modelinin daha gerçekçi bir kanal modeli olduğu bilinmektedir. Bu yüzden bu tezin 2. bölümünde bu tezde ele alınan her 3 farklı sistemde de kanal olarak seçilen araçlar arası genelleştirilmiş-K kanallar üzerinde durulmuştur.

Telsiz haberleşmesinde, çok girişli çok çıkışlı (ÇGÇÇ), maksimum oranda birleştirme (MOB), anten seçimi, eşit kazançlı birleştirme (EKB), huzmeleme gibi performansı artıran çeşitlilik tekniklerini geliştirmek ve uygulamak önemlidir. Bu çeşitliliklerden bir tanesi de alıcının kompleksliğini azaltan, pratikte güvenilir araçların uygulanabilirliğini mümkün kılabilen maksimum oranlı iletim (MOİ) tekniğidir. Bu yüzden, Bu tezin 3. bölümünde, hata oranları ve kesinti olasılığı göz

önünde bulundurularak genelleştirilmiş-k kanallarda MOİ ile elde edilen perfromans arttırımı araştırılmıştır.

Son yıllarda, dikey olmayan çoklu erişim (DOÇE) tekniği, aynı kaynaklarda (aynı frekans bandı ve aynı zaman diliminde) birden fazla kullanıcı ile haberleşmeyi mümkün kıldığından dolayı oldukça dikkat çekmiştir. DOÇE, bunu vericide süperpozisyon kodlama ile güç domaininde birden fazla kullanıcının olmasını sağlayarak ve alıcıda başarılı karışım iptaili (BKİ) kullanarak gerçekleştirir. Bu yüzden dikey çoklu erişim (DÇE) tekniklerine kıyasla, frekans kıtlığını ve gecikmeyi önemli ölçüde düşürür. Bu yüzden bu tezin 4. Bölümünde frekans bandından önemli kazanç sağlayan ve gecikmeyi oldukça azaltan ve 5. Kuşak haberleşme tekniğinde kullanılması öngörülen dikey olmayan çoklu erişim (DOÇE) tekniğinin, araçlar arası genelleştirilmiş-k kanallarda aşağı yönde performansı incelenmiştir.

Bu tezin 5. Bölümünde araçlar arası genelleştirilmiş-k kanallarda yukarı yönde DOÇE tekniğinin performansı incelenmiştir. Frekans kıtlığı ve gecikme doğal olarak araçlar arası haberleşmede hız ve güvenilir haberleşme gereksiniminden dolayı daha büyük bir problemlere yol açar. Bu yüzden DOÇE, araçlar arası kanallar için diğer kanallardan daha önemlidir. Bu amaçla ele alınan sistemde Kesinti olasılığı, Ortalama Kanal Kapasitesi, Ortalama Sembol Hata Olasılığı gibi çeşitli performans metrikleri matematiksel olarak analiz edilmiştir.

**Anahtar Kelimeler:** Araçlar arası haberleşme kanalları, Genelleştirilmiş-k kanallar, Maksimum oranlı iletim, NOMA

#### YILDIZ TEKNİK ÜNİVERSİTESİ FEN BİLİMLERİ ENSTİTÜSÜ

# 1 INTRODUCTION

#### 1.1 Literature Review

As the number of vehicles is increasing, the traffic problems are expected to increase more in the near future since the road infrastructure is not developing proportionally, especially due to continuing urbanization [1]. However, researchers continue to investigate improving vehicles and transportation systems for more safety, comfort, and efficiency [2]. Intelligent transportation systems (ITS) coined in 1999 had been developed to avoid major problems [1]. It integrates sensors, pedestrians, roadside infrastructures, vehicles, traffic management centers, satellites, cameras, global positioning system (GPS) receivers, and multiple programs [2]. These technological advancements lead vehicles to collect data via sensors and share information with each other and with roadside units (RSUs), vehicle to infrastructure (V2I) in the future [3]. Thus, vehicles can prevent a collision by transmitting valuable information, and they can inform each other about environmental hazards, traffic conditions, and other location-relevant information [4]. It can be considered artificial intelligence. ITS systems are organized by IEEE Standard 802.11p based on IEEE 802.11a with the physical and medium access control layers. They are modified to support low latency communication among vehicles [5]. The most popular research topics about ITS are RSU and V2I devices, autonomous (pilotless) vehicles, platoon driving patterns using fog, and cloud computing. Delegating most of the human responsibilities to control systems allows comfortable, efficient, and safer voyages while reducing accidents caused by drivers [1]. Nowadays, heterogeneous autonomous vehicles of Google such as Freight liner Trucks, ISRobotCar, and European Cyber Cars are getting attention [6]. Another hot research topic related to vehicular technology is platoon driving where a group of vehicles moves together by communicating with each other which can be called cooperative driving. Vehicles follow each other by keeping a constant space among them and thus optimize the use of the road. In the literature, its benefits are highlighted as the increase of transportation capacity and reduction of energy consumption and pollution [7]. All these new technologies do not only require the performance of vehicular communication networks to be improved but also require storing enormous data from vehicles and RSUs at fog and cloud data centers. The traffic and vehicle database can be utilized for various goals such as improving ITS. RSUs enable the data transmission between infrastructure-to-vehicle (I2V) and vehicle-to-vehicle (V2V) communications [8]. Thus, they support traffic applications by transmitting periodic updates to remote traffic control centers Network providing communication in V2V and I2V is called vehicular ad hoc network (VANET) couple to connect to the internet [7]. Some RSUs can act as gateways by routing packets from VANETs to the internet. Obviously, the success of ITS highly depends on the condition of vehicular communication channels. In a wireless transmission system, the signals propagate from the transmitter to the receiver via different paths due to reflection, refraction, diffraction, and scattering. These paths give rise to attenuated, delayed, and phase-shifted components of the transmitted signal affecting the impulse response of the channel which is random and time-varying [9].

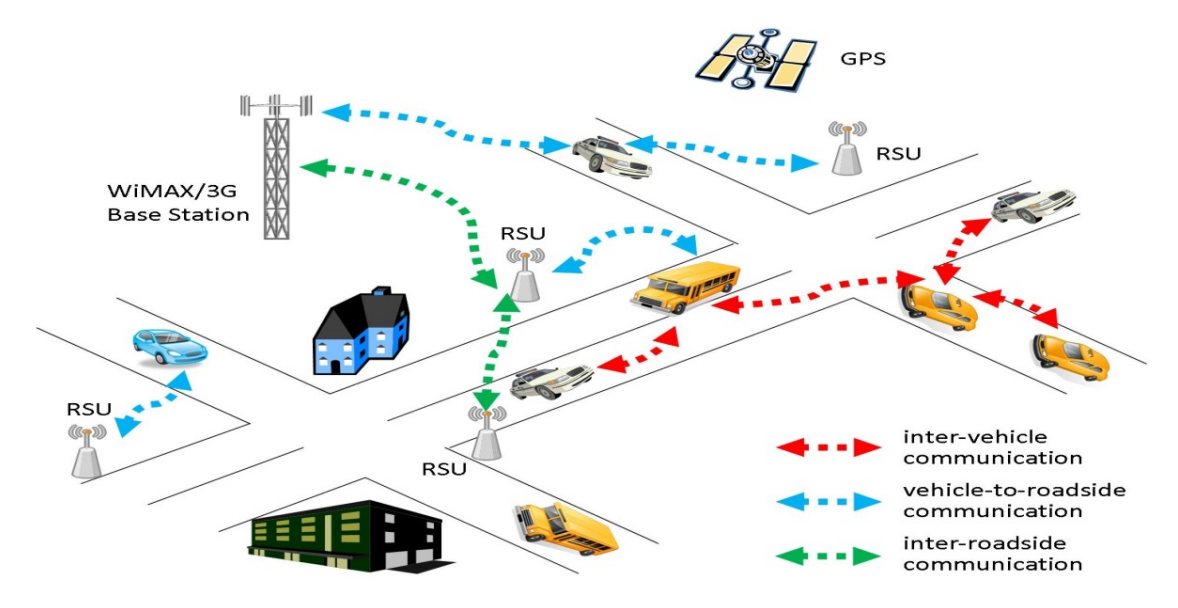


Figure 1.1 Vehicle-to-vehicle communication

#### 1.1.1 Characteristic of Vehicular Channels

Since the environment of wireless channels is dynamic, they are time-variant. However, while cellular channels with low-speed are accepted quasi-wide sense stationary (WSS), vehicular communication channels can be a stationary or a non-stationary random process characterized by a transfer function h(f,t) or impulse response  $h(\tau,t)$  [10]. Although the statistical properties of non-WSS vary with position or time, the statistical properties of WSS channels do not vary with position or time, and thus it allows simplified analysis. Being a non-WSS channel leads to Doppler spreading or Doppler shifting phenomena due to high speed. It can cause time selectivity to arise as well as frequency selective stemming from multipath components

that can emerge in WSS channels. Therefore, the propagation characteristics of V2V communication channels are significantly different from those of cellular channels, especially in terms of the time and frequency selectivity and the associated fading statistics. Here, time selectivity describes the temporal fluctuations of the channel quality, whereas frequency selectivity relates to the occurrence of "spectral holes" in the channel; both are very important for system performance. Dedicated measurements are needed for the accurate characterization of V2V propagation aspects, and dedicated V2V channel models are urgently needed to evaluate the reliability and latency of data packet transmissions among vehicles [9]. In wireless channels, sounders, which are an essential tool in studying and modeling the wireless propagation channels, are used to determine channel impulse response (CIR). They sound the channel with known narrowband or wideband signals, measure the received signals, and then estimate channel impulse. They use 2 types of tests called multi-tone and single tone. A wideband signal is applied to the channel, and then it is measured in the output of the channel in multi-tone. In a single tone, a monochromatic signal is used for this purpose. On side of the receiver, algorithms such as minimum mean square error, least-square (LS), linear minimum mean square error, maximum likelihood estimation algorithms, etc., are used for channel estimation [11] that can be performed in frequency or in time domains. While channel estimation in the frequency domain reduces the complexity of the receiver, it increases the channel's performance with the long delay in the time domain.

It is necessary to first characterize vehicular channels in order to cope with encountered problems or increase their performance. In other words, it is necessary to figure out them. The most important problem encountered in the V2V channels as the difference from cellular channels is doppler spreading that induces frequency shifting and time-selectivity. At present, derivations of power Doppler spectra (PDS) are intensively tried to make. PDS is obtained by determining autocorrelation function which is also determined by using distributions of the angle-of-departure (AoD) and the angle-of-arrival (AoA) of electromagnetic wave by geometrically modeling V2V channel as elliptic, circular, or cylindrical.

In [12], it is highlighted that non-WSS uncorrelated scattering (WSSUS) can be analyzed with functions in Figure 1.2 where  $\tau$ , v denote delay and spread, respectively. Local scattering function (LSF) and channel correlation function (CCF) as well as functions in Figure 1.2 are developed to estimate channel function. They give knowledge about all parameters in Figure 1.2 simultaneously. LSF estimates WSSUS fading processes under additive White Gaussian noise [13]. CCF being dual of LSF is defined to estimate vehicular channel in [12]. The other two important functions are the envelope LCR and average fade duration (AFD) functions for V2V channels, which

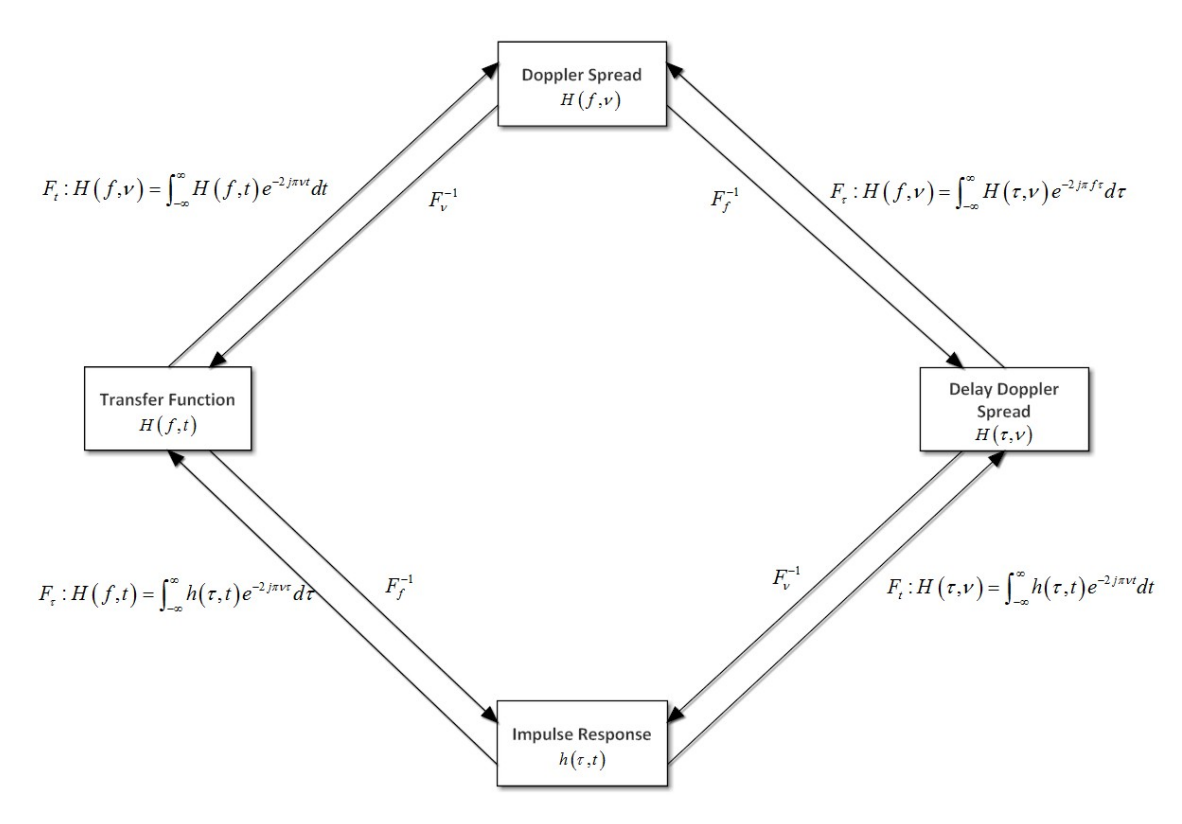


**Figure 1.2** Relationship among different channel functions.

can be used to observe the undesired effect of signal attenuation. The LCR defines how often the envelope crosses a specific level in the positive/negative direction. The AFD indicates the average time over which the envelope stays below a certain level. According to Cheng *et al.* [14], their effects are fairly dominant in V2V channels. In [10, Eq. 31], the spatial time correlation function (STCF) is presented, and then the time-correlation and spatial-correlation function are derived by using it. Fourier transform of time correlation function leads to the derivation of the power spectrum. All these functions depend on the AoD, AoA, and velocity of transceivers and scatters. On the other hand, AoD and AoA are correlated to scatters. Therefore, the statistics of scatters affect the statistics of the above-mentioned parameters in V2V channels. Hence, V2V channels in some works are modeled based on the distribution of scatters in the communication environment.

#### 1.1.2 Modeling of Vehicular Channels

In this section, firstly V2V channel models are described, compared, their common aspects with cellular channels are explained, and finally, recent papers considering V2V channels are presented.

Vehicular channels can be modeled in three categories [15] in order to derive delay Doppler spread, CIR, LSF, Doppler shift, power delay spread, Rms delay spread, and so on. One of those categories is the empirical method used for initial coverage estimation. It offers an advantage such as giving rapid results, but it needs calibration based on measurements to ensure an adequate fit of the results according to initial regression methods. This model is appropriate for the slow channel variation since it can enable the understanding of the V2V communication channel. Herbert *et al.* [16] state that slow channel variation affects very little Doppler spread. However, characterizing it allows the channel to be estimated. Thus, it can provide the improvement of communication performance. Therefore, they address the empirical methods to model slow channel variation. Researchers in [17] analyze the V2V propagation channels by characterizing coherence time, signal strength versus distance, Doppler analysis, and fading models based on empirical models. Likewise, authors of [18] study empirically the multi-path properties of the V2V channel across the suburban, highway, and rural environments. Acosta *et al.* [19] investigate Doppler delay profiles in V2V channels with frequency selective based on the empirical method.

A second category is the stochastic channel models that characterize the channel based on a frequency selection by modeling PDPs, Doppler spectrum, Doppler shift, AoA, and fadings, etc. The main idea of the stochastic scheme is to produce synthetic channel responses representing physical propagation channels with an acceptable level of accuracy. The stochastic approach can be classified into two major groups, namely the correlation-based approach and the geometry-based approach, which are most commonly used for propagation prediction in non-stationary mobile communication channels, e.g., the geometrical model predicts the Doppler spectrum and AoA distribution associated with the diffuse component for various V2V scenarios. The geometry-based approach builds on placing (diffuse or discrete) scatterers at random, specifying their properties, and based on certain statistical distributions. The incident signals from the scatters are determined with Ray tracing and finally all reflections overlap at the receiver. Benefits of this modeling approach: (i) it can easily model non-WSSUS channels, (ii) it ensures not only PDS and delay, but inherently models the MIMO properties of the channel, (iii) modifying easily the antenna influence by including a different antenna pattern is possible, (iv) the environment can be easily changed, and (v) it is much faster than deterministic ray-tracing since only single (or double) scattering needs to be simulated. A few geometry-based approaches such as two-ring models and two-cylinder models where scatters are placed on regular shapes around transmitter and receiver have been developed for V2V communication. Such approaches are useful for analytical studies of the joint space-time correlation function since they enable the derivation of closed-form expressions. However, their underlying assumption of all scatters being static does not agree with the results reported in measurements. A more realistic placement of scatters, rather than reproducing the physical reality, can remedy this. The drawback compared to regular-shaped models is that closed-form expressions generally cannot be derived, but there is a major advantage in terms of easily reproducing realistic temporal channel variations. In [20], a three-dimensional (3D) cluster-based non-stationary channel model is proposed for V2V communications. Scatters are located with the Poisson distribution. In that paper, scatters in the environment are grouped according to line-of-sight (LOS), single bounced, and double bounced, and CIR is obtained according to these groups and then, STCF is derived. In [21], PDSs and the autocorrelation functions (ACFs) are derived and simulated based on the geometry-based elliptical and circular scattering models, in V2V outdoor scenarios where the scatters are moving in arbitrary directions and with random velocities.

The third category is deterministic methods, which are widely used for propagation prediction, given a specific environment. The deterministic approach has two major subcategories, namely the measurement-based approach and the ray-tracing approach. Channel models based on measurement are developed from empirical data collected by measurements performed in real-world propagation environments. Thus, measured channel impulses are fairly accurate, which also offers to obtain accurate channel models. However, this approach has a disadvantage such that the measured data is considerably scenario-dependent. On the other hand, channel measurements are quite costly, thus the amount of data capable to be collected is very restricted. In the ray-tracing scheme, a simulation tool provides to launch and trace the propagation mechanism in a simulated wireless environment. Their principle is based mainly on ray optics (advanced ray-tracing techniques) or, more generally, on solving Maxwell's equations. These methods are precise but time-consuming due to their inherent computational complexity. Thus, methods based on geometrical optics [ray launching and ray tracing for radio planning purposes, with strong diffractive elements, offer a reasonable tradeoff between precision and required calculation time. In the ray launching technique, rays are launched from a transmitter and, at the locations where rays intersect an object; at least one new reflected, absorbed, diffracted, or scattered ray begins. On the other hand, in the ray-tracing approach, imaging techniques are usually employed, leading to a number of possible paths that rays follow from the transmitter to the receiver over the direct, reflected, and diffracted rays [3]. In this scheme, it is necessary that Maxwell's equations must be often solved under some boundary conditions imposed by the underlying site-specific wireless propagation environment. To develop a channel model based on this scheme, characteristics of the topographic and electromagnetic of the related propagation environment are required known. Despite this scheme is less costly than the approach based on the measurement, it is more expensive in terms of computation. Similar to channel models based on measurement, the channel models designed by the ray-tracing technique are very site-specific. Therefore, they are not preferred to employ for extensive system-level simulations of communication systems. A ray-tracing approach is exploited to model V2V the channel, which leads for wide-band as well as narrow-band analysis in [22]. A geometry-based path interpolation [23] tool is proposed to deal with the high computational complexity problem of the ray-tracing technique. It utilizes knowledge of the specific movement of transmitting and receiving nodes and their environment.

In this paragraph, the comparison of the aforementioned model types is discussed. Empirical model and stochastic channel models do not take into account all the elements of the environment and therefore, they could fail in situations where the surroundings have a great impact on the electromagnetic propagation (i.e., where such things as vegetation, different types of scatters, or other materials are present). Mathematically, deterministic channel models are generally more complex than stochastic ones. Nevertheless, some realistic approaches may make a stochastic channel model very complex due to the mobile radio channel being non-stationary. Different from the deterministic approach, stochastic channel models can be set to emulate various propagation environments, which is the main advantage of these models [24].

Channel types termed based on the amplitude of channel coefficients in cellular channels are also valid for V2V channels, due to distributions of scatters and channel coefficients are statistically independent in the wireless channel. However, it is clearly not stated in the literature. Articles in the sequel investigate V2V channels by also considering the amplitude distribution of channel coefficients. Yuan et al. [25] propose a novel 3D theoretical regular-shaped geometry-based stochastic model and the corresponding sum-of-sinusoids simulation model for non-isotropic MIMO V2V Rician fading channels. Scatterers in the channel are distributed by using von Mises Fisher distribution. According to that model, CIR is derived as a sum of LOS, single bounced, and double bounced paths. While Rician phase distribution in cellular communication has uniform distribution between  $-\pi$  and  $\pi$  its phase does not have a uniform distribution in the V2V channel. Channel characteristics such as amplitude and phase distribution of CIR, STFC, PDS density, envelope level crossing rate (LCR), and AFD are obtained in both proposed two models. In that paper, any performance analysis is not performed. In the same such, channel estimation, which is obtaining of CIR, also is done in [26] by using a geometry-based stochastic channel model for V2V. The LS estimation algorithm is used for channel estimation. In [33], a 3D geometry-based stochastic scattering model for wideband MIMO V2V relay-based cooperative fading channel based on geometrical three-cylinder is proposed.

is an amplify-and-forward Rayleigh channel. Channel characteristics, which are STCF, channel envelope, averaging PDP, are obtained through CIR. As a result, modeling channels as based-geometry does not change channel type (Rician, Rayleigh, Nakagami). In [27], the impact of outdated CSI in a TAS system that operates in the V2V communication environment is investigated by analyzing the performance of the channel. The V2V channel is modeled by the double-Weibull distribution, a widely adopted distribution for modeling scenarios where both the transmitter and the receiver are in motion. Double distribution for V2V channels is used in some papers. Its reason is that all reflections in the channel are assumed to be double bounced. In [28], a V2V MIMO system using an MRT scheme is proposed, and its performance is investigated. The cascaded Nakagami-m channel model is used for distribution. Symbol error rate (SER) and moment generating function (MGF) statements in the receiver are derived by carrying out MRT on the transmitter side and MRC on the receiver side. A different number of antennas for MRT is used in order to examine error performance. In this dissertation, the distribution of the amplitude of channel coefficients is assumed as a generalized-k ( $K_G$ ) one.

In this paragraph, recently published articles dealing with V2V channels are subjected. Abbas *et al.* [29] highlight that gains of cellular communication are higher than V2V ones because the base-station (BS) antenna is at an elevated position. Therefore, they investigate the effects of antennas mounted to different vehicle locations to gain, delay and Doppler spread. In [30], it is investigated whether the 22-23 GHz band is feasible for V2I communications. Schack *et al.* [31] also study receiver diversity and MIMO capacity by mounting three antennas to the different locations of the vehicle and applying a ray-tracing model. In [32], characteristics of the V2V channel are analyzed in the low TeraHertz band. A novel geometry-based model (3D scenario) [33] is proposed to model V2I channels with deep learning.

#### 1.2 Objective of the Thesis

Nowadays, vehicular communications are quite an attractive research field. Providing safety of road, efficient transportation, fuel-saving, preventing traffic congestion and road tolls is aimed with vehicular communication. Thanks to vehicular communications, vehicles can provide different types of data to each other, such as information about available parking spaces, accidents, emergency braking, obstacles in the road, real-time traffic information, or information relative to the coordination of vehicles in emergency situations [34]. On the other hand, one of the most important reasons for death worldwide is road crashes. It is estimated that 1.2 million people are killed, and over 50 million are injured each year due to road crashes which are

the second cause of death in the 5–29 year old age group [35]. For this purpose, it is predicted that all vehicles will aggregate data providing from the road with sensors and will share it with each other and infrastructure via wireless channels.

All these reasons and the developed new vehicle technologies enforce researchers to investigate vehicular channels. In this dissertation, performance analysis is made by applying MRT in order to increase performance in vehicular  $K_G$  fading channels. Another problem is spectral efficiency and latency which constitute a considerable problem in the future due to the increasing wireless communication. It is especially much significant in vehicular communication because it is sensitive. Therefore, downlink and uplink NOMA systems providing gain from spectrum and latency are investigated.

#### 1.3 Hypothesis

In the near future, new technologies within the scope of ITS will be released to prevent current problems and to provide high efficiency e.g. fuel consumption. Vehicles communicate via the VANET network and most of them will not be controlled by humans. Operation with high performance depends on the performance of reliability of vehicular communication channels. Furthermore, all vehicular communication systems are required to have low latency and high spectral efficiency because speedy responses are essential in crowded vehicular systems. Contributions of this dissertation can be sorted as follows:

- 1. In vehicular  $K_G$  fading channels, outage probability (OP), average channel capacity (AVC), bit error rate (BER), asymptotic OP, and asymptotic BER in the receiver are derived by applying MRT in the transmitter with 4, 6, and 8 antennas, and obtained results are validated with simulations. Thus, the performance success enabled by MRT is verified.
  - Results of this work were published called Performance of Maximal Ratio Transmission over  $K_G$  fading channels in the Institution Engineering and Technology (IET).
- 2. In vehicular  $K_G$  fading channels and downlink-NOMA ensuring low latency and high spectral efficiency; OP, AVC, BER, asymptotic OP, and asymptotic BER for systems with 2, 3, 4, 5 users are analyzed as mathematically and results are verified with simulations. Thus, it is demonstrated that downlink-NOMA is applicable for V2V due to it provides enough performance in spite of high interference. Furthermore, it is proved downlink-NOMA provides fairness between users.

- Results of this work were published by the Physical Communication journal with the title of Performance Analysis of Downlink-NOMA over  $K_G$  fading channels.
- 3. Likewise, in vehicular  $K_G$  fading channels uplink-NOMA offering low latency and high spectral efficiency; OP, AVC, BER, asymptotic OP, and asymptotic BER for a system with 3 users are analyzed as mathematically and results are verified with simulations.
  - Results of this work were submitted to Wiley online library journal with the title of Performance Analysis of NOMA Uplink Transmission over  $K_G$  fading channels.

The rest of this thesis is organized as follows:  $K_G$  fading channels are presented in Chapter 2, performance analysis is carried out in vehicular  $K_G$  fading channels with MRT in chapter 3, downlink-NOMA and uplink-NOMA in vehicular  $K_G$  fading channels are investigated in chapters 4 and 5, respectively. Finally, chapter 6 concludes and summarizes this dissertation.

#### 2.1 Generalized-k Fading Channels

In the space (Outside of the atmosphere), while only pathloss is critical in wireless communication, multipath (small-scale fading) and shadowing (large-scale fading) due to diffraction, refraction, reflection, and scattering can severely distort communication signals. These propagation mechanisms can also enable communication even though transmitter and receiver antennas do not directly see each other. On the other hand, they can lead to problems such as frequency selectivity which emerges if symbols interfere with each other due to late arrivals of multipath components. Time selectivity emerges due to Doppler spreading when mobile objects are in the environment, or transmitter or receiver are moving. The probability of its occurrence is quite high in vehicular channels. Both time and frequency selectivities can significantly corrupt received signals. Thus, increasing performance is needed with various techniques such as multiple antenna transmissions.

Friis formula is valid for free-space where only pathloss (attenuation) is present.

$$\frac{P_r}{P_t} = G_t G_r \left(\frac{\lambda}{4\pi d}\right)^2 \tag{2.1}$$

In contrast to free-space, multipath fading and shadowing constituted by scattering, refraction, diffraction, and reflection are present in the earth's face as well as pathloss. In [36, Eq 1.4], due to pathloss originated distance, large-scale and small-scale fading, received power in the receiver in terms of dB is as follows

$$\Omega_{p(dBm)}(d) = \mu \Omega_{p(dBm)}(d_0) - 10\beta \log_{10}(d/d_0) + \epsilon(dB) + y(dB)$$
 (2.2)

In (2.2),  $\mu\Omega_{p(dBm)}(d_0)$  is received power in reference distance  $d_0$ .  $\beta$  is pathloss order which some papers addressed especially its calculation as empirically.  $\epsilon(dB)$ 

is a large-scale fading random variable having gauss distribution (it has a gauss distribution because it is written in terms of dB. If it is not written in terms of dB it has log-normal distribution). y(dB) is small-scale fading random variables that can be Rayleigh, Rician, Nakagami, or Weilbull distribution.  $\mu\Omega_{p(dBm)}(d_0) - 10\beta\log_{10}(d/d_0)$  is the expected value of y(dB) random variables. If parameters in (2.2) are not written in terms of dB, they are written in such that way multiplication as in equation (2.3). As a result, pathloss is the mean of the shadowing, and shadowing is also the mean of the multipath fading (Figure 2.1).

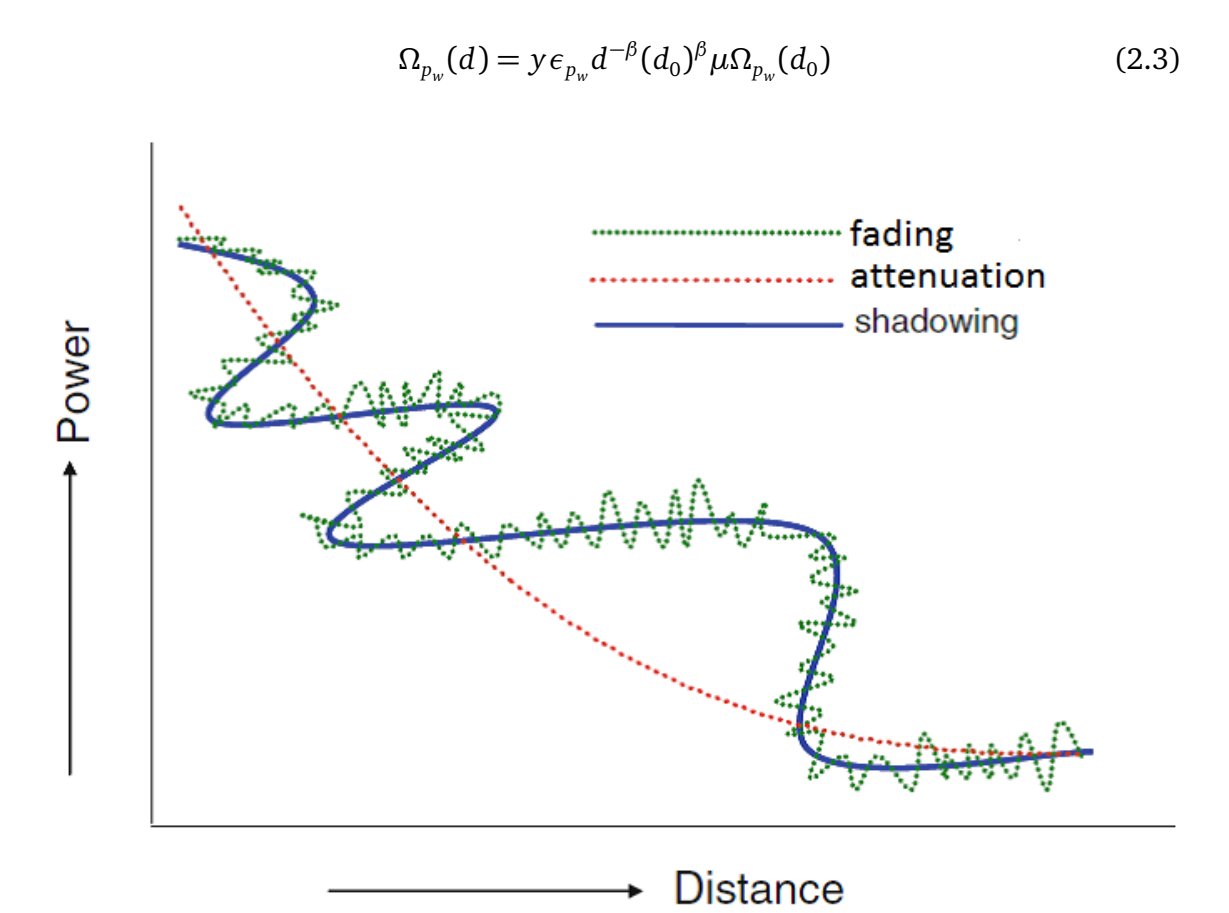


Figure 2.1 Pathloss, Shadowing and Multipath Fadings. [37, Fig. 4.3]

The shadowing fading for a variety of terrains was firstly described in [38], and it is detected that it has log-normal distribution. While shadowing fading is originated buildings, trees, and terrain according to Alouini [39], Matz and Hlawatsch state that it is originated buildings and dense vegetation. According to [40], buildings and hills cause it. Authors of [41] express that multipath and shadowing fadings arise simultaneously in many practical situations. Furthermore, they classify shadowing fading into three groups, namely, frequent heavy shadowing (FHS), overall results, which are Loo's models, and the third one performed by Karsawa [42]. They are classified according to the standard deviation of log-normal. In [43], multipath and

shadowing fadings and pathloss emerge simultaneously in many cases. Miridakis [44] emphasize that shadowing is always available in a wireless channel. It is expressed that shadowing specifies the average of multipath fading envelope [45]. Bithas [46] describes it affects transmission quality with its slow variation. While [47] explain in which situation shadowing disappear, [48] present situation in which its effect is neglected. In [49] and [50], relationship of received power with pathloss and shadowing is presented. Al-Hussaini [51] and Dwivedi [52] determine values for heavy and light shadowing. While Al-Husaini decides to heavy or light shadowing according to the standard deviation of normal distribution. As a consequence, although the impact of shadowing is mostly neglected, incorporated it into the channel model gives a much realistic channel model [53]. As mentioned above, shadowing is modeled with a log-normal distribution. However, it is not tractable mathematically, so gamma distribution being a general distribution is preferred instead. Therefore, composite fading models for wireless transmissions (e.g.,  $(K_G)$  distribution introduced in [54]) combine the effects of both multipath fading and shadowing. The use of  $K_G$ model has been increasing since it is applicable to the unmanned aerial vehicle (UAV) [55], V2V [56] as well as cellular communications. Decode-and-forward (DF) relaying over  $K_G$  fading channels is considered in [57] to analyze secrecy outage and capacity, and similarly simultaneous wireless information and power transfer (SWIPT) system is investigated for  $K_G$  fading channels to explore the secrecy OP [58]. Blagojevic et al. [59] analyze the ergodic and outage capacities for energy harvesting and information transmission based on time-switching and power-splitting relaying protocols over  $K_G$ fading channels. Efthymoglou et al. [60] evaluate the SER performance of several modulation schemes and the capacity of various transmission policies while Dziri et al. [61] derive the SER and OP for DF relaying multi-hop IoT networks over  $K_G$ fading channels. Zhang et al. [62] derive the secrecy OP, secrecy diversity order, and array gain over  $K_G$  fading channels. On the other hand, Blagojevic and Cvetkovic [63] analyze OP of DF energy harvesting relaying over  $K_G$  fading channels.

The  $K_G$  fading model is quite general as it includes the K distribution as a special case and accurately approximates many other fading models, such as Rayleigh-Lognormal (RL) and Nakagami-Lognormal (NL) fading [49]. In many papers, it is not stated  $K_G$  distribution created by the product of two Nakagami random variables. Thus, its derivation is presented below.

#### 2.2 Derivation of Generalized-K Probability Density Function

The probability density function (PDF) of the amplitude of  $K_G$  fading channels is derived by multiplying two Nakagami-m random variables one of which represent

multipath fading coefficients and the other one represent shadowing coefficients. Nakagami-m distribution representing multipath fading is as follows,

$$f_X(x) = \frac{2(m_m)^{m_m} x^{2m_m - 1} e^{-\frac{m_m}{\Omega_X} x^2}}{\Gamma(m_m)(\Omega_x)^{m_m}}, \qquad x > 0$$
 (2.4)

where  $m_m \ge 0.5$  multipath fading shaping parameter. Nakagami-m distribution representing shadowing is as follows,

$$f_{Y}(y) = \frac{2(m_{s})^{m_{s}} y^{2m_{s}-1} e^{-\frac{m_{s}}{\Omega_{y}} y^{2}}}{\Gamma(m_{s})(\Omega_{y})^{m_{s}}}, \qquad y > 0$$
 (2.5)

where  $m_s > 0$  shadowing shaping parameter. The level of impact of  $m_m$  and  $m_s$  on OP, AVC, BER is studied by Bithas *et al.* [64]. X and Y having Nakagami-m distributions are independent and not identically distributed (i.n.i.d.) random variables, and then  $\alpha = XY$  random variable gives the amplitude of  $K_G$  fading channel coefficients and its distribution is obtained as

$$f_{\alpha}(\alpha) = \int_{y=0}^{\infty} \frac{1}{y} f_X(\frac{\alpha}{y}) f_Y(y) dy$$
 (2.6)

When  $\frac{\alpha}{y}$  is substituted into (2.4), it reverts as

$$f_X(\frac{\alpha}{y}) = \frac{2(m_m)^{m_m} \alpha^{2m_m - 1} e^{-\frac{m_m}{\Omega_X} (\frac{\alpha}{y})^2}}{\Gamma(m_m)(\Omega_X) m_m y^{2m_m - 1}}, \qquad 0 \le \alpha \le \infty$$
 (2.7)

When (2.5) and (2.7) are substituted into (2.6), it becomes

$$f_{\alpha}(\alpha) = \frac{4(m_m)^{m_m} \alpha^{2m_m - 1}(m_s)^{m_s}}{\Gamma(m_m)(\Omega_x)^{m_m} \Gamma(m_s)(\Omega_y)^{m_s}} \int_{\gamma=0}^{\infty} (y^2)^{m_s - m_m - 1} e^{-\frac{m_m \alpha^2}{y^2 \Omega_x} - \frac{m_s}{\Omega_y} y^2} 2y \, dy \tag{2.8}$$

The change variable  $r=y^2$  is applied in (2.8), integral transforms in the following form,

$$f_{\alpha}(\alpha) = \frac{4(m_m)^{m_m} \alpha^{2m_m - 1} (m_s)^{m_s}}{\Gamma(m_m)(\Omega_x)^{m_m} \Gamma(m_s)(\Omega_y)^{m_s}} \int_{r=0}^{\infty} r^{m_s - m_m - 1} e^{-\frac{m_m \alpha^2}{r\Omega_x} - \frac{m_s}{\Omega_y} r} dr$$
(2.9)

According to [65, Eq. 3.471/9], integral in (2.9) is derived as follows

$$f_{\alpha}(\alpha) = \frac{4\alpha^{m_s + m_m - 1}}{\Gamma(m_m)\Gamma(m_s)} \Xi^{\frac{m_s + m_m}{2}} K_{m_s - m_m} \left( 2\alpha\sqrt{\Xi} \right)$$
 (2.10)

where  $\Xi=\frac{m_m m_s}{\Omega_0}$ , namely  $\Omega_0=\Omega_x\Omega_y$  which is mean of  $\gamma=\alpha^2$ .  $K_{m_s-m_m(.)}$  is the modified Bessel function with order  $m_s-m_m$ . Square of  $K_G$  random variable ( $\alpha$ ) or multiplying two gamma random variables conclude with Gamma-Gamma (GG) one and it is presented as,

$$f_{\gamma}(\gamma) = \frac{2\gamma^{m_s + m_m - 1}}{\Gamma(m_m)\Gamma(m_s)} \Xi^{\frac{m_s + m_m}{2}} K_{m_s - m_m} \left(2\sqrt{\Xi\gamma}\right)$$
(2.11)

#### 2.3 **NOMA**

With the advances of new applications and services, data traffic has been growing which leads to problems such as reduced bandwidths and increased delays. The demand for higher capacity enforces new wireless transmission techniques to be developed. Recently, NOMA [66] has attracted great attention since it can improve spectral efficiency by exploiting all time and frequency resources without any guard band or guard interval [67] unlike orthogonal multiple access (OMA) techniques such as time division multiple access (TDMA) and frequency division multiple access (FDMA). Therefore, NOMA is a strong candidate for increasing the throughput of next-generation wireless systems as it can approach the capacity limits of the downlink broadcast channels. On the other hand, investigation of its availability and reliability are highly essential since multiple access interference becomes significant due to non-orthogonal signaling. Signals of multiple users can be transmitted in the same resource blocks at different power levels by using superposition coding (SC) and successive interference cancellation (SIC) at the receivers can be used in NOMA to increase spectral efficiency [68]. Wunder et al. [69] explain the necessity of non-orthogonal communications for 5G and Benjebbour [70] presents a comprehensive overview of NOMA. Kızılırmak [71] describes the decoding of signals for uplink and downlink NOMA and compares NOMA and OFDMA in terms of rate, and energy, spectral efficiencies. Duan et al. [72] study resource allocation for UAV BSs to aggregate data from IoT nodes from NOMA uplink and compare with OMA. Kwon et al. [73] deal with power allocation in UAV-aided NOMA uplink with carrier sense multiple access with collision avoidance (CSMA/CA) networks. Chen et al. [74] derives channel capacity for NOMA with spatial modulation in the vehicular system over the Rician channel. Even though the advance of NOMA systems is promising,

the co-channel interference can reduce signal quality, and thus its capacity and error performance for both downlink and uplink scenarios need extensive research.

#### 2.4 Performance Evaluation Tools

#### 2.4.1 Outage Probability

OP is a widely used performance metric providing information about the availability of the system. It is defined as the probability of the received signal-to-interference-plus-noise ratio (SINR) falling below a threshold value ( $\gamma_{th}$ ) which can be determined based on the desired level of quality of service or receiver sensitivity. Thus, the OP can be simply written in terms of the CDF of SINR as,

$$F_{\gamma}(\gamma_{th}) = Pr(\gamma < \gamma_{th}). \tag{2.12}$$

#### 2.4.2 Outage Capacity

Channel capacity gives information about the limits on error-free transmission speed and it can be computed by using the signal-to-noise ratio (SNR),

$$C = W \log_2(1+\gamma),\tag{2.13}$$

where *W* denotes the bandwidth. The cumulative distribution function (CDF) of the capacity (aka outage capacity) can be derived from the CDF of SNR as follows,

$$F_C(c) = Pr(C < c) = Pr(\gamma < 2^{\frac{C}{W}-1}) = F_{\gamma}(2^{\frac{c}{W}} - 1),$$
 (2.14)

where  $\gamma = 2^{\frac{C}{W}} - 1$  is used.

#### 2.4.3 Average Channel Capacity

AVC for any channel can be found by taking the average of *C* above over the PDF of SINR as below,

$$\bar{C} = \int_{\gamma=0}^{\infty} W \log_2(1+\gamma) f_{\gamma}(\gamma) d\gamma. \tag{2.15}$$

#### 2.4.4 Symbol Error Rate

A widely used error performance metric is average SER which can be found by using the PDF of SNR as

$$\bar{P}_{se} = \int_{\gamma=0}^{\infty} P_e(\gamma) f_{\gamma}(\gamma) d\gamma. \tag{2.16}$$

 $P_e(\gamma)$  is error probability for a fixed SNR and in general it can be written as  $P_e(\gamma) = Aerf c(\sqrt{B\gamma})$  where A and B are constants depending on the specific modulation scheme [75, Table I].

#### 2.4.5 Asymptotic Analysis, Diversity and Array Gain

Outage diversity and outage coding gains can be found by studying asymptotic OP expression. Based on [76, Assumption 3], PDF of  $\beta$  (i.e.  $f(\beta)$ ) can be approximated by a single polynomial for  $(\beta \longrightarrow 0^+)$  which is called as asymptotic PDF and it can be expressed as,

$$f(\beta) = a\beta^t + o(\beta^t), \tag{2.17}$$

where a is a positive constant and t represents the order of smoothness at the origin and they must be computed in order to find diversity and coding gains.

3

## PERFORMANCE OF MAXIMAL RATIO TRANSMISSION OVER GENERALIZED-K FADING CHANNELS

#### 3.1 Introduction

MIMO techniques utilize multiple antennas at the transmitter and receiver sides to achieve diversity in order to improve reliability performance. Considering size, power and processing constraints of mobile units, diversity combining with the use of multiple receiver antennas may not be desirable. Therefore, transmit diversity approaches such as space time codes (STC) have become popular. For example Peppas et al. analyze the performance of orthogonal space-time block code (STBC) over cascaded  $K_G$  fading channels in [77]. Salahat and Saleh [78] obtain a unified performance analysis of SER for STBCs for coherent modulation schemes over  $K_G$ fading channels. Similarly, the performance of orthogonal STBC systems with M-ary quadrature amplitude modulation transmission is investigated over independent but not necessarily identically distributed (i.n.i.d.)  $K_G$  fading channels in [79]. Li et al. [80] present an approximate capacity analysis for distributed MIMO system over  $K_G$ channels. Diversity combining techniques such as MRC, EGC and selection combining (SC) can also be used at the multi-antenna receiver to improve the reliability. However, similar to space-time coding, these methods can also increase the receiver complexity which is not desirable for size and power constrained mobile units such as sensors. Dwivedi et al. [81] provide the channel capacity by using MRC over the  $K_G$  fading channel. Jung et al. [82] investigate the capacity and error probability for MRC and SC over  $K_G$  fading channels. Bithas et al. [46] evaluate OP for diversity combining techniques over  $K_G$  fading channels.

Similar to STC, MRT [83] is another widely used transmit diversity technique which can maximize the SNR and obtain full diversity while not increasing the complexity of the receiver. Unlike STBC, it can be used with any number of transmit antennas and thus MRT has been widely employed in massive MIMO schemes thanks to its simplicity. The performance of a single cell massive MIMO downlink system using

MRT is analyzed in the presence of both jammers and eavesdroppers in [84]. Recently, the average SER of quadrature phase-shift keying (QPSK) transmission with MRT over a Rayleigh fading channel is obtained in [85]. Chauhan and Kumar [86] study channel capacity, OP and SER of the MRT with receive antenna selection over correlated Nakagami-m fading. Badarneh *et al.* [87] investigate OP, throughput, BER for wireless power and information transfer under Nakagami-m fading where the source uses MRT. Yang and Zhang [88] present outage performance of MIMO relay channels with MRT. Aladwani et al [89] deal with a system with amplify-and-forward (AF) two-way relay network exposed to co-channel interference where MRT is employed at the sources. Similarly, MRT with DF relaying over Nakagami-m fading is studied in [90]. Ibrahim *et al.* investigate the performance of MRT in free space optical links which is modeled by Malaga distribution [91].

In this chapter, the performance metrics of MRT technique over  $K_G$  channels are explored. The contributions of the chapter can be listed as follows:

- PDF and CDF of the received SNR for the considered system is studied.
- OP, outage diversity and coding gains are obtained.
- Statistics of channel capacity and average channel capacity are provided.
- SER is analyzed by using the PDF of SNR.
- Diversity and coding gains are also computed from asymptotic SER.
- The impact of estimation errors on the performance is explored.
- Finally, numerical examples are illustrated to corroborate our theoretical findings.

The rest of this chapter is organized as follows. In section 2, the system model and the PDF of SNR in MRT over  $K_G$  channel are explained. In section 3, performance metrics such as OP, channel capacity, SER, diversity and coding gains are derived. Simulation results are discussed in Section 4 and finally Section 5 concludes the chapter.

## 3.2 System Description

The block diagram of the considered system model is shown in Figure 3.1 where the multiple antenna transmitter employs MRT and the low complexity receiver has a

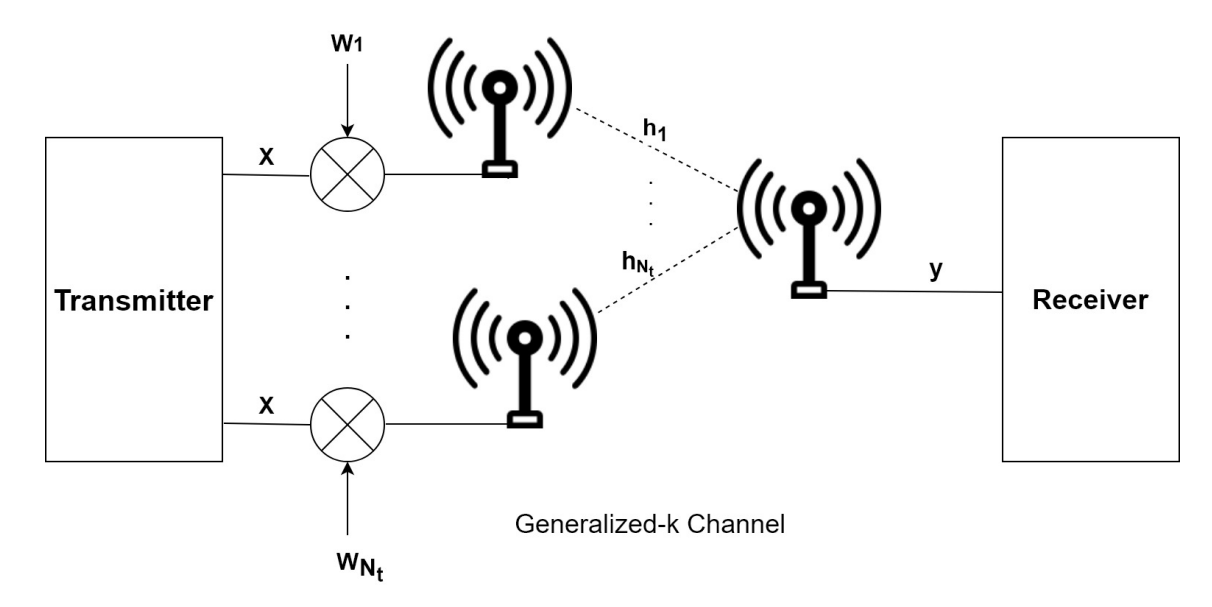


**Figure 3.1** Block diagram of the maximum-ratio transmission over generalized-K channel

single antenna. The symbols to be transmitted are weighted in order to maximize the recieved SNR [83]. The received signal can be written as,

$$y = \sum_{i=1}^{N_t} h_i w_i x + n,$$
 (3.1)

where x is the symbol with average energy  $E_s$  transmitted from  $N_t$  transmit antennas.  $h_i$  is the complex channel coefficient between i-th transmit antenna and the receiver whose magnitude follows  $K_G$  distribution. n denotes zero mean additive white Gaussian noise sample with one sided power spectral density  $N_0$ .  $w_i$  ( $i=1,2,...,N_t$ ) is the weighting factor for the i-th transmit antenna found by  $w_i = \frac{h_i^*}{\|h_F\|}$ ,  $h_F$  below represents the Frobenius norm of channel vector  $\mathbf{h} = [h_1, h_2, ...h_{N_t}]$ ,

$$||h_F|| = \sqrt{\sum_{i=1}^{N_t} |h_i|^2},$$
 (3.2)

where  $|h_i|$  is the magnitude of channel coefficient whose square  $|h_i|^2$  has GG distribution. By employing MRT at transmitter, total instantaneous SNR at the receiver can be written as follows,

$$\gamma_{\varsigma} = \frac{E_{s}}{N_{0}} \sum_{i=1}^{N_{t}} |\mathbf{h}_{i}|^{2}.$$
 (3.3)

In order to find the performance metrics such as SER, channel capacity, and OP, the PDF of  $\gamma_{\varsigma}$  in (3.3) needs to be computed. For  $K_G$  fading channel, the PDF of  $\gamma_{\varsigma}$  can be obtained by using MGF [64] of  $|\mathbf{h}_i|^2$ ,  $i=1,...,N_t$ ,

$$M_{|h_i|^2}(s) = \left(\frac{\Xi}{s}\right)^{\frac{m_s + m_m - 1}{2}} e^{\frac{\Xi}{2s}} W_{-\frac{m_s + m_m - 1}{2}, \frac{m_s - m_m}{2}} \left(\frac{\Xi}{s}\right), \tag{3.4}$$

Usually, when multiple random variables are added, the MGF of each random variable is computed first to derive the PDF of their summation. Then, all MGFs are multiplied and inverse MGF of the obtained final term is computed. In the above case, multiplying Whittaker functions and calculating inverse MGF are not tractable. Therefore, approximated PDF of  $\gamma_c$  can be used as shown in [47, p. 9],

$$f_{\gamma_{\varsigma}}(\gamma_{\varsigma}) \stackrel{\triangle}{=} \frac{2(b_{\varsigma})^{m_{m,\varsigma}+m_{s,\varsigma}}}{\Gamma(m_{m,\varsigma})\Gamma(m_{s,\varsigma})} (\gamma_{\varsigma})^{(m_{m,\varsigma}+m_{s,\varsigma})/2-1} K_{m_{s,\varsigma}-m_{m,\varsigma}} (2b_{\varsigma}\sqrt{\gamma_{\varsigma}}), \qquad \gamma_{\varsigma} > 0. \quad (3.5)$$

where  $a=\frac{m_m}{m_s}$ ,  $m_{s,\varsigma}=\frac{m_{m,\varsigma}}{a}$  and  $b_{\varsigma}=\sqrt{\frac{m_{s,\varsigma}m_{m,\varsigma}}{\Omega_{0,\varsigma}}}$ ,  $\Omega_{0,\varsigma}=N_t\Omega_0$  is the mean of  $\gamma_{\varsigma}$ .  $m_{s,\varsigma}$  and  $m_{m,\varsigma}$  are fading parameters depending on  $m_m$  and  $m_s$ .  $m_{m,\varsigma}$  is given by,

$$m_{m,\varsigma} = \frac{(1+a)\sqrt{(1+a)^2 + \frac{4}{N_t m_s^2} k_1}}{2\left(a + \frac{1}{m_s} + 1\right)},$$
(3.6)

which is obtained by equating amount fadings statistics [47] where  $k_1 = m_m + m_s + 1$ .

## 3.3 Performance Analysis

In this section, the OP of the system (i.e CDF of SNR), channel capacity, SER, diversity, coding gain and the impact of channel estimation error are analyzed.

#### 3.3.1 Outage Probability

In order to obtain OP expression, CDF of SNR can be computed by integrating the PDF in (3.5),

$$F_{\gamma_{\varsigma}}(\gamma_{\varsigma}) = \int_{\tau=0}^{\gamma_{\varsigma}} f_{\tau}(\tau) d\tau = \frac{2(b_{\varsigma})^{m_{m,\varsigma}+m_{s,\varsigma}}}{\Gamma(m_{m,\varsigma})\Gamma(m_{s,\varsigma})} \times \int_{\tau=0}^{\gamma_{\varsigma}} \tau^{(m_{m,\varsigma}+m_{s,\varsigma})/2-1} K_{m_{s,\varsigma}-m_{m,\varsigma}}(2b_{\varsigma}\sqrt{\tau}) d\tau,$$

$$(3.7)$$

(3.7) can be rearranged as follows,

$$F_{\gamma_{\varsigma}}(\gamma_{\varsigma}) = \frac{2(b_{\varsigma})^{2}}{\Gamma(m_{m,\varsigma})\Gamma(m_{s,\varsigma})2^{m_{m,\varsigma}+m_{s,\varsigma}-2}} \times \int_{\tau=0}^{\gamma_{\varsigma}} (2b_{\varsigma}\sqrt{\tau})^{m_{m,\varsigma}+m_{s,\varsigma}-2} K_{m_{s,\varsigma}-m_{m,\varsigma}} (2b_{\varsigma}\sqrt{\tau})d\tau,$$

$$(3.8)$$

The term  $(2b_{\varsigma}\sqrt{\tau})^{m_{m,\varsigma}+m_{s,\varsigma}-2}K_{m_{s,\varsigma}-m_{m,\varsigma}}(2b_{\varsigma}\sqrt{\tau})$  in (3.8) can be written in terms of Meijer-G function [92, Section 2.6], then (3.8) can be rewritten as follows,

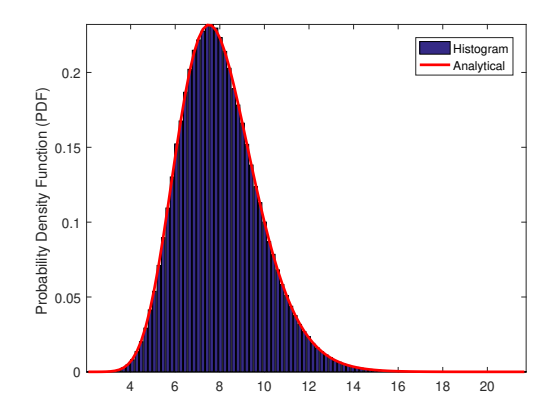
$$F_{\gamma_{\varsigma}}(\gamma_{\varsigma}) = \frac{(b_{\varsigma})^{2}}{\Gamma(m_{m,\varsigma})\Gamma(m_{s,\varsigma})} \int_{\tau=0}^{\gamma_{\varsigma}} G_{0,2}^{2,0} \left(\tau(b_{\varsigma})^{2} \Big|_{m_{\varsigma,\varsigma}, m_{m,\varsigma}}\right) d\tau, \tag{3.9}$$

By using [93], CDF of SNR can be obtained as follows,

$$F_{\gamma_{\varsigma}}(\gamma_{\varsigma}) = \frac{(b_{\varsigma})^{2}}{\Gamma(m_{m,\varsigma})\Gamma(m_{s,\varsigma})} G_{1,3}^{2,1} \left( (b_{\varsigma})^{2} \gamma_{\varsigma} \Big|_{m_{s,\varsigma}+1, m_{m,\varsigma}+1, 0}^{1, 0} \right). \tag{3.10}$$

Analytical expressions of PDF and CDF are validated by comparing with their simulation plots shown in Figure 3.2 and Figure 3.3 respectively where the number of transmit antennas is selected as 8. In Figure 3.2 blue bars represent the histogram values and red lines represent approximate PDF.

In order to derive outage diversity and outage coding gain, the instantaneous SNR at the receiver can be written as  $\gamma_{\varsigma} = \beta \Omega_{0,\varsigma}$  where  $\Omega_{0,\varsigma}$  is given by  $\mathbb{E}[\gamma_{\varsigma}] = \Omega_{0,\varsigma} = N_t(E_s/N_0)$  with  $\beta = \frac{1}{N_t} \sum_{i=1}^{N_t} |h_i|^2$ ,  $\mathbb{E}[\beta] = 1$ . a and t in (2.17) are computed as follows



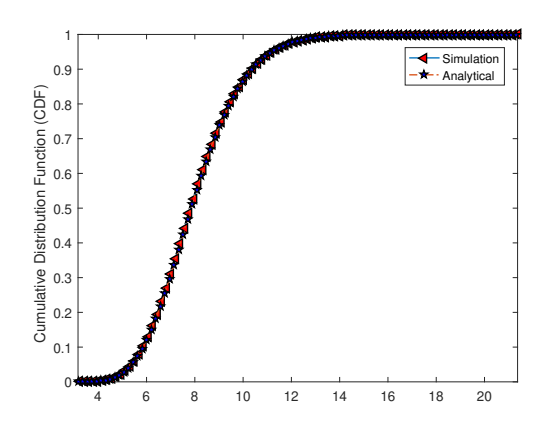


**Figure 3.2** Histogram and analytical plots PDF of the SNR

**Figure 3.3** Simulation and analytical plots of CDF of the SNR

for the considered system (Details of derivation can be seen in Appendix A),

$$t = \frac{1}{2} \left( m_{s,\varsigma} + m_{m,\varsigma} - \frac{5}{2} \right), \tag{3.11}$$

$$a = \frac{(\sqrt{m_{s,\varsigma}} m_{m,\varsigma})^{(m_{s,\varsigma} + m_{m,\varsigma} - \frac{1}{2})} \pi^{\frac{1}{2}}}{\Gamma(m_{m,\varsigma}) \Gamma(m_{s,\varsigma})}.$$
(3.12)

According to [76], when the average SNR is large enough, the asymptotic OP can be evaluated as,

$$F_{\gamma_{\varsigma}}(\gamma_{\varsigma_{th}}) = \frac{a}{t+1} \left(\frac{\gamma_{\varsigma_{th}}}{\bar{\gamma}_{\varsigma}}\right)^{t+1} + o\left(\bar{\gamma}_{\varsigma}^{-(t+1)}\right). \tag{3.13}$$

Thus, while average SNR approaches to infinity  $(\bar{\gamma}_{\varsigma} \longrightarrow \infty)$ , the term  $o(\bar{\gamma}_{\varsigma}^{-(t+1)})$  can be neglected, and  $F_{\gamma_{\varsigma}}(\gamma_{\varsigma_{th}})$  can be written as,

$$F_{\gamma_{\varsigma}}(\gamma_{\varsigma_{th}}) \approx \frac{a}{t+1} \left(\frac{\gamma_{\varsigma_{th}}}{\bar{\gamma}_{\varsigma}}\right)^{t+1} \approx (O_{c}\bar{\gamma}_{\varsigma})^{-O_{d}}, \tag{3.14}$$

where  $O_d = t + 1$  is outage diversity and  $O_c = \frac{1}{\gamma_{\varsigma_{th}}} \left(\frac{a}{t+1}\right)^{-\frac{1}{t+1}}$  is outage coding gain. When a and t are substituted into  $O_d$  and  $O_c$ , they can be shown as,

$$O_d = \frac{1}{2} \left( m_{s,\varsigma} + m_{m,\varsigma} - \frac{5}{2} \right) + 1 = \frac{1}{2} \left( m_{s,\varsigma} + m_{m,\varsigma} - \frac{1}{2} \right). \tag{3.15}$$

$$O_{c} = \frac{1}{\gamma_{\varsigma_{th}}} \left[ \frac{\left(\sqrt{m_{s,\varsigma}m_{m,\varsigma}}\right)^{(m_{s,\varsigma}+m_{m,\varsigma}-\frac{1}{2})}}{\left(m_{s,\varsigma}+m_{m,\varsigma}-\frac{1}{2}\right)} \frac{\pi^{\frac{1}{2}}}{\frac{1}{2}\Gamma(m_{s,\varsigma})\Gamma(m_{m,\varsigma})} \right]^{-\frac{1}{\frac{1}{2}(m_{s,\varsigma}+m_{m,\varsigma}-\frac{1}{2})}}.$$
 (3.16)

It can be easily understood from (3.15) and (3.16) that diversity and coding gain depend on multipath fading and shadowing parameters  $(m_m, m_s)$  and number of transmitter antennas.

#### 3.3.2 Channel Capacity

With the help of (3.10), the CDF in (2.14) can be written as below,

$$F_C(c) = \frac{(b_{\varsigma})^2}{\Gamma(m_{m,\varsigma})\Gamma(m_{s,\varsigma})} G_{1,3}^{2,1} \left( (b_{\varsigma})^2 (2^{\frac{c}{W}} - 1) \Big|_{m_{s,\varsigma}+1, m_{m,\varsigma}+1, 0}^{1, } \right).$$
(3.17)

Another statistical function of the capacity is its PDF which can be obtained by derivation of the above CDF as below,

$$f_C(c) = \frac{2^{\frac{c}{W}} \ln(2)(b_{\varsigma})^2}{W\Gamma(m_{m,\varsigma})\Gamma(m_{s,\varsigma})} G_{0,2}^{2,0} \left( (b_{\varsigma})^2 (2^{\frac{c}{W}} - 1) \Big|_{m_{\varsigma,\varsigma}, m_{m,\varsigma}} \right), \tag{3.18}$$

AVC can be obtained by using the PDF of capacity, or by substituting the PDF of SNR in (3.5) into (2.15) below,

$$\bar{C} = \frac{2W(b_{\varsigma})^{m_{m,\varsigma}+m_{s,\varsigma}}}{\Gamma(m_{m,\varsigma})\Gamma(m_{s,\varsigma})ln(2)} \int_{\gamma_{\varsigma}=0}^{\infty} ln(1+\gamma_{\varsigma})(\gamma_{\varsigma})^{(m_{m,\varsigma}+m_{s,\varsigma})/2-1} K_{m_{s,\varsigma}-m_{m,\varsigma}}(2b_{\varsigma}\sqrt{\gamma_{\varsigma}})d\gamma_{\varsigma},$$
(3.19)

and then with the help of [94], the term  $ln(1 + \gamma_{\varsigma})\gamma_{\varsigma}^{(m_{m,\varsigma}+m_{s,\varsigma})/2-1}$  in (3.19) can be written in terms of Meijer-G functions [65, p. 9.301],

$$\gamma_{\varsigma}^{(m_{m,\varsigma}+m_{s,\varsigma})/2-1}ln(1+\gamma_{\varsigma}) = G_{1,2}^{2,2} \left(\gamma_{\varsigma} \Big|_{(m_{m,\varsigma}+m_{s,\varsigma})/2, (m_{m,\varsigma}+m_{s,\varsigma})/2-1}^{(m_{m,\varsigma}+m_{s,\varsigma})/2}\right).$$
(3.20)

Likewise, the modified Bessel function of the second kind in (3.19) can be expressed

in terms of a Meijer-G function [95],

$$K_{m_{s,\varsigma}-m_{m,\varsigma}}\left(\sqrt{4b_{\varsigma}^{2}\gamma_{\varsigma}}\right) = \frac{1}{2}G_{0,2}^{2,0}\left(\frac{4b_{\varsigma}^{2}\gamma_{\varsigma}}{4}\Big|_{\frac{m_{s,\varsigma}-m_{m,\varsigma}}{2}, -\frac{m_{s,\varsigma}-m_{m,\varsigma}}{2}}\right). \tag{3.21}$$

By substituting (3.20) and (3.21) into (3.19) and using [65, pp. 7.811/1], the AVC is obtained as,

$$\bar{C} = \frac{W(b_{\varsigma})^{m_{m,\varsigma}+m_{s,\varsigma}}}{ln(2)\Gamma(m_{m,\varsigma})\Gamma(m_{s,\varsigma})}G_{2,4}^{4,1}\left((b_{\varsigma})^{2}\Big|_{-\frac{m_{s,\varsigma}+m_{s,\varsigma}}{2}, -\frac{m_{s,\varsigma}+m_{m,\varsigma}}{2}, -\frac{m_{s,\varsigma}+m_{m,\varsigma}}{2}, -\frac{m_{s,\varsigma}+m_{m,\varsigma}}{2}, \frac{m_{s,\varsigma}-m_{m,\varsigma}}{2}, -\frac{m_{s,\varsigma}-m_{m,\varsigma}}{2}}\right).$$
(3.22)

## 3.3.3 Symbol Error Rate

erfc(.) can be written in terms of Meijer-G function as in [96], and thus,

$$P_{e}(\gamma_{\varsigma}) = \frac{A}{\sqrt{\pi}} G_{1,2}^{2,0} \left( B \gamma_{\varsigma} \Big|_{0, \frac{1}{2}}^{1} \right). \tag{3.23}$$

By substituting (3.5) and (3.23) into (2.16),  $\bar{P}_{se}$  can be written as,

$$\bar{P}_{se} = \frac{2A(b_{\varsigma})^{m_{m,\varsigma}+m_{s,\varsigma}}}{\sqrt{\pi}\Gamma(m_{m,\varsigma})\Gamma(m_{s,\varsigma})} \int_{\gamma_{\varsigma}=0}^{\infty} (\gamma_{\varsigma})^{(m_{m,\varsigma}+m_{s,\varsigma})/2-1} \times K_{m_{s,\varsigma}-m_{m,\varsigma}} \left(2\sqrt{\gamma_{\varsigma}(b_{\varsigma})^{2}}\right) G_{1,2}^{2,0} \left(B\gamma_{\varsigma}\Big|_{0,\frac{1}{2}}^{1}\right) d\gamma_{\varsigma},$$

$$(3.24)$$

when integral in (3.24) is computed, the average SER is obtained as follows (Derivation details are shown in Appendix B),

$$\bar{P}_{se} = \frac{A}{\Gamma(m_{m,\varsigma})\Gamma(m_{s,\varsigma})\sqrt{\pi}} G_{3,2}^{2,2} \left(\frac{B}{(b_{\varsigma})^2}\Big|_{0,\frac{1}{2}}^{1-m_{s,\varsigma}, 1-m_{m,\varsigma}, 1}\right).$$
(3.25)

## 3.3.4 Diversity and Coding Gain

In order to find diversity and coding gains, asymptotic SER at high SNR can be put in the following form as in [76],

$$P_{E} = \frac{2^{t} a \gamma_{\varsigma}(t + \frac{3}{2})}{\sqrt{\pi}(t + 1)} (k \bar{\gamma}_{\varsigma})^{-(t+1)} + o(\bar{\gamma}_{\varsigma}^{-(t+1)}), \tag{3.26}$$

where the term  $o(\bar{\gamma}_{\varsigma}^{-(t+1)})$  becomes negligible when the average SNR approaches to infinity  $(\bar{\gamma}_{\varsigma} \longrightarrow \infty)$ , and thus asymptotic  $P_E$  can be approximated as,

$$P_E \approx \frac{2^t a \Gamma(t + \frac{3}{2})}{\sqrt{\pi}(t+1)} (k\bar{\gamma}_\varsigma)^{-(t+1)}, \tag{3.27}$$

where k is a constant depending on the modulation scheme. The coding gain is written as  $G_c = k \left( \frac{2^t a \Gamma(t + \frac{3}{2})}{\sqrt{\pi}(t+1)} \right)^{-\frac{1}{t+1}}$ , and the diversity gain becomes  $G_d = t+1$  which is same as  $O_d$ . When a and t derived in Appendix A are substituted into  $G_c$ , it can be obtained as

$$G_{c} = \left[ \frac{2^{\frac{1}{2}(m_{s,\varsigma} + m_{m,\varsigma} - \frac{5}{2})} \Gamma(\frac{1}{2}[m_{s,\varsigma} + m_{m,\varsigma} + \frac{1}{2}])}{\frac{1}{2}(m_{s,\varsigma} + m_{m,\varsigma} - \frac{1}{2}) \Gamma(m_{s,\varsigma}) \Gamma(m_{m,\varsigma})} \times \left( \sqrt{m_{s,\varsigma}} m_{m,\varsigma} \right)^{(m_{s,\varsigma} + m_{m,\varsigma} - \frac{1}{2})} \right]^{-\frac{1}{2}(m_{s,\varsigma} + m_{m,\varsigma} - \frac{1}{2})}.$$
(3.28)

## 3.3.5 Impact of Channel Estimation Errors

Channel coefficients are estimated at the receiver with some errors due to limited number of pilot symbols and noise. In practice, the relationship between actual and estimated values can be written as,

$$h_i = \hat{h}_i + e_i, \tag{3.29}$$

where  $h_i$  is actual channel coefficient for the i-th antenna,  $\hat{h}_i$  is estimated channel coefficient with channel estimation error (CEE)  $e_i$  which is denoted as complex normal random variable  $\mathscr{CN}(0, \sigma^2)$  [97]. Therefore the resulting channel impact on the

transmitted signal can be written as,

$$\sum_{i=1}^{N_t} h_i w_i = \sum_{i=1}^{N_t} \frac{\hat{h}_i^*}{\|h_F\|} h_i, \tag{3.30}$$

and thus the received signal becomes,

$$y = \sqrt{P_t} ||h_F|| x + \sqrt{P_t} \frac{x}{||h_F||} \sum_{i=1}^{N_t} \hat{h}_i^* e_i + n.$$
 (3.31)

The second term in (3.31) can cause error floor when the estimation error becomes dominant as shown in the next section. Let  $\gamma_{\varsigma_s} = (\sqrt{P_t} \|h_F\|)^2$ ,  $\gamma_{\varsigma_i} = (\frac{\sqrt{P_t}}{\|h_F\|} \sum_{i=1}^{N_t} \hat{h}_i^* e_i)^2$ , then the new SNR at the receiver is reduced as follows,

$$\gamma_{\varsigma} = \frac{\gamma_{\varsigma_{s}}}{N_{0} + \gamma_{\varsigma_{i}}} = \frac{(\sqrt{P_{t}} || h_{F} ||)^{2}}{N_{0} + \left(\frac{\sqrt{P_{t}}}{||h_{F}||} \sum_{i=1}^{N_{t}} \hat{h}_{i}^{*} e_{i}\right)^{2}}.$$
(3.32)

When complex  $K_G$  and complex Gaussian random variables are added, PDFs of their real and imaginary parts are needed to derive the PDF of the new SNR. However, it requires a lengthy and mathematically intractable computation, thus, we resort to simulations to observe the impact of CEE on performance.

#### 3.4 Simulation Results

In this section, simulation and analytical results are illustrated with several cases. At least  $10^6$  channel vectors are randomly generated for all simulation curves and  $K_G$  coefficients  $m_m$  and  $m_s$  are selected as 5 and 6, respectively. Since we focus on the performance improvement with MRT, the receiver is assumed to have a single antenna and the number of transmit antennas can be 4, 6 or 8.

SER plots of the considered system are illustrated in Figure 3.4. QPSK modulation is used with 4 transmit antennas and a receiver with a single antenna. Obviously, QPSK has higher SER than binary phase shift keying (BPSK) as expected, for example, SER values of QPSK and BPSK are  $2.23 \times 10^{-1}$  and  $4.69 \times 10^{-2}$ , respectively at SNR 5 dB when 4 transmit antennas are used. As the number of antennas increases, SER decreases, e.g.  $4.69 \times 10^{-2}$  for  $N_t = 4$ ,  $1.93 \times 10^{-2}$  for  $N_t = 6$  and  $7.9 \times 10^{-3}$  for  $N_t = 8$  at SNR=5 dB. As can be seen, as the number of antennas is increased both SER results

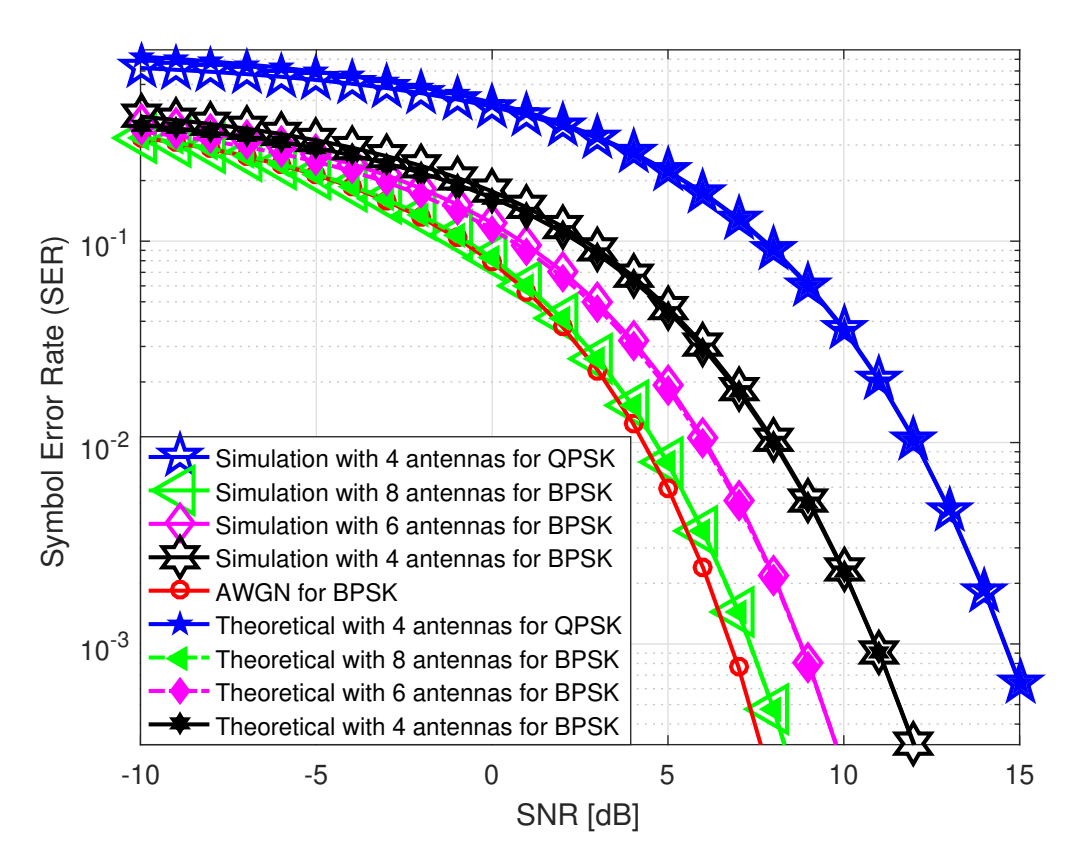


Figure 3.4 Symbol error rate for different number of transmit antennas

approach to that of the additive Gaussian white noise (AWGN) channel therefore MRT can be highly useful to increase reliability.

OP plots are compared in Figure 3.5 where the SNR threshold is selected as 5 dB. As can be seen, theoretical and simulation results matches perfectly. As the number of antennas is increased, OP decreases and diversity increases, and at SNR 9 dB OP values are  $8.107 \times 10^{-1}$ ,  $2.854 \times 10^{-1}$  and  $2.75 \times 10^{-2}$  for 4, 6 and 8 antennas, respectively.

The AVC curves are depicted in Figure 3.6 where markers represent theoretical results and solid lines represent simulations. It can be seen that as the number of antennas increases, the AVC also increases. For example, values of AVC for 4, 6 and 8 antennas are approximately 12 b/s/Hz, 17 b/s/Hz and 21 b/s/Hz, respectively at SNR=14 dB. When the value of  $m_s$  is decreased from 6 to 3, the capacity decreases from 12 b/s/Hz to 7.5 b/s/Hz for the system with 4 antennas.

Asymptotic SER results from (3.25) and (3.27) are illustrated in Figure 3.7. As observed, asymptotic results approach actual SERs at high SNR values. Theoretical  $G_d$  findings are verified as theoretical results and the slope of asymptotic plots are equal. Similarly, asymptotic OP results by using (3.10) and (3.14) illustrated in Figure 3.8 also shows the validity of the analytical derivations.

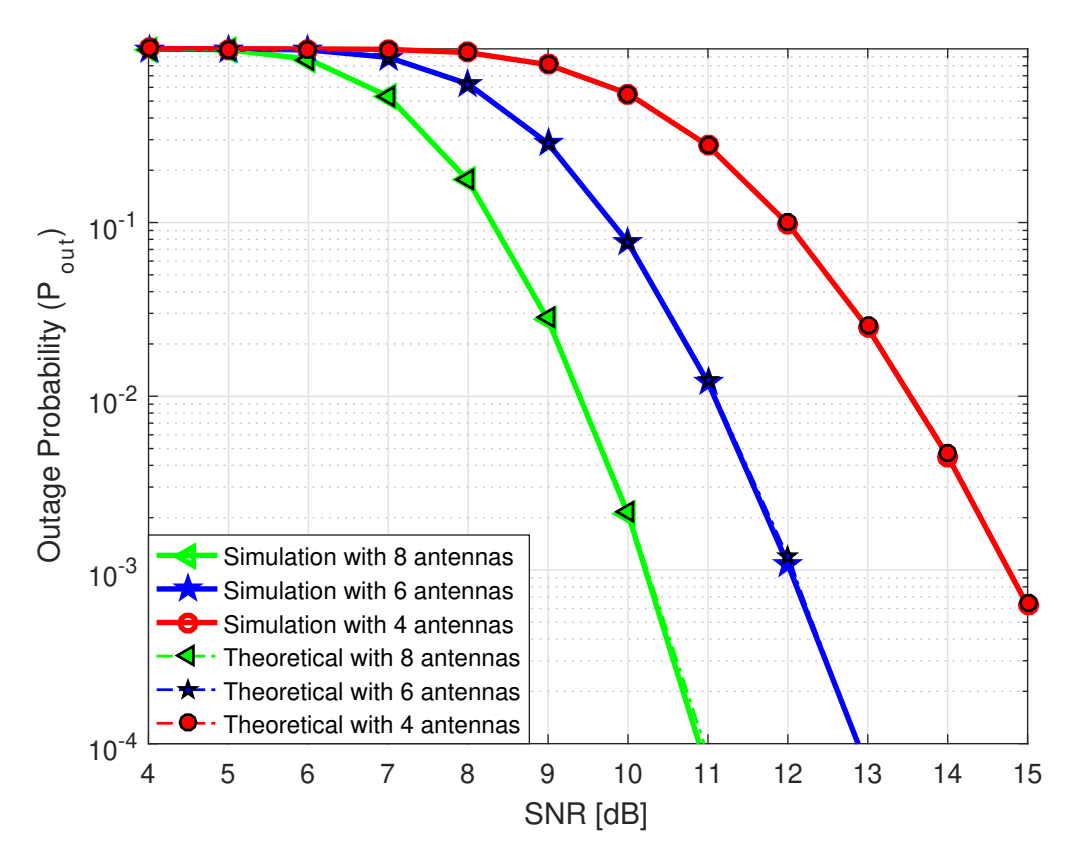


Figure 3.5 Outage probability of MRT over  $K_G$  channels

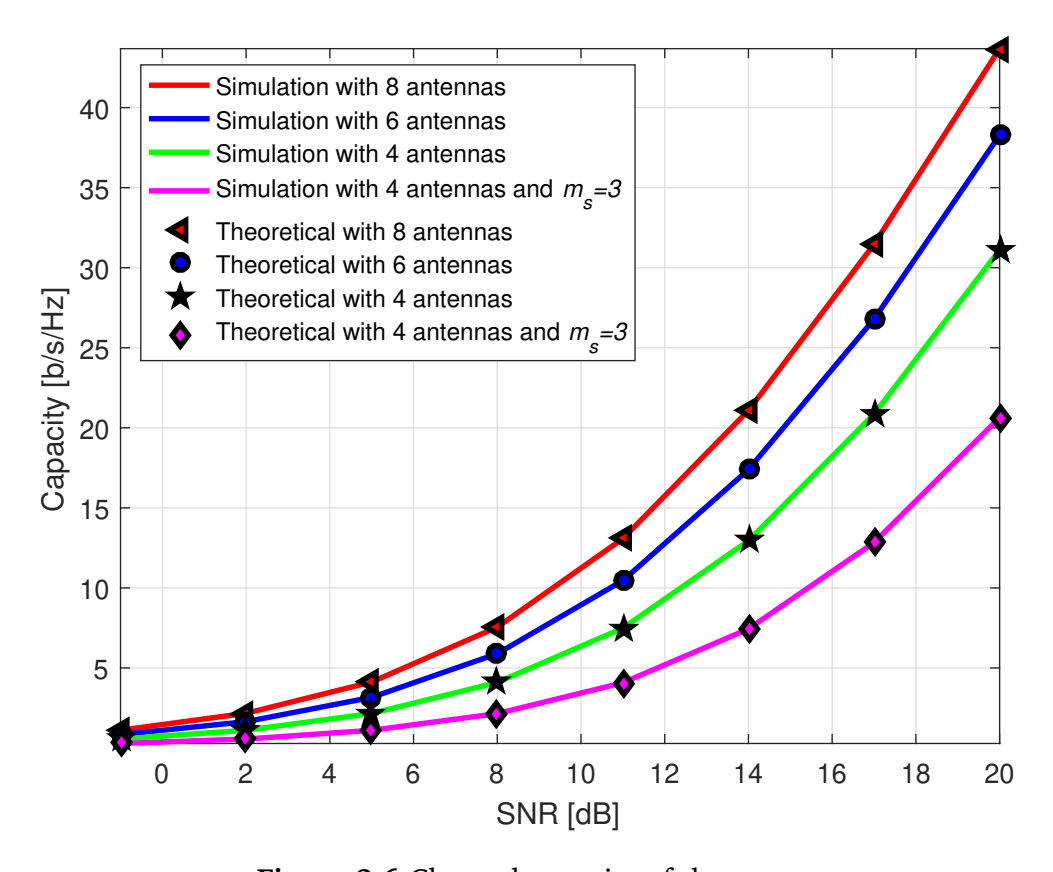
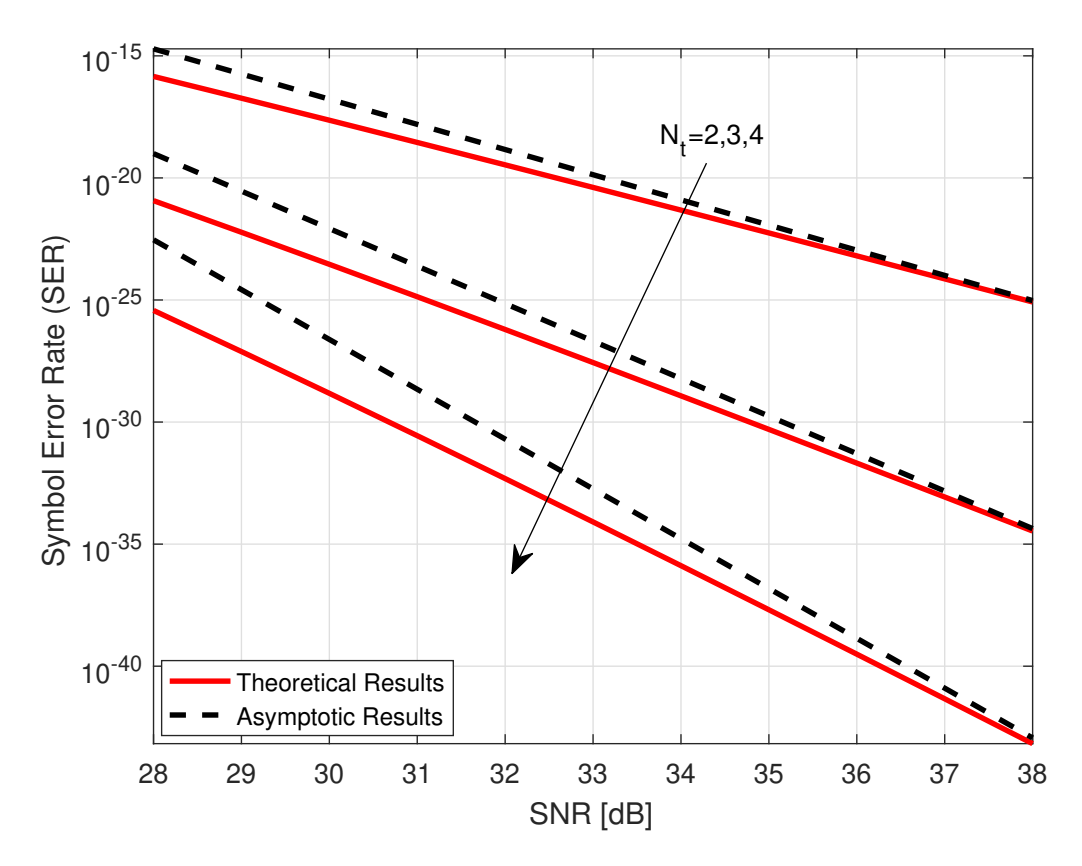


Figure 3.6 Channel capacity of the system



**Figure 3.7** Asymptotic SER of BPSK for MRT over  $K_G$  channel

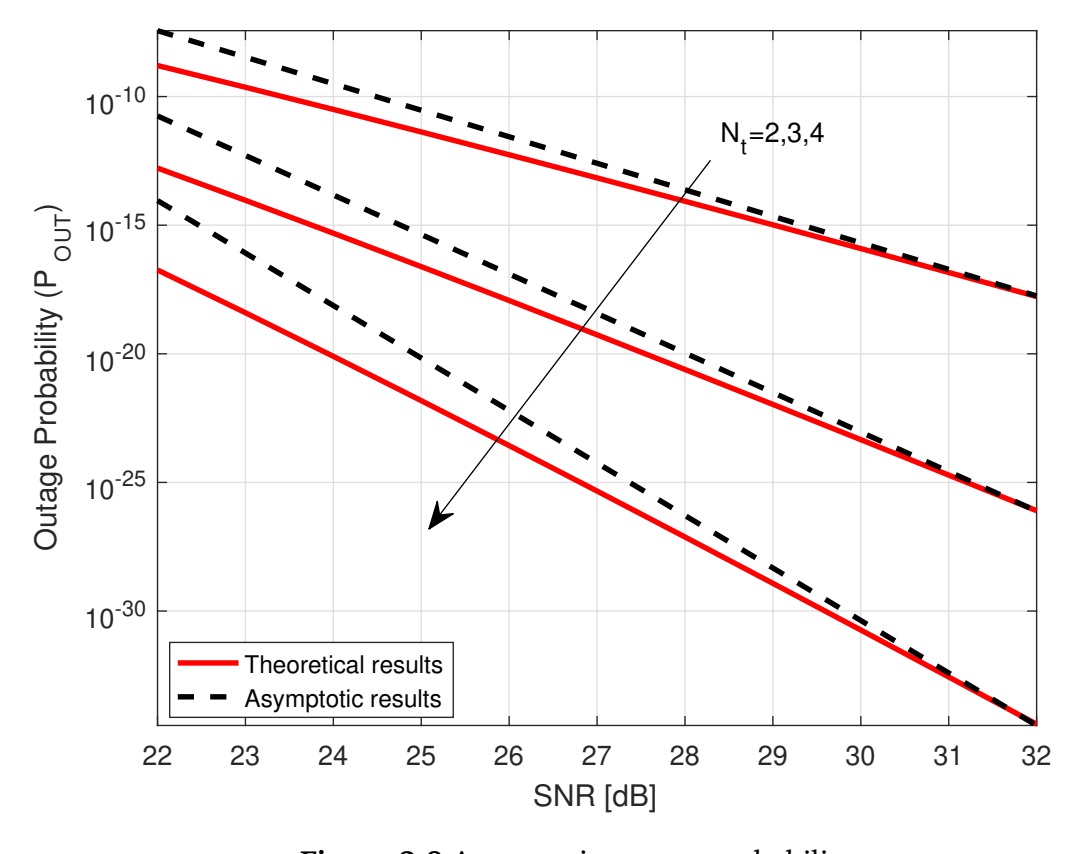


Figure 3.8 Asymptotic outage probability

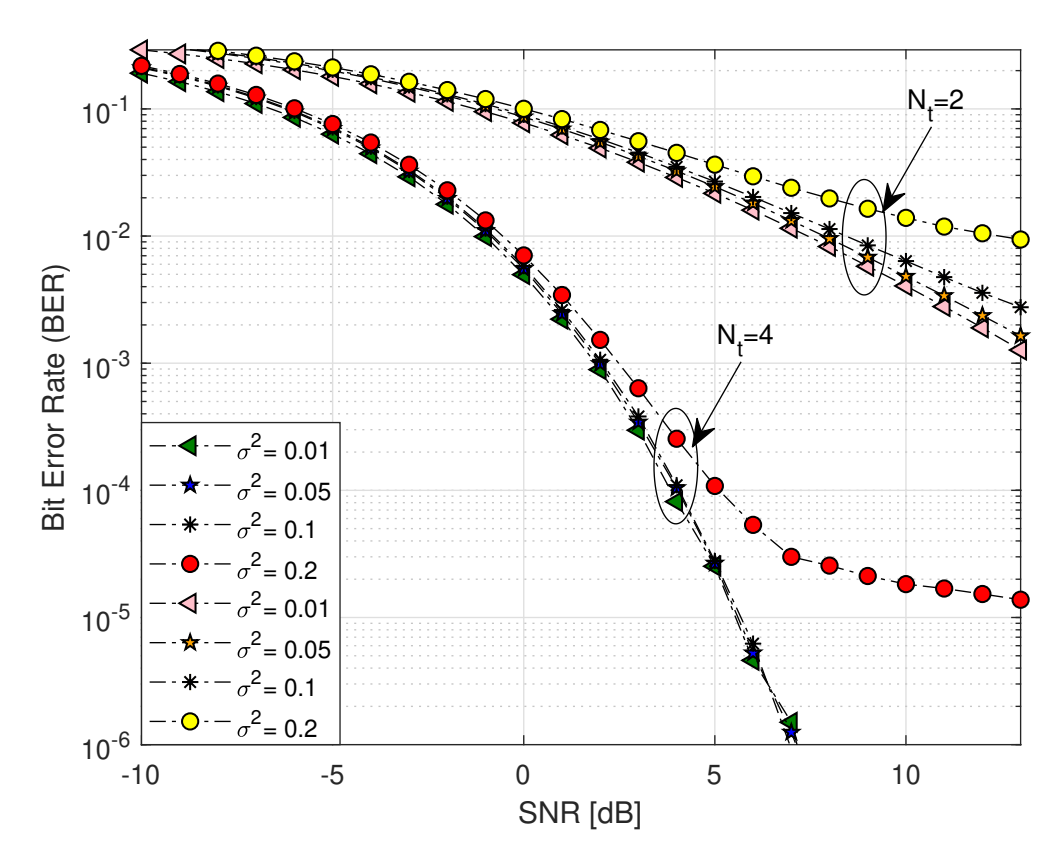


Figure 3.9 SER when imperfect channel estimation is used

SER curves in the presence of channel estimation errors are shown in Figure 3.9 for two different systems. The number of antennas, multipath fading and shadowing parameters for the first system are selected as  $N_t=2$ ,  $m_m=1$  and  $m_s=2$ , respectively and for second system, they are selected as  $N_t=4$ ,  $m_m=5$  and  $m_s=6$ , respectively. As can be seen, the increase of variance of CEE degrades the error performance. For the system with 4 antennas, while CEEs with variances 0.01, 0.05 and 0.1 do not have almost any considerable impact on SER while increasing the variance to 0.2 causes a significant error floor approximately at SER=2 × 10<sup>-6</sup>. On the other hand, CEE variance larger than 0.01 can easily impact SER of the system with 2 antennas. Our results indicate that as the number of antennas increases, the variance value affecting SER increases as well which indicates that MRT transmission with higher diversity can make the receiver more robust that can be preferable by low complexity IoT devices.

## 3.5 Chapter Summary

In this chapter, approximate PDF and CDF of SNR for MRT over  $K_G$  channels, SER, OP, channel capacity are obtained analytically which are validated by simulation results. Furthermore, by deriving asymptotic expressions, diversity and coding are provided.

Performance results are observed to be robust even if imperfect channel estimation is used. Numerical examples demonstrate that the desirable performance increase achieved by low complexity MRT over  $K_G$  channels as the number of transmit antennas increases while the receiver complexity is kept the same, makes it a desirable candidate for vehicular, drone and cellular communication systems. Our theoretical findings can be useful for getting further insight about multiple antenna transmissions exposed to both shadowing and fading distortions.

## 4

# PERFORMANCE ANALYSIS OF DOWNLINK-NOMA OVER GENERALIZED-K FADING CHANNELS

#### 4.1 Introduction

Performance analysis of NOMA based systems has been increasing in the literature. For example, the OP of downlink-NOMA with fixed power allocation over Nakagami-m fading channels is studied in [98], and Choi et al. [99] deal with the OP of NOMA over block fading channels. Similarly, Arzykulov et al. [100] explore the OP of a downlink DF cooperative underlay cognitive radio NOMA transmission over Rayleigh fading channels. Ding et al. [101] evaluate the OP and ergodic sum-rate of downlink-NOMA over Rayleigh fading. SER and BER for downlink-NOMA with two users over Rayleigh fading channels are obtained in [102] and [103], respectively. Furthermore, Sashiganth et al. [104] analyze the BER of a full-duplex relaying with NOMA in both downlink and uplink over Nakagami-m fading channels. Can et al. provide the union bound on BER for a downlink-NOMA with DF relaying over Rayleigh fading channel where media based modulation is used [105]. Yu et al. [106] investigate block error rate over Rayleigh-fading channel to obtain optimum block length for short-packet communication. Most of the previous NOMA studies considered Rayleigh or Nakagami fading models with only two users for mathematical simplicity. Obviously, research on emerging NOMA systems over more realistic channel models is essential to get better insights about their practical performance.

The performance of NOMA over  $K_G$  fading channels has not been studied in the literature. In this chapter, the reliability of downlink-NOMA transmission in the presence of arbitrary number of users over  $K_G$  channels is investigated by studying OP, AVC and SER expressions. The contributions can be listed as follows:

- PDF of signal-to-interference-plus-noise ratio (SINR) coefficients are obtained.
- Outage Probability is explored by deriving the CDF of SINR.

- Average channel capacity is also provided by using the PDF of SINR.
- Symbol error rate is found by using the PDF of SINR.
- Diversity and coding gains are derived from both asymptotic OP and SER expressions.
- OP, AVC and SER are also obtained by using mixture-gamma function based SINR
   PDF to provide alternative expressions.
- Novel diversity and coding gains are derived for OMA system over  $K_G$  channel and compared with NOMA performance.
- Theoretical findings are verified by numerical examples.

The rest of the chapter is organized as follows. In Section 2, the system model and the PDF of SINR for downlink-NOMA over  $K_G$  channel are provided. In Section 3, OP, AVC, and SER are derived. Simulation results are discussed in Section 4 and finally, Section 5 concludes the chapter.

## 4.2 System Description

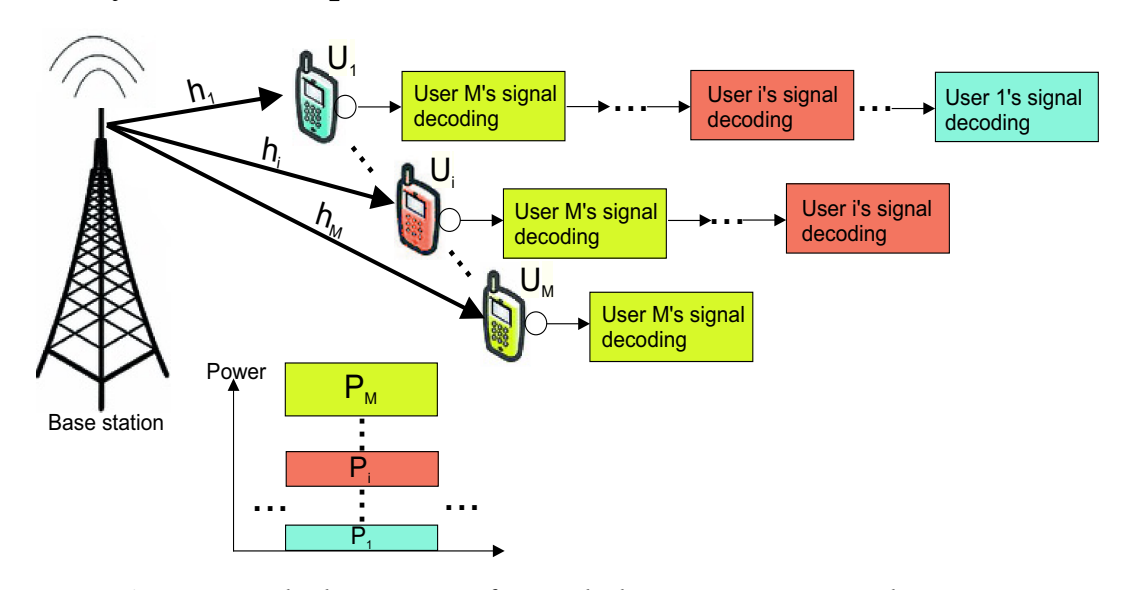


Figure 4.1 Block Diagram of Downlink-NOMA System with M Users

The block diagram of the considered system model which consists of a single BS and M users with the distances  $d_M > d_M - 1 \cdots d_i \cdots > d_2 > d_1$ , is shown in Figure 4.1. The BS transmits the superposition of all user signals in the same resource blocks (time slot and frequency band). Each user has to decode the stronger signals first in order to get its signal after removing their interference via SIC. The total transmit power at

the BS is assumed to be  $P_T$ . The power allocated to the user i is shown by  $P_i$  below which is directly proportional to the square of its distance from BS,

$$P_i = P_T \frac{(d_i)^2}{D},$$
 (4.1)

where  $d_i$  is the distance of *i*-th user from BS and  $D = [(d_1)^2 + (d_2)^2 + \cdots + (d_M)^2]$  is the summation of squares of all distances. The received signal for *j*-th user can be written as,

$$y_{j} = \frac{h_{j}}{d_{j}} \sum_{i=1}^{M} \sqrt{P_{i}} x_{i} + n_{j}, \tag{4.2}$$

where transmitted signal for user i is shown by  $x_i$ .  $n_j$  denotes zero mean White Gaussian noise sample at j-th user.  $h_j$  denotes complex channel coefficient for the j-th user and its magnitude  $\alpha$  has  $K_G$  distribution (2.11). Instantaneous SINR at the j-th user is given as below [107, Eq. 3],

$$\gamma_{j} = \frac{P_{j}(\frac{\alpha_{j}}{d_{j}})^{2}}{N_{0} + \sum_{i=1}^{j-1} P_{i}(\frac{\alpha_{j}}{d_{j}})^{2}} = \frac{P_{j}}{\frac{N_{0}(d_{j})^{2}}{(\alpha_{j})^{2}} + \sum_{i=1}^{j-1} P_{i}},$$
(4.3)

where  $P_j$  is the allocated power to targeted j-th user and  $\sum_{i=1}^{j-1} P_i$  is the allocated total power to users having less power than j-th user. For the sake of simplicity, variables are changed as  $P_j = \kappa$ ,  $N_0(d_j)^2 = \delta$  and  $\sum_{i=1}^{j-1} P_i = \rho$  where  $d_j \ge d_{j-1} \cdots \ge d_2 \ge d_1$ , thus SINR becomes,

$$\gamma_j = \frac{\kappa}{\frac{\delta}{(\alpha_i)^2} + \rho}.\tag{4.4}$$

Note that channel power  $(\alpha_j)^2 = \lambda_j$  has GG distribution in (2.11). Appendix C shows the derivation of the PDF of SINR  $\gamma_j$  in (4.4) and it is found as,

$$f_{\gamma}(\gamma) = \begin{cases} \frac{2\kappa \delta \Xi^{\frac{m_s + m_m}{2}}}{\Gamma(m_s)\Gamma(m_m)(\kappa - \gamma \rho)^2} \left(\frac{\delta \gamma}{\kappa - \gamma \rho}\right)^{\frac{m_s + m_m - 2}{2}} \times \\ K_{m_s - m_m} \left(2\sqrt{\frac{\delta \gamma}{\kappa - \gamma \rho}}\Xi\right), & 0 \le \gamma \le \frac{\kappa}{\rho}. \\ 0, & \text{otherwise.} \end{cases}$$

$$(4.5)$$

## 4.3 Performance Analysis

In this section, firstly, the OP is studied by finding the CDF from the derived PDF in (4.5), and then its asymptotic behavior is explored. Secondly, AVC is found by averaging the capacity over the SINR distribution. Finally, the SER of the system and its asymptotic behavior are analyzed to obtain diversity and coding gains.

## 4.3.1 Outage Probability

In order to obtain this CDF, the PDF in (4.5) can be integrated,

$$F_{\gamma}(\gamma) = \int_{\tau=0}^{\gamma} f_{\gamma}(\tau) d_{\tau} = \frac{2\Xi^{\frac{m_{s}+m_{m}}{2}}}{\Gamma(m_{s})\Gamma(m_{m})} \times \int_{\tau=0}^{\gamma} \frac{\kappa \delta}{(\kappa - \tau \rho)^{2}} \left(\frac{\delta \tau}{\kappa - \tau \rho}\right)^{\frac{m_{s}+m_{m}-2}{2}} K_{m_{s}-m_{m}} \left(2\sqrt{\frac{\delta \tau}{\kappa - \tau \rho}}\Xi\right) d_{\tau}.$$

$$(4.6)$$

Then, the change of variable  $x = \frac{\delta \tau}{\kappa - \tau \rho}$  is applied with  $dx = \frac{\kappa \delta}{(\kappa - \tau \rho)^2} d_{\tau}$ ,

$$F_{\gamma}(\gamma) = \frac{2\Xi^{\frac{m_s + m_m}{2}}}{\Gamma(m_s)\Gamma(m_m)} \int_{x=0}^{\frac{\delta\gamma}{\kappa - \gamma\rho}} x^{\frac{m_s + m_m - 2}{2}} K_{m_s - m_m} \left(2\sqrt{x\Xi}\right) dx. \tag{4.7}$$

This integration can be put into the following form after simple manipulations,

$$F_{\gamma}(\gamma) = \frac{2\Xi}{\Gamma(m_s)\Gamma(m_m)2^{m_s+m_m-2}} \times \int_{x=0}^{\frac{\delta\gamma}{\kappa-\gamma\rho}} \left(2\sqrt{x\Xi}\right)^{m_s+m_m-2} K_{m_s-m_m} \left(2\sqrt{x\Xi}\right) dx.$$

$$(4.8)$$

The term  $\left(2\sqrt{x\Xi}\right)^{m_s+m_m-2} K_{m_s-m_m}\left(2\sqrt{x\Xi}\right)$  in (4.8) can be written in terms of Meijer's G-function [92, Section 2.6], and then (4.8) becomes,

$$F_{\gamma}(\gamma) = \frac{\Xi}{\Gamma(m_s)\Gamma(m_m)} \int_{x=0}^{\frac{\delta\gamma}{\kappa-\gamma\rho}} G_{0,2}^{2,0} \left(x\Xi\Big|_{m_s-1, m_m-1}\right) dx, \tag{4.9}$$

Indefinite integral of Meijer's G-function in [93] and definite integral of Meijer's

G-function in (4.9) are of the same form. Hence, integral of Meijer's G-function in (4.9) is written below,

$$\int_{x=0}^{\frac{\delta \gamma}{\kappa - \gamma \rho}} G_{0,2}^{2,0} \left( x \Xi \bigg|_{m_s - 1, m_m - 1} \right) dx = G_{1,3}^{2,1} \left[ \Xi \left( \frac{\delta \gamma}{\kappa - \gamma \rho} \right) \bigg|_{m_s, m_m, 0}^{1,} \right]. \tag{4.10}$$

As a result, the CDF of SINR (i.e. OP) is found as,

$$F_{\gamma}(\gamma) = \begin{cases} 0, & \gamma < 0. \\ \frac{\Xi}{\Gamma(m_s)\Gamma(m_m)} G_{1,3}^{2,1} \left[ \Xi \left( \frac{\delta \gamma}{\kappa - \gamma \rho} \right) \Big|_{m_s, m_m, 0}^{1,} \right], & 0 \le \gamma \le \frac{\kappa}{\rho}. \\ 1, & \frac{\kappa}{\rho} < \gamma. \end{cases}$$
(4.11)

The distribution functions in (4.5) and (4.11) can be used to obtain performance metrics in the sequel.

In order to derive outage diversity and outage coding gains, the instantaneous SINR at the receiver can be written as  $\gamma = \beta \Omega_0$  where  $\Omega_0$  is given by  $\mathbb{E}[\gamma] = \Omega_0 = E_s/N_0$  and  $\mathbb{E}[\beta] = \tau = 1$ . To find  $\alpha$  and t in (2.17), OP can be written as follows by using (4.8),

$$F_{\gamma}(\gamma_{th}) = \int_{\beta=0}^{\frac{\delta \gamma_{th}}{\kappa - \gamma_{th} \rho}} f(\beta) d\beta. \tag{4.12}$$

By noting that the only difference between OP in [76, Eq. 17] and OP in (4.12) is at the upper limits of the integrals, one can get,

$$f(\beta) = \frac{2\Psi}{\Gamma(m_m)\Gamma(m_s)2^{m_s+m_m-2}} \times \left(2\sqrt{\beta\Psi}\right)^{m_s+m_m-2} K_{m_s-m_m} \left[2\sqrt{\beta\Psi}\right], \qquad \beta > 0$$

$$(4.13)$$

where  $\Psi = \frac{m_s m_m}{\tau} = m_s m_m$  due to  $\tau = 1$ . By using the PDF in (4.13), derivations of a

and t are presented in Appendix D,

$$t = \frac{1}{2} \left( m_s + m_m - \frac{5}{2} \right), \tag{4.14}$$

$$a = \frac{(\sqrt{m_s m_m})^{(m_s + m_m - \frac{1}{2})} \pi^{\frac{1}{2}}}{\Gamma(m_m) \Gamma(m_s)}.$$
 (4.15)

As shown in [76], when the average SINR is large enough, the asymptotic OP can be evaluated as,

$$F_{\gamma}(\gamma_{th}) = \frac{a}{t+1} \left(\frac{\frac{\delta \gamma_{th}}{\kappa - \rho \gamma_{th}}}{\Omega_0}\right)^{t+1} + o\left(\Omega_0^{-(t+1)}\right). \tag{4.16}$$

Thus, while average SINR approaches to infinity  $(\Omega_0 \longrightarrow \infty)$ , the term  $o(\Omega_0^{-(t+1)})$  can be omitted, and  $F_{\gamma}(\gamma_{th})$  can be written as,

$$F_{\gamma}(\gamma_{th}) \approx \frac{a}{t+1} \left(\frac{\frac{\delta \gamma_{th}}{\kappa - \rho \gamma_{th}}}{\Omega_0}\right)^{t+1} \approx (O_c \Omega_0)^{-O_d},$$
 (4.17)

where  $O_d = t+1$  is outage diversity and  $O_c = \frac{1}{\frac{\delta \gamma_{th}}{\kappa - \rho \gamma_{th}}} \left(\frac{a}{t+1}\right)^{-\frac{1}{t+1}}$  is outage coding gain. When a and t are substituted into  $O_d$  and  $O_c$ , they can be shown as,

$$O_d = \frac{1}{2} \left( m_s + m_m - \frac{5}{2} \right) + 1 = \frac{1}{2} \left( m_s + m_m - \frac{1}{2} \right), \tag{4.18}$$

$$O_{c} = \frac{\kappa - \rho \gamma_{th}}{\delta \gamma_{th}} \left[ \frac{(\sqrt{m_{s} m_{m}})^{(m_{s} + m_{m} - \frac{1}{2})} \pi^{\frac{1}{2}}}{\frac{1}{2} (m_{s} + m_{m} - \frac{1}{2}) \Gamma(m_{s}) \Gamma(m_{m})} \right]^{-\frac{1}{\frac{1}{2} (m_{s} + m_{m} - \frac{1}{2})}}.$$
 (4.19)

It can be easily observed from (4.18) and (4.19) that while  $O_d$  depends only on multipath fading and shadowing parameters  $(m_m, m_s)$ ,  $O_c$  depends also on allocated power and distances of users as well as  $m_m$  and  $m_s$ .

## 4.3.2 Average Channel Capacity

Substituting (4.5) into (2.15) results in,

$$\bar{C} = \frac{2W}{\Gamma(m_s)\Gamma(m_m)ln(2)} \times 
\int_{\gamma=0}^{\frac{\kappa}{\rho}} ln(1+\gamma) \frac{\kappa \delta \Xi}{(\kappa-\gamma\rho)^2} \left(\frac{\delta \Xi \gamma}{\kappa-\gamma\rho}\right)^{\frac{m_s+m_m-2}{2}} K_{m_s-m_m} \left(2\sqrt{\frac{\delta \Xi \gamma}{\kappa-\gamma\rho}}\right) d\gamma.$$
(4.20)

When variables are changed as  $x = \frac{\delta \Xi \gamma}{\kappa - \gamma \rho}$ ,  $dx = \frac{\delta \kappa \Xi}{(\kappa - \gamma \rho)^2} d_{\gamma}$ . The new parameters are substituted in (4.20) and after some simple mathematical manipulations, it becomes,

$$\bar{C} = \frac{2W}{\Gamma(m_s)\Gamma(m_m)\ln(2)2^{m_s+m_m-2}} \times \int_{x=0}^{\infty} \ln\left(\frac{x(\rho+\kappa)+\delta\Xi}{x\rho+\delta\Xi}\right) (2\sqrt{x})^{m_s+m_m-2} K_{m_s-m_m}(2\sqrt{x}) dx.$$
(4.21)

The term  $(2\sqrt{x})^{m_s+m_m-2}K_{m_s-m_m}(2\sqrt{x})$  in (4.21) can be expressed in terms of Meijer's G-function [92, Section 2.6], and thus AVC becomes,

$$\bar{C} = \frac{W}{\Gamma(m_s)\Gamma(m_m)ln(2)} \times \int_{x=0}^{\infty} ln \left(\frac{x(\rho+\kappa)+\delta\Xi}{x\rho+\delta\Xi}\right) G_{0,2}^{2,0} \left(x\Big|_{m_s-1, m_m-1}\right) dx.$$
(4.22)

Applying integration by parts and changing variables as  $u=ln\Big(\frac{x(\rho+\kappa)+\delta\Xi}{x\rho+\delta\Xi}\Big)$  and  $d\nu=G_{0,2}^{2,0}\Big(x\bigg|_{m_s-1,\ m_m-1}\Big)dx$  with  $du=\Big(\frac{1}{x+\frac{\delta\Xi}{\kappa+\rho}}-\frac{1}{x+\frac{\delta\Xi}{\rho}}\Big)dx,\ \nu=G_{1,3}^{2,1}\Big[x\bigg|_{m_s-m_s=0}^{1,1}\Big] \text{ according to [93], one can obtain the }$ 

following equation,

$$\int_{x=0}^{\infty} ln \left( \frac{x(\rho + \kappa) + \delta \Xi}{x\rho + \delta \Xi} \right) G_{0,2}^{2,0} \left( x \Big|_{m_s - 1, m_m - 1} \right) dx = [uv]_{x=0}^{\infty} - \int_{x=0}^{\infty} v du$$

$$= \left[ ln \left( \frac{x(\rho + \kappa) + \delta \Xi}{x\rho + \delta \Xi} \right) G_{1,3}^{2,1} \left[ x \Big|_{m_s, m_m, 0}^{1,} \right] \right]_{x=0}^{\infty}$$

$$- \int_{x=0}^{\infty} G_{1,3}^{2,1} \left[ x \Big|_{m_s, m_m, 0}^{1,} \right] \left( \frac{1}{x + \frac{\delta \Xi}{\kappa + \rho}} - \frac{1}{x + \frac{\delta \Xi}{\rho}} \right) dx,$$
(4.23)

where  $[uv]_{x=0}^{\infty} = ln\left(1+\frac{\kappa}{\rho}\right)G_{1,3}^{2,1}\left[\infty\Big|_{m_s, m_m, 0}^{1,}\right]$  and the term  $G_{1,3}^{2,1}\left[\infty\Big|_{m_s, m_m, 0}^{1,}\right]$  converges to zero when variable x goes to infinity. Therefore,  $[uv]_{x=0}^{\infty} = ln\left(1+\frac{\kappa}{\rho}\right)G_{1,3}^{2,1}\left[\infty\Big|_{m_s, m_m, 0}^{1,}\right] = 0$ . Another change of variables as  $\beta_1 = \frac{\delta\Xi}{\kappa+\rho}$ ,  $\beta_2 = \frac{\delta\Xi}{\rho}$  can be helpful in simplification as follows,

$$\int_{x=0}^{\infty} v du = \int_{x=0}^{\infty} \frac{1}{x + \beta_1} G_{1,3}^{2,1} \left[ x \Big|_{m_s, m_m, 0}^{1,} \right] dx 
- \int_{x=0}^{\infty} \frac{1}{x + \beta_2} G_{1,3}^{2,1} \left[ x \Big|_{m_s, m_m, 0}^{1,} \right] dx.$$
(4.24)

When  $\rho$ ,  $\sigma$ ,  $\alpha$  in [65, Eq. 7.811/5] are selected as  $\rho = 1$ ,  $\sigma = 1$  and  $\alpha = 1$ , then the integral in (4.24) becomes,

$$\int_{r=0}^{\infty} v du = G_{2,4}^{3,2} \left[ \frac{\delta \Xi}{\rho + \kappa} \Big|_{0, m_{0}, m_{0}=0}^{0, 1} \right] - G_{2,4}^{3,2} \left[ \frac{\delta \Xi}{\rho} \Big|_{0, m_{0}, m_{0}=0}^{0, 1} \right]. \tag{4.25}$$

When the derived results for  $[uv]_{x=0}^{\infty}$  and  $\int_{x=0}^{\infty} v du$  are substituted in (4.22), AVC can be written as,

$$\bar{C} = \frac{W}{\Gamma(m_s)\Gamma(m_m)ln(2)} \times \left( G_{2,4}^{3,2} \left[ \frac{\delta \Xi}{\rho} \right]_{0, m_s, m_m, 0}^{0, 1} \right] - G_{2,4}^{3,2} \left[ \frac{\delta \Xi}{\rho + \kappa} \right]_{0, m_s, m_m, 0}^{0, 1} \right] \right).$$
(4.26)

#### 4.3.3 Asymptotic AVC

When asymptotic AVC based on [108, Eq. 1] is computed, it is derived as follows since  $\beta_1 = 0$  in (4.24),

$$\bar{C} = \frac{W}{\Gamma(m_s)\Gamma(m_m)ln(2)} \left( G_{2,4}^{3,2} \left[ \frac{\delta \Xi}{\rho} \right]_{0, m_s, m_m, 0}^{0, 1} \right) \right). \tag{4.27}$$

#### 4.3.4 Symbol Error Rate

When integration by parts is applied to (2.16) by changing variables as  $u = erfc(\sqrt{B\gamma})$ ,  $dv = f_{\gamma}(\gamma)d\gamma$ ,  $du = -\frac{\sqrt{B}e^{-B\gamma}}{\sqrt{\gamma\pi}}d\gamma$ ,  $v = F_{\gamma}(\gamma)$ , and then one can obtain,

$$\begin{split} \bar{P}_{se} &= \left[ uv \right]_{\gamma=0}^{\frac{\kappa}{\rho}} - \int_{\gamma=0}^{\frac{\kappa}{\rho}} v du \\ &= A \left( \left[ erfc(\sqrt{B\gamma}) F_{\gamma}(\gamma) \right]_{\gamma=0}^{\frac{\kappa}{\rho}} - \int_{\gamma=0}^{\frac{\kappa}{\rho}} F_{\gamma}(\gamma) \left( -\frac{\sqrt{B}e^{-B\gamma}}{\sqrt{\gamma\pi}} \right) d\gamma \right), \end{split} \tag{4.28}$$

where  $[uv]_{\gamma=0}^{\frac{\kappa}{\rho}}=[erfc(\sqrt{B\gamma})F_{\gamma}(\gamma)]_{\gamma=0}^{\frac{\kappa}{\rho}}=erfc\bigg(\sqrt{\frac{B\kappa}{\rho}}\bigg)$ . Due to  $F_{\gamma}(\gamma)=1$  for  $F_{\gamma}(\gamma)\geq\frac{\kappa}{\rho}$ , the integral in (4.28) can be divided into two parts as follows,

$$\int_{\gamma=0}^{\frac{\kappa}{\rho}} F_{\gamma}(\gamma) \left( -\frac{\sqrt{B}e^{-B\gamma}}{\sqrt{\gamma\pi}} \right) d\gamma 
= \int_{\gamma=0}^{\infty} F_{\gamma}(\gamma) \left( -\frac{\sqrt{B}e^{-B\gamma}}{\sqrt{\gamma\pi}} \right) d\gamma - \int_{\gamma=\frac{\kappa}{\rho}}^{\infty} \left( -\frac{\sqrt{B}e^{-B\gamma}}{\sqrt{\gamma\pi}} \right) d\gamma.$$
(4.29)

Substituting  $erfc\left(\sqrt{\frac{B\kappa}{\rho}}\right)$  and (4.29) into (4.28), average SER is obtained as,

$$\begin{split} \bar{P}_{se} &= A \bigg[ erfc \bigg( \sqrt{\frac{B\kappa}{\rho}} \bigg) + \int_{\gamma=0}^{\infty} F_{\gamma}(\gamma) \bigg( \frac{\sqrt{B}e^{-B\gamma}}{\sqrt{\gamma\pi}} \bigg) d\gamma - erfc \bigg( \sqrt{\frac{B\kappa}{\rho}} \bigg) \bigg] \\ &= A \int_{\gamma=0}^{\infty} F_{\gamma}(\gamma) \bigg( \frac{\sqrt{B}e^{-B\gamma}}{\sqrt{\gamma\pi}} \bigg) d\gamma. \end{split} \tag{4.30}$$

It can be further simplified as follows when (4.11) is substituted into (4.30),

$$\bar{P}_{se} = \frac{A\sqrt{B}\Xi}{\Gamma(m_s)\Gamma(m_m)\sqrt{\pi}} \times \int_{\gamma=0}^{\infty} \gamma^{-\frac{1}{2}} e^{-B\gamma} G_{1,3}^{2,1} \left[\Xi\left(\frac{\delta\gamma}{\kappa - \gamma\rho}\right)\Big|_{m_s, m_m, 0}^{1,}\right] d\gamma.$$
(4.31)

Changing of variable  $\vartheta = B\gamma$  results in

$$\bar{P}_{se} = \frac{A\Xi}{\Gamma(m_s)\Gamma(m_m)\sqrt{\pi}} \times \int_{\vartheta=0}^{\infty} \vartheta^{-\frac{1}{2}} e^{-\vartheta} G_{1,3}^{2,1} \left[ \Xi \left( \frac{\delta \vartheta}{B\kappa - \vartheta \rho} \right) \Big|_{m_s, m_m, 0}^{1,} \right] d\vartheta, \tag{4.32}$$

which allows us to use Gauss-Hermite quadrature formula in [109],

$$\int_{x=0}^{\infty} x^{-\frac{1}{2}} e^{-x} f(x) dx = \sum_{k=1}^{\iota} H_k f(a_k) + E_{\iota}, \tag{4.33}$$

where  $a_k$  is the k-th zero of the Laguerre polynomial  $L_i^{\beta}(x)$ ,  $H_k$  represents the weight coefficients and  $E_i$  is the truncation error. When the normalization of Laguerre polynomials is chosen as,

$$L_{\iota}^{\beta}(x) = \sum_{\nu=0}^{\iota} {\binom{\iota+\nu}{\iota-\nu}} \frac{(-x)^{\nu}}{\nu!},$$
(4.34)

then the weight coefficients are given by,

$$H_k = \frac{\Gamma(\iota + \beta + 1)}{\iota! a_k \left[\frac{d}{dx} L_\iota^\beta(a_k)\right]^2},\tag{4.35}$$

and the truncation error by,

$$E_{\iota} = \frac{\iota!\Gamma(\iota + \beta + 1)}{(2\iota)!} f(2\iota)(\xi). \tag{4.36}$$

The term  $f(a_k)$  in (4.33) corresponds to  $G_{1,3}^{2,1} \left[ \mathcal{E} \left( \frac{\delta a_k}{B \kappa - a_k \rho} \right) \Big|_{m_{*,*}}^{1,*} \right]$  in (4.32). Thus,

SER can be found as,

$$\bar{P}_{se} \sim \frac{A\Xi}{\Gamma(m_s)\Gamma(m_m)\sqrt{\pi}} \times \left( \sum_{k=1}^{\iota} H_k G_{1,3}^{2,1} \left[ \Xi \left( \frac{\delta a_k}{B\kappa - a_k \rho} \right) \right|_{m_s, m_m, 0}^{1,} \right] + E_{\iota} \right).$$
(4.37)

In [109, Table II], values for  $a_k$  and  $H_k$  are given depending on  $\iota$ .

## 4.3.5 Diversity and Coding Gains

In order to find diversity and coding gains from the SER expression, it can be written as follows after (4.5) is substituted into (2.16) by taking  $\Omega_0 = 1$ ,

$$\bar{P}_{se} = \int_{\gamma=0}^{\frac{\kappa}{\rho}} Q(\sqrt{B\gamma}) \frac{2\kappa \delta \Psi^{\frac{m_s + m_m}{2}}}{\Gamma(m_s)\Gamma(m_m)(\kappa - \gamma \rho)^2} \left(\frac{\delta \gamma}{\kappa - \gamma \rho}\right)^{\frac{m_s + m_m - 2}{2}} \times K_{m_s - m_m} \left(2\sqrt{\frac{\delta \gamma}{\kappa - \gamma \rho}}\Psi\right) d\gamma.$$
(4.38)

By changing variable as  $\beta = \frac{\delta \gamma}{\kappa - \gamma \rho}$ , and  $d\beta = \frac{\delta \kappa}{(\kappa - \gamma \rho)^2} d\gamma$ , SER is simplified as,

$$\bar{P}_{se} = \int_{\beta=0}^{\infty} Q\left(\sqrt{B\frac{\beta\kappa}{\delta + \beta\rho}\Omega_0}\right) f(\beta) d\beta. \tag{4.39}$$

Considering high SINR in (4.39) and using [76, Eq. 4a], asymptotic SER can be obtained as follows,

$$P_{E} = \frac{2^{t} a \Gamma(t + \frac{3}{2})}{\sqrt{\pi}(t+1)} \left( B \frac{\kappa}{\delta + \rho} \Omega_{0} \right)^{-(t+1)} + o(\Omega_{0}^{-(t+1)}), \tag{4.40}$$

where the term  $o\left(\Omega_0^{-(t+1)}\right)$  becomes negligible when the average SINR approaches to infinity  $(\Omega_0 \longrightarrow \infty)$ , and thus asymptotic SER,  $P_E$  can be approximated as,

$$P_{E} \approx \frac{2^{t} a \Gamma(t + \frac{3}{2})}{\sqrt{\pi}(t+1)} \left( B \frac{\kappa}{\delta + \rho} \Omega_{0} \right)^{-(t+1)}. \tag{4.41}$$

The diversity gain is  $G_d = t+1$  which is the same as  $O_d$  in (4.18) and the coding gain is  $G_c = \frac{B\kappa}{\delta + \rho} \left( \frac{2^t a \Gamma(t + \frac{3}{2})}{\sqrt{\pi}(t+1)} \right)^{-\frac{1}{t+1}}$ . When a in (4.14) and t in (4.15) are used,  $G_c$  is found as,

$$G_{c} = \left(\frac{B\kappa}{\delta + \rho}\right) \left[\frac{2^{\frac{1}{2}(m_{s} + m_{m} - \frac{5}{2})}\Gamma(\frac{1}{2}[m_{s} + m_{m} + \frac{1}{2}])}{\frac{1}{2}(m_{s} + m_{m} - \frac{1}{2})\Gamma(m_{s})\Gamma(m_{m})} \times \left(\sqrt{m_{s}m_{m}}\right)^{(m_{s} + m_{m} - \frac{1}{2})}\right]^{-\frac{1}{\frac{1}{2}(m_{s} + m_{m} - \frac{1}{2})}}.$$

$$(4.42)$$

(4.42) shows that  $G_c$  depends on multipath fading and shadowing parameters  $(m_m, m_s)$ , allocated powers and distances of users.

## 4.3.6 Performance Analysis of Downlink-NOMA over $K_G$ Fading Channels Using Mixture-Gamma Function

Atapattu *et al.* [110] prove that most PDFs such as RL and NL, K,  $K_G$  and so on can be written in terms of mixture gamma (MG) function to facilitate easier numerical computations. In order to obtain alternative forms for performance results, (4.5) can be written in terms of MG function [110, Eq. 8] as follows,

$$f_{\gamma}(\gamma) = \begin{cases} \frac{\kappa \delta}{(\kappa - \gamma \rho)^2} \sum_{i=1}^{N} \eta_i \left( \frac{\delta \gamma}{\kappa - \gamma \rho} \right)^{\epsilon_i - 1} \times \\ e^{-\varphi_i \frac{\delta \gamma}{\kappa - \gamma \rho}}, & 0 \le \gamma \le \frac{\kappa}{\rho}. \\ 0, & \text{otherwise.} \end{cases}$$
(4.43)

In order to obtain OP, AVC, and SER by using MG, change of variables can be applied by using  $x = \frac{\delta \gamma}{\kappa - \gamma \rho}$ ,  $dx = (\frac{\delta \gamma}{\kappa - \gamma \rho})^2 d\gamma$  in (4.43) and then substituted into (2.12), (2.15) and (2.16). For example, CDF of SINR can be written from (2.12) as

$$F_{\gamma}(\gamma) = \begin{cases} 0, & \gamma < 0. \\ \sum_{i=1}^{N} \eta_{i} \left(\frac{1}{\varphi_{i}}\right)^{\epsilon_{i}} \left[\Gamma(\epsilon_{i}) - \Gamma(\epsilon_{i}, \frac{\delta \gamma \varphi_{i}}{\kappa - \gamma \rho})\right], & 0 \leq \gamma \leq \frac{\kappa}{\rho}. \\ 1, & \frac{\kappa}{\rho} < \gamma. \end{cases}$$
(4.44)

Similarly, when (4.43) is substituted into (2.15), AVC becomes

$$\bar{C} = \frac{W}{\ln(2)} \sum_{i=1}^{N} \eta_i \left[ \int_{x=0}^{\infty} x^{\epsilon_i - 1} e^{-\varphi_i x} \ln\left(1 + \frac{x\kappa}{\delta + x\rho}\right) dx \right]. \tag{4.45}$$

By changing variable  $t = \varphi_i x$  and using  $dt = \varphi_i dx$ , (4.45) is transformed as follows,

$$\bar{C} = \frac{W}{\ln(2)} \sum_{i=1}^{N} \eta_i \left(\frac{1}{\varphi_i}\right)^{\epsilon_i} \left[ \int_{t=0}^{\infty} t^{\epsilon_i - 1} e^{-t} \ln\left(1 + \frac{t\kappa}{\delta \varphi_i + t\rho}\right) dt \right]. \tag{4.46}$$

Integral in (4.46) is the same form of Gauss-Laguerre quadrature [109] where  $f(a_k) = ln\left(1 + \frac{t\kappa}{\delta\varphi_i + x\rho}\right)$ . Hence, AVC can be obtained as,

$$\bar{C} = \frac{W}{\ln(2)} \sum_{i=1}^{N} \eta_i \left(\frac{1}{\varphi_i}\right)^{\epsilon_i} \left[\sum_{k=1}^{\iota} H_k \ln\left(1 + \frac{a_k \kappa}{\delta \varphi_i + a_k \rho}\right) + E_{\iota}\right]. \tag{4.47}$$

When (4.44) is substituted into (4.30), SER becomes,

$$\bar{P}_{se} = A \sqrt{\frac{B}{\pi}} \left[ \sum_{i=1}^{N} \eta_i \left( \frac{1}{\varphi_i} \right)^{\epsilon_i} \times \left( \Gamma(\epsilon_i) \int_{x=0}^{\infty} x^{-\frac{1}{2}} e^{-Bx} dx - \int_{x=0}^{\infty} x^{-\frac{1}{2}} e^{-Bx} \Gamma\left(\epsilon_i, \frac{x \delta \varphi_i}{\kappa - x \rho}\right) dx \right) \right].$$
(4.48)

With the change of variable t = Bx and using dt = Bdx, (4.48) can be written in the following form

$$\bar{P}_{se} = \frac{A}{\sqrt{\pi}} \left[ \sum_{i=1}^{N} \eta_i \left( \frac{1}{\varphi_i} \right)^{\epsilon_i} \times \left( \Gamma(\epsilon_i) \int_{t=0}^{\infty} t^{-\frac{1}{2}} e^{-t} dt - \int_{t=0}^{\infty} t^{-\frac{1}{2}} e^{-t} \Gamma\left( \epsilon_i, \frac{t \delta \varphi_i}{B \kappa - r \rho} \right) dr \right) \right],$$
(4.49)

where  $\int_{t=0}^{\infty} t^{-\frac{1}{2}} e^{-t} dt = \sqrt{\pi}$ . Then it can be substituted into (4.49) to find SER as,

$$\bar{P}_{se} = A \left( \sum_{i=1}^{N} \eta_{i} \left( \frac{1}{\varphi_{i}} \right)^{\epsilon_{i}} \Gamma(\epsilon_{i}) - \frac{1}{\sqrt{\pi}} \sum_{i=1}^{N} \eta_{i} \left( \frac{1}{\varphi_{i}} \right)^{\epsilon_{i}} \left( \int_{t=0}^{\infty} t^{-\frac{1}{2}} e^{-t} \Gamma\left(\epsilon_{i}, \frac{t \delta \varphi_{i}}{B \kappa - t \rho}\right) dt \right) \right).$$
(4.50)

Integral in (4.50) is the same form in (4.33) where  $f(a_k) = \Gamma\left(\epsilon_i, \frac{t\delta\varphi_i}{B\kappa - t\rho}\right)$ , and then Gauss-Hermite quadrature is substituted into (4.50), thus SER can be obtained as,

$$\bar{P}_{se} = A \left( \sum_{i=1}^{N} \eta_{i} \left( \frac{1}{\varphi_{i}} \right)^{\epsilon_{i}} \Gamma(\epsilon_{i}) - \frac{1}{\sqrt{\pi}} \sum_{i=1}^{N} \eta_{i} \left( \frac{1}{\varphi_{i}} \right)^{\epsilon_{i}} \left[ \sum_{k=1}^{l} H_{k} \Gamma\left( \epsilon_{i}, \frac{x \delta \varphi_{i}}{B \kappa - x \rho} \right) + E_{\iota} \right] \right).$$
(4.51)

The above results can be used as an alternative forms to get insight about the considered system. It is evident from [110] that although using MG function in PDF results in more theoretically tractable performance expressions for OMA, it provides lengthy expressions especially for AVC and SER in downlink-NOMA system.

## 4.3.7 Performance of OMA over Generalized-K Fading Channels

OP, AVC, and BER for OMA systems over  $K_G$  channels are derived in [64, Eqs 3, 7, 8], however, asymptotic OP and BER are not available in the literature. In order to compare performances of NOMA and OMA at high SNRs, one can find the asymptotic OP for OMA as,

$$F_{\lambda}(\lambda_{th}) = \frac{a}{t+1} \left(\frac{\lambda_{th}}{\Omega_0}\right)^{t+1} + o\left(\Omega_0^{-(t+1)}\right),\tag{4.52}$$

where outage coding gain is  $O_c = \frac{1}{\lambda_{th}} \left(\frac{a}{t+1}\right)^{-\frac{1}{t+1}}$  [76] although  $O_d$  is the same as that one in (4.18). When t in (4.14) and a in (4.15) are substituted into  $O_c$ , it becomes

$$O_{c} = \frac{1}{\lambda_{th}} \left[ \frac{\pi^{\frac{1}{2}} (\sqrt{m_{s} m_{m}})^{(m_{s} + m_{m} - \frac{1}{2})}}{\frac{1}{2} (m_{s} + m_{m} - \frac{1}{2}) \Gamma(m_{s}) \Gamma(m_{m})} \right]^{-\frac{1}{\frac{1}{2} (m_{s} + m_{m} - \frac{1}{2})}}.$$
 (4.53)

Note that the only difference between (4.53) and (4.19) is the term  $\frac{\kappa - \rho \gamma_{th}}{\delta}$ .

In order to find diversity and coding gains for OMA, asymptotic SER at high SNR can be approximated as in [76],

$$P_E \approx \frac{2^t a \Gamma(t + \frac{3}{2})}{\sqrt{\pi}(t+1)} (B\Omega_0)^{-(t+1)},$$
 (4.54)

where the coding gain is written as  $G_c = B\left(\frac{2^t a \Gamma(t+\frac{3}{2})}{\sqrt{\pi}(t+1)}\right)^{-\frac{1}{t+1}}$ , and the diversity gain becomes  $G_d = t+1$  which is same as  $O_d$  in (4.18). When t in (4.14) and a in (4.15) are substituted into  $G_c$ , it can be obtained as,

$$G_{c} = B \left[ \frac{2^{\frac{1}{2}(m_{s}+m_{m}-\frac{5}{2})} \Gamma(\frac{1}{2}[m_{s}+m_{m}+\frac{1}{2}])}{\frac{1}{2}(m_{s}+m_{m}-\frac{1}{2})\Gamma(m_{s})\Gamma(m_{m})} \times \left( \sqrt{m_{s}m_{m}} \right)^{(m_{s}+m_{m}-\frac{1}{2})} \right]^{-\frac{1}{2}(m_{s}+m_{m}-\frac{1}{2})},$$

$$(4.55)$$

where the only difference between (4.42) and (4.55) is the term  $\frac{\kappa}{\delta m_s m_m + \rho}$ .

## 4.4 Simulation Results

In this section, numerical results for OP, SER, AVC are illustrated for several shadowing and multipath parameters where the NOMA system consists of up to five users whose distances from the BS are selected as 4, 16, 64, 256, and 1024. At least  $10^6$  BPSK symbols and channel coefficients are randomly generated for each simulation curve where  $m_m$  and  $m_s$  parameters for  $K_G$  coefficients are selected as 5 and 6, respectively unless otherwise stated. Although simulation and analytical results of all users are obtained in each system, only the performance of the first user is plotted to present clearly and the performance of other users are almost the same due to power allocation based on distances. In the figures, dashed lines and markers represent simulation and analytical results of users and the dotted lines represent asymptotic results.

In Figure 4.2 and Figure 4.3, analytical PDF and CDF expressions are compared with simulations in order to check their validity. In Figure 4.2 blue bars represent the histogram values and the red line represents the theoretical PDF in (4.5). Likewise, in Figure 4.3 the red line with the left-pointing triangle represents the simulated CDF, and the dashed red line with the pentagram represents the theoretical CDF result in

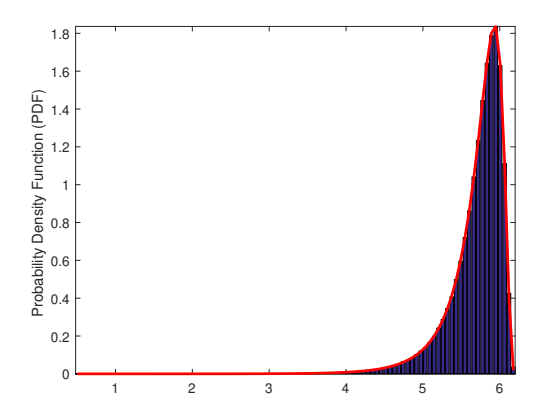


**Figure 4.2** Histogram and theoretical PDF of SINR of downlink-NOMA over  $K_G$  channel

**Figure 4.3** CDF of SINR for downlink-NOMA over  $K_G$  channel from simulation and derivation

(4.11). As can be observed from Figure 4.2 and Figure 4.3, theoretical and simulation results perfectly match.

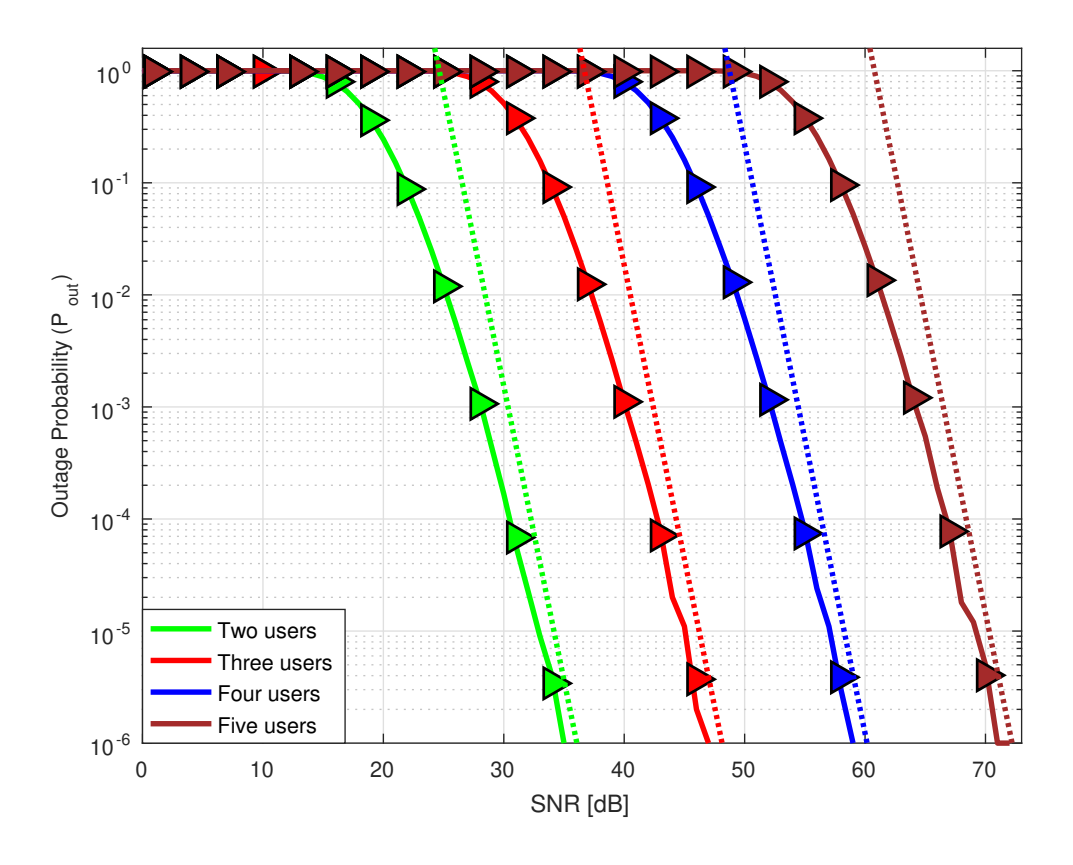
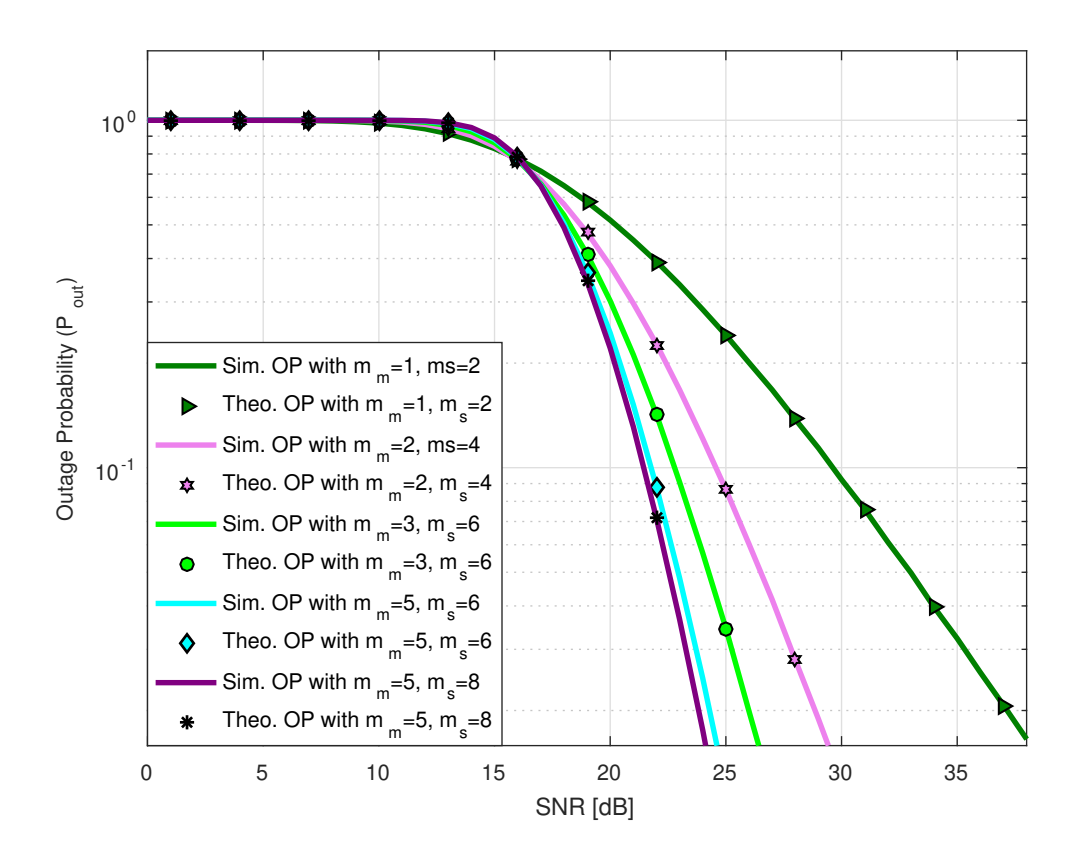


Figure 4.4 OPs of first users in all systems

Figure 4.4 shows the OP performance of NOMA systems with the different number of users where theoretical and asymptotic results are based on expressions (4.11) and (4.17). The SINR threshold is selected as 0.2 dB. At each system, all users

have the same OP thus only a single marker is used as simulation results overlap. It demonstrates that downlink-NOMA have perfect fairness in the network. As the number of users increases in the system, the OP of the same user also increases. It is expected because as the number of users increases allocated power to the same user decreases. Users in all systems reach to  $10^{-6}$  OP value at 33 dB, 45 dB, 57 dB, 69 dB, respectively. Furthermore, as expected, asymptotic results converge simulation and analytical ones at high SINR values. The slopes of asymptotic lines validate theoretically obtained  $O_d$  values in (4.18) and  $O_d$ 's of all users are equal.



**Figure 4.5** OPs of first user in system with two users for different multipath and shadowing parameters

In Figure 4.5, OPs results are depicted for several  $m_m$  and  $m_s$  values. Analytical and simulation results match perfectly in each case. OP values for  $m_m = 1$ ,  $m_s = 2$ ;  $m_m = 2$ ,  $m_s = 4$ ;  $m_m = 3$ ,  $m_s = 6$ ;  $m_m = 5$ ,  $m_s = 6$ ; and  $m_m = 5$ ,  $m_s = 8$  cases are  $39.19 \times 10^{-2}$ ,  $22.6 \times 10^{-2}$ ,  $14.2 \times 10^{-2}$ ,  $8.81 \times 10^{-2}$ , and  $7.14 \times 10^{-2}$  at SINR 22 dB, respectively. As can be seen from figure, when  $m_m$  or  $m_s$  increases (i.e. Random distortion of the channel decreases), OP decreases. On the other hand, it can be concluded that as values  $m_m$  and  $m_s$  increase, decrease in OP diminishes.

The AVC curves are depicted in Figure 4.6 where theoretical results are obtained from the expression (4.26) with W=1. AVC values of all systems with two, three, four,

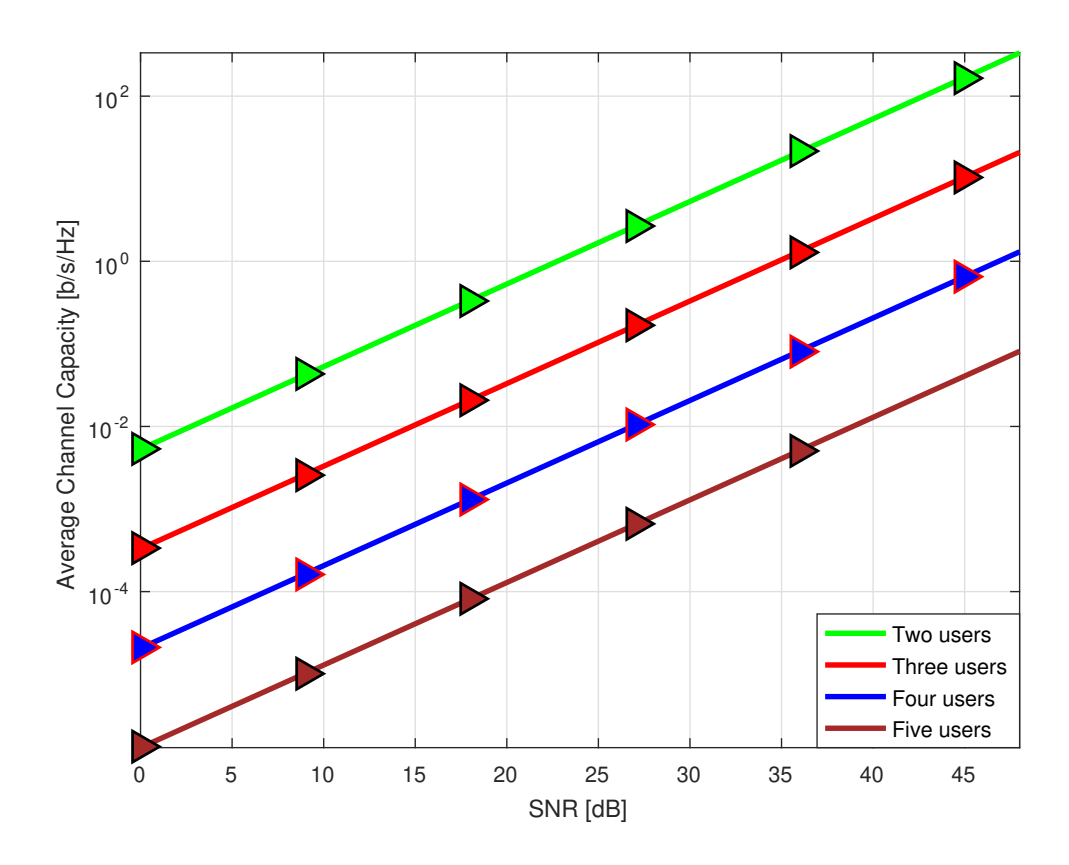


Figure 4.6 AVCs of first users in all systems

five users are equal and their simulation and theoretical results match perfectly. As can be observed, when the number of users increases in a downlink-NOMA system, the AVC of each user decreases as the allocated power is reduced. AVC values at SINR 18 dB are  $3,35\times10^{-1}$ ,  $2.1\times10^{-2}$ ,  $1.3\times10^{-3}$ , and  $8\times10^{-5}$  b/s/Hz for two, three, four and five user systems, respectively. Although not shown, simulation and theoretical results for other  $m_m$  and  $m_s$  values also match perfectly. Unlike OP results, it is found that changing channel parameters do not create significant difference in AVC.

In Figure 4.7, AVC results in NOMA system with three users are depicted. Asymptotic result is plotted based on (4.27). According to [108, Figure 1], the power offset corresponding to an isotropic input is the distance between the origin and the point where the value of asymptotic AVC is zero. Therefore, the power offset for the considered NOMA system is 87 dB and the high-SNR slope is found as 0.83.

SER performance of NOMA systems with different number of users are illustrated in Figure 4.8. Theoretical and asymptotic results are plotted according to (4.37) and (4.41), respectively. As can be seen, the theoretical and simulation results of each user match perfectly. SER of all users are approximately same and SER increases when the number of users are increased since allocated power becomes lower. Users

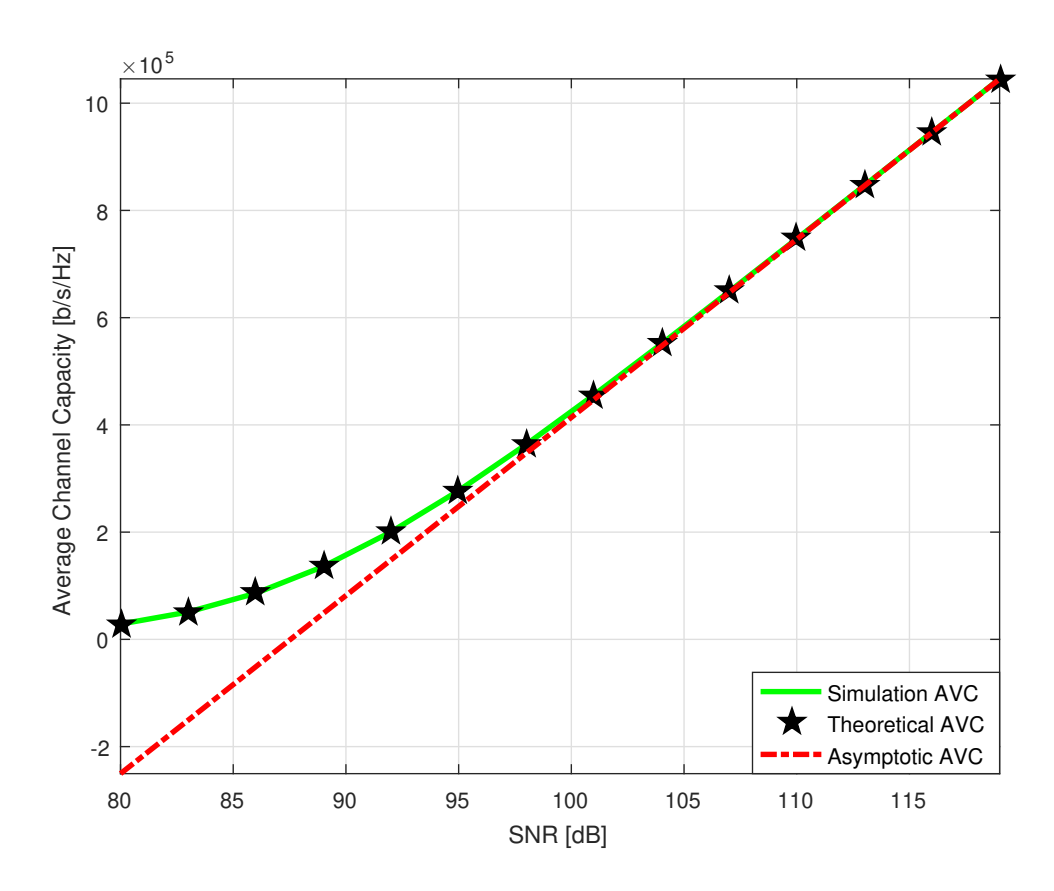


Figure 4.7 AVC of first user in system with three users

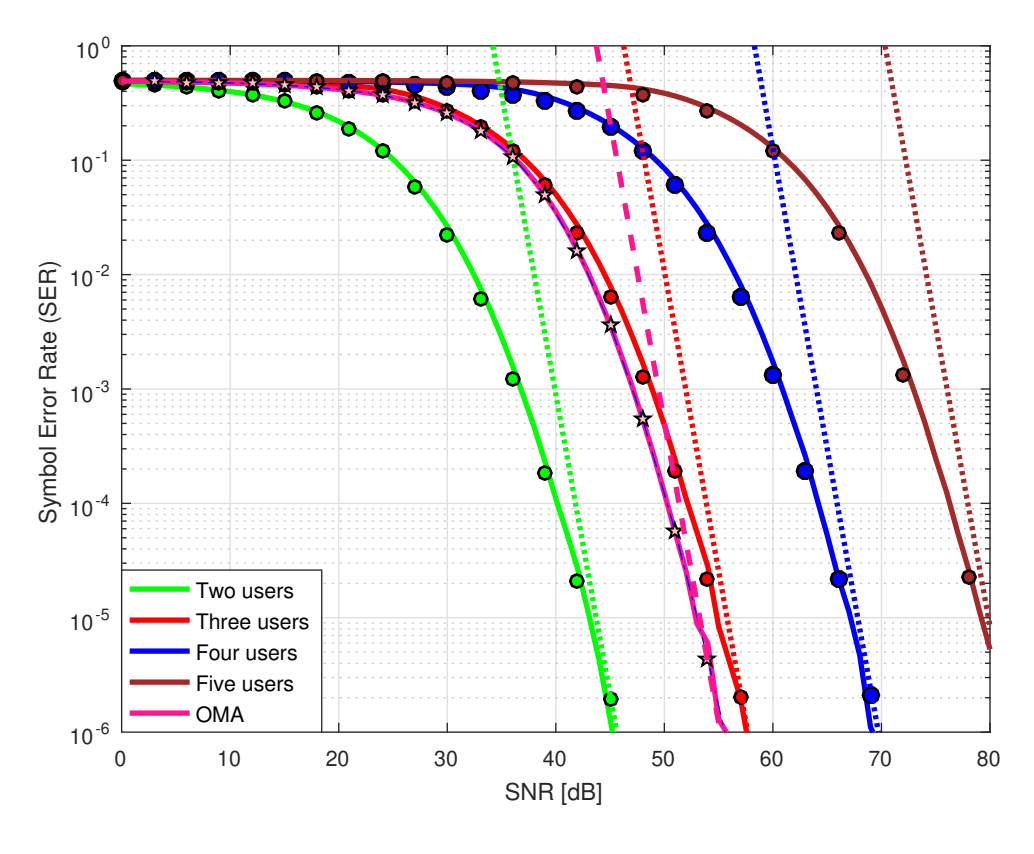
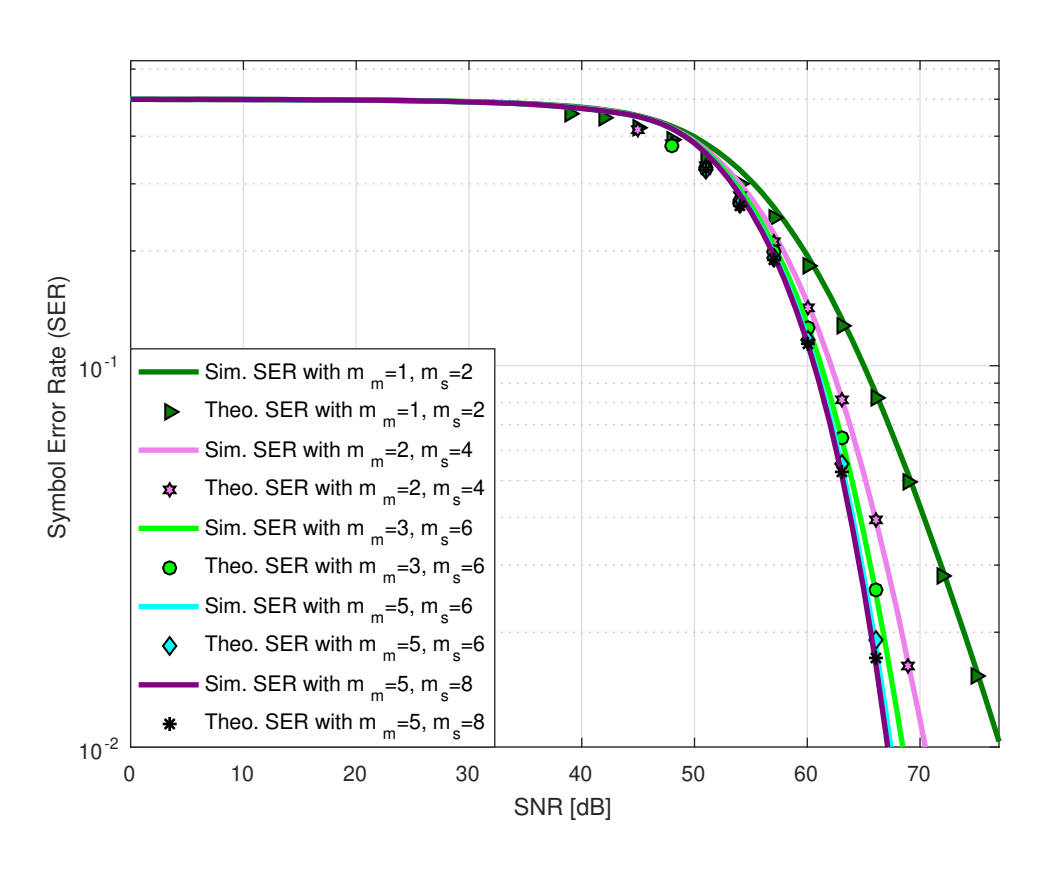


Figure 4.8 SERs of first users in all systems

in all systems reach SER=10<sup>-5</sup> at SINRs 41 dB, 53 dB, 65 dB and 77 dB, respectively. Moreover, SER result for only a single user OMA system is also illustrated in order to compare it with NOMA. Its distance from BS is selected as equal to that of the third user (i.e. 64). Theoretical and asymptotic results are plotted according to [64, Eq 8] and (4.54), respectively. As can be seen, OMA SER performance is slightly better than that of NOMA as expected. For example, an OMA user has SER=10<sup>-5</sup> at SNR 53 dB while NOMA user needs SNR 55 dB. Furthermore, one can observe that asymptotic results approach analytical SERs at high SINR values and the slopes of the curves validate theoretical diversity gains in (4.18).



**Figure 4.9** SERs of first user in system with five users for different multipath and shadowing parameters

In Figure 4.9, simulations and analytical SER results are given for different  $m_s$  and  $m_m$  values. Analytical and simulation results match perfectly in each case. SER values for  $m_m = 1$ ,  $m_s = 2$ ;  $m_m = 2$ ,  $m_s = 4$ ;  $m_m = 3$ ,  $m_s = 6$ ;  $m_m = 5$ ,  $m_s = 6$ ; and  $m_m = 5$ ,  $m_s = 8$  cases are  $1.8 \times 10^{-1}$ ,  $1.4 \times 10^{-1}$ ,  $1.3 \times 10^{-3}$ ,  $1.2 \times 10^{-1}$ , and  $1.1 \times 10^{-1}$  at SINR 60 dB, respectively. As can be observed from the figure, when  $m_m$  or  $m_s$  increases, SER decreases. Similar to OP results, as  $m_m$  or  $m_s$  increases, decrease of SER is reduced.

Figure 4.10 shows the SER of the signals for three users computed at the first user (U1). As aforementioned, any user receives signals of all users in a downlink-NOMA system,

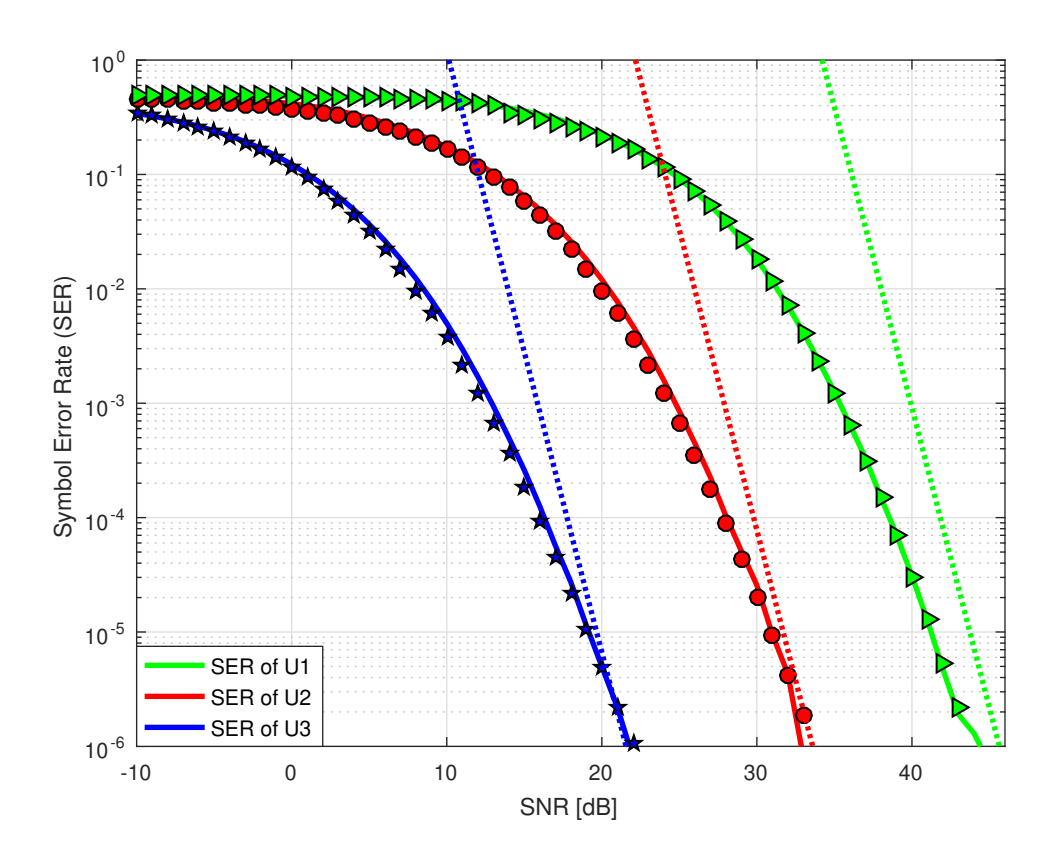


Figure 4.10 SERs of all users in the nearest user.

and at each user, signals of farther users are stronger. Theoretical and asymptotic results are plotted based on (4.37) and (4.41), respectively. SER values of U1, U2, U3 users are  $3.8 \times 10^{-1}$ ,  $5.3 \times 10^{-2}$  and  $2.9 \times 10^{-6}$ , respectively at SINR=19 dB. Obviously, near users get the signals of farther users with higher reliability although they do not need it. However, this observation motivates the use of cooperative communication in a NOMA system. In addition, it also shows the necessity of physical layer security in a IoT system since an eavesdropper close to BS can easily capture all of the user signals.

## 4.5 Chapter Summary

In this chapter, PDF and CDF of SINR, OP, AVC and SER of users for a downlink-NOMA transmission over  $K_G$  fading channels are analytically derived and validated by simulations for several channel parameters with different number of users. The outage diversity and coding gains are also obtained by deriving asymptotic expressions and verified by the slopes of asymptotic OP and SER curves. Performance analysis is made by using MG function over  $K_G$  channel. However, by theoretical analysis made by using MG function for downlink-NOMA, it is demonstrated that MG function does not provide much more simplest. This study can be helpful in getting insights about the performance of NOMA systems in vehicular communications, IoT, and sensor networks

when the shadowing impact is not negligible. Furthermore, our findings demonstrate that downlink-NOMA systems provide perfect fairness in the network regardless of the number of users and the system can highly benefit from the use of cooperative/relay transmissions significantly since users decode the signals of far users with lower errors.

### 5

# PERFORMANCE ANALYSIS OF NOMA UPLINK OVER GENERALIZED-K FADING CHANNELS

#### 5.1 Introduction

In the literature, the studies on the performance of uplink-NOMA systems have been increasing since asynchronous transmissions from mobile stations with limited power are becoming popular especially with the advance of IoT and sensor networks. For example, Khan et al. [111] study optimization of power allocation of uplink-NOMA over Nakagami-m fading channels and show that it can outperform the conventional OMA in terms of sum-rate. Shen et al. [112] consider beamforming design for multi-cell MIMO uplink NOMA. Dai et al. [113] design a low-complexity multi-antenna system with a zero-forcing detector where users are divided into two groups based on their power levels and then they derive an average sum rate in Rayleigh fading channels. Sedaghat and Müller [114] investigate optimum user pairing in multiple uplink-NOMA scenarios. Seo et al. explore energy efficiency, throughput, and access delay for uplink-NOMA over Rayleigh fading channels in [115]. Xie et. al [116] investigate a cooperative uplink-NOMA system with a novel relay transmission scheme that receives the combined signal from two users, then transmits to the BS with amplify-and-forward transfer protocol. They evaluate the ergodic sum rate and OP of the considered system over Rayleigh fading channels. Wang et al. [117] derive the OP expression using dynamically ordered SIC over Rayleigh fading channels. Tegos et al. [118] deal with the OP of uplink NOMA for land mobile satellite communication with only two users. Tahir et. al [119] investigate the OP of an intelligent reflecting surface-assisted uplink-NOMA to boost the signal of one of the users over Nakagami-m fading channels. Singh and Bansal [120] derives an exact closed-form expression for the OP of a NOMA-based full-duplex decode-and-forward relay system. Xu et. al [121] analyze buffer-aided relay hybrid uplink-NOMA/OMA cooperative system with two users by deriving closed-form expressions of throughput, OP, average packet delay, and diversity gain for Rayleigh fading channels. Le et. al [122] address uplink-NOMA system over composite

fading channels by using mixture gamma distribution, and obtain expressions of delay-limited throughput, OP, and effective capacity with imperfect SIC stemming the presence of residual hardware impairments and delay constraints. Sharma et. al [123] derive secrecy OP of the uplink and downlink NOMA cooperative system. Rabee and Gitlin [124] present the BER simulation results for two users. Theoretical BER expression for QPSK signaling at an uplink NOMA system is obtained in [125] where two users employ a single-carrier frequency division multiplexing scheme at the transmitter. Obviously getting insights for NOMA uplink systems are useful before implementing them in practical scenarios. Bae et al [126] analyze uplink-NOMA-based IoT system utilizing a space time line code and a BPSK modulation and evaluate SER over complex Gaussian channels. As stated in the current literature, the SWIPT in NOMA systems can offer performance improvement in many aspects compared to OMA ones.

Although the impact of fading is mostly considered in NOMA studies, shadowing needs to be taken into account for a more realistic wireless system. On the other hand, there has been no research considering NOMA uplink transmission over  $K_G$  channels. With the motivation of exploring the performance of uplink NOMA schemes for an arbitrary number of users over composite  $K_G$  channels, OP, AVC, and SER are provided in this chapter. The contributions are listed as follows:

- The PDF of SINR is obtained.
- OP is derived by finding the CDF of SINR.
- Analytical expression for average channel capacity is provided.
- SER is found by using the PDF of SINR.
- Theoretical findings are verified via numerical examples.

This chapter is organized as follows. In Section 5.2, the system model and SINR for uplink-NOMA over the  $K_G$  channel are presented. In Section 5.3, performance metrics OP, AVC, SER are derived and then simulation results are discussed in Section 5.4. Finally, conclusions are presented in Section 5.5.

### 5.2 System Description

The block diagram of the considered system model is shown in Figure 5.1. All M users transmit their signals at equal power P in the same resource blocks to the BS

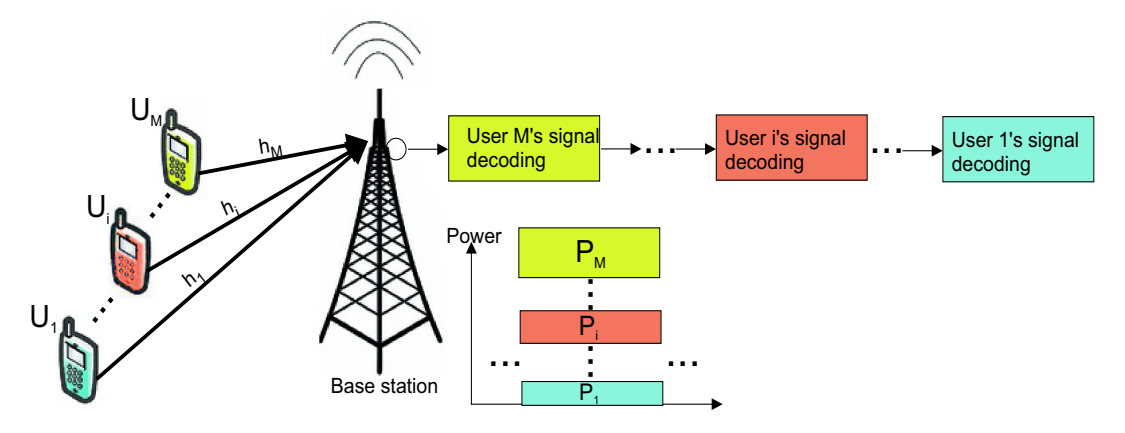


Figure 5.1 System Model

which decodes the user symbols with the stronger magnitude first before dealing with weaker signals. The received power of each user at the BS is inversely proportional to the square of the distance as shown below,

$$P_i = \frac{P}{(d_i)^2},\tag{5.1}$$

where  $d_i$  is the distance of *i*-th user to BS and  $d_M < d_{M-1} < ... < d_i < ... < d_1$ . The received signal at the BS can be written as,

$$y = \sum_{i=1}^{M} \sqrt{P} \frac{h_i}{d_i} x_i + n, \tag{5.2}$$

where  $h_i$  is the channel coefficient between i-th user and the BS,  $x_i$  is signal transmitted by i-th user, and n denotes white Gaussian noise with zero mean. Therefore, instantaneous SINR of j-th user can be written as,

$$\gamma_{j} = \frac{P \frac{|\mathbf{h}_{j}|^{2}}{(d_{j})^{2}}}{N_{0} + \sum_{i=1}^{j-1} P \frac{|\mathbf{h}_{i}|^{2}}{(d_{i})^{2}}} = \frac{P|\mathbf{g}_{j}|^{2}}{N_{0} + P \sum_{i=1}^{j-1} |\mathbf{g}_{i}|^{2}} = \frac{|\mathbf{g}_{j}|^{2}}{\frac{N_{0}}{P} + \sum_{i=1}^{j-1} |\mathbf{g}_{i}|^{2}}.$$
 (5.3)

where  $\mathbf{g}_j$ ,  $\mathbf{g}_i$  are channel gain coefficients of j-th and i-th users, respectively.  $N_0$  denotes the one sided power spectral density of white Gaussian noise. While  $|\mathbf{g}_j|^2$  is channel power between j-th user and the BS,  $\sum_{i=1}^{j-1} |\mathbf{g}_i|^2$  is total interference impact of users whose signals are weaker than j-th user. For the sake of simplicity, if variables are changed such that  $\frac{N_0}{P} = \kappa$ ,  $|\mathbf{g}_j|^2 = \alpha$  and  $\sum_{i=1}^{j-1} |\mathbf{g}_i|^2 = \beta$  are performed, (5.3) can

be transformed into the following form,

$$\gamma = \frac{\alpha}{\kappa + \beta},\tag{5.4}$$

In order to determine SER, AVC, OP, the PDF of  $\gamma$  in (5.4) needs to be derived. Therefore, PDFs of  $\beta$ ,  $\kappa + \beta$  and  $\frac{\alpha}{\kappa + \beta}$  have to be computed, respectively. In the considered system, it is assumed that all channels between each user and the BS has  $K_G$  distribution, thus  $|h_i|^2$  has GG distribution [61, Eq. 2] and it is given as,

$$f(|\boldsymbol{h}_{i}|^{2}) \stackrel{\triangle}{=} \frac{2(b_{i})^{m_{s}+m_{m}}}{\Gamma(m_{s})\Gamma(m_{m})} (|\boldsymbol{h}_{i}|^{2})^{\frac{m_{s}+m_{m}-2}{2}} K_{m_{s}-m_{m}} \left(2b_{i}\sqrt{|\boldsymbol{h}_{i}|^{2}}\right), \quad |\boldsymbol{h}_{i}|^{2} \ge 0$$
 (5.5)

where  $m_s>0$  and  $m_m\geq 0.5$  are shadowing and multipath fading parameters, respectively.  $b_i=\sqrt{\frac{m_sm_m}{\Omega_{0,i}}}$ ,  $\Omega_{0,i}$  is the mean of  $|\boldsymbol{h}_i|^2$  for channel coefficients between i-th user and the BS,  $K_{m_s-m_m}(.)$  is the modified Bessel function with order  $m_s-m_m$  and  $\Gamma(.)$  is Gamma function. There is any difference between  $f(|\boldsymbol{h}_i|^2)$  and  $f(|\boldsymbol{g}_i|^2)$  except their means. Because, when channel coefficients are divided to any number, the mean of their SNR is divided to the square of that number such that  $\mathbb{E}[|\boldsymbol{h}_i|^2]=\Omega_{0,i}$  and  $\mathbb{E}[|\boldsymbol{h}_i|^2]=\frac{\Omega_{0,i}}{(d_i)^2}=\mu_{0,i}$ . Although all SNR coefficients  $(|\boldsymbol{h}_i|^2)$  in (5.3) are independent and identically distributed (i.i.d.) random variables, channel gain coefficients  $(|\boldsymbol{g}_i|^2)$  in the same equation are i.n.i.d. ones. Because, their means are different in spite of their shadowing and multipath fading parameters are the same.

When multiple random variables are summed, their PDFs are convolved. Multiple vectors are convolved, their Laplace transforms are multiplied. Performing process over Laplace transforms of random variables, which are called MGFs, is preferred since the convolution process is more challenging. However, the MGF of a GG random variable is equal to the Whittaker function, and multiplications of Whittaker functions are not tractable. Therefore, approximated PDF is proposed [47, Eq. 9] to compute PDF of summation of multiple i.n.i.d GG random variables in (5.4),

$$f_{\beta}(\beta) = \frac{2(b_{\varsigma})^{m_{m,\varsigma}+m_{s,\varsigma}}}{\Gamma(m_{m,\varsigma})\Gamma(m_{s,\varsigma})} \beta^{(m_{m,\varsigma}+m_{s,\varsigma})/2-1} K_{m_{s,\varsigma}-m_{m,\varsigma}} (2b_{\varsigma}\sqrt{\beta}), \qquad \beta > 0, \quad (5.6)$$

where  $b_{\varsigma} = \sqrt{\frac{m_{s,\varsigma}m_{m,\varsigma}}{\mu_{0,s}}}$ ,  $\mu_{0,s} = \sum_{i=1}^{j-1} \mu_{0,i}$  is the mean of  $\beta$ .  $m_{s,\varsigma} = \frac{m_{m,\varsigma}}{a_{\varsigma}}$  and  $m_{s,\varsigma}$ ,  $m_{m,\varsigma}$  are fading parameters depending on  $m_m$  and  $m_s$ .  $m_{m,\varsigma}$  is computed by equating amount of fadings [47, Eqs. 12, 14] ( $AF_{\varsigma}$ ,  $AF_{sum,i.n.i.d}$ ) of N i.i.d GG random variables and N

i.n.i.d GG random variables,

$$m_{m,\varsigma} = \frac{(1+a_{\varsigma})(\mu_{0,s})^{2} + \mu_{0,s}\sqrt{(1+a_{\varsigma})^{2}(\mu_{0,s})^{2} + 4a_{\varsigma}\sum_{i=1}^{j-1}AF_{i}(\mu_{0,i})^{2}}}{2\sum_{i=1}^{j-1}AF_{i}(\mu_{0,i})^{2}}.$$
 (5.7)

where  $AF_i$  is amount fading of each GG random variable and it is assumed that  $a_{\varsigma} = 1$ . SINR PDF of any user in (5.2) is derived at Appendix E and it is as follows,

$$f_{\gamma}(\gamma) = \frac{1}{\Gamma(m_{s})\Gamma(m_{m})\Gamma(m_{m,\varsigma})\Gamma(m_{s,\varsigma})} \times \sum_{k=0}^{\infty} \frac{(-(b_{\alpha})^{2}\kappa)^{k}\gamma^{k-1}}{k!} G_{3,3}^{2,3} \left(\frac{(b_{\varsigma})^{2}}{(b_{\alpha})^{2}\gamma}\right|_{\{m_{s,\varsigma}, m_{m,\varsigma}\}, 1+k}^{\{1,1+k-m_{s},1+k-m_{m}\}, \{\}}$$
(5.8)

### 5.3 Performance Analysis

In this section, all derivations are performed according to M users. Firstly, the OP is obtained by finding the CDF from the derived PDF above. Secondly, AVC is obtained by averaging the capacity for a fixed SINR over the SINR distribution. Finally, the SER of the system is analyzed.

#### 5.3.1 Outage Probability

In order to find OP, CDF of SINR can be computed by integrating the PDF in (5.8),

$$F_{\gamma}(\gamma) = \int_{\tau=0}^{\gamma} f_{\tau}(\tau) d_{\tau} = \frac{1}{\Gamma(m_{s})\Gamma(m_{m})\Gamma(m_{m,\varsigma})\Gamma(m_{s,\varsigma})} \times \int_{\tau=0}^{\gamma} \sum_{k=0}^{\infty} \frac{(-(b_{\alpha})^{2}\kappa)^{k}\tau^{k-1}}{k!} G_{3,3}^{2,3} \left(\frac{(b_{\varsigma})^{2}}{(b_{\alpha})^{2}\tau}\Big|_{\{m_{s,\varsigma}, m_{m,\varsigma}\}, 1+k}^{\{1,1+k-m_{s},1+k-m_{m}\}, \{\}}\right) d_{\tau}.$$
(5.9)

The summation and integral in (5.9) can be replaced as below,

$$F_{\gamma}(\gamma) = \frac{1}{\Gamma(m_{s})\Gamma(m_{m})\Gamma(m_{m,\varsigma})\Gamma(m_{s,\varsigma})} \times \sum_{k=0}^{\infty} \frac{(-(b_{\alpha})^{2}\kappa)^{k}}{k!} \left[ \int_{\tau=0}^{\gamma} \tau^{k-1} G_{3,3}^{2,3} \left( \frac{(b_{\varsigma})^{2}}{(b_{\alpha})^{2}\tau} \Big|_{\{m_{s,\varsigma}, m_{m,\varsigma}\}, 1+k}^{\{1,1+k-m_{s},1+k-m_{m}\}, \{\}} \right) d_{\tau} \right].$$
 (5.10)

When change of variable with  $x=\frac{1}{\tau}$  is applied, then  $x=\tau^{-1} \implies \frac{d}{d\tau}x=\frac{d}{d\tau}\tau^{-1}$ ,  $dx=-\tau^{-2}d\tau$ . Furthermore,  $x=\tau^{-1} \implies \tau=x^{-1}$ . The integral in (5.10) must be firstly multiplied  $\frac{-\tau^{-2}}{-\tau^{-2}}$  term to enable  $dx=-\tau^{-2}d\tau$  condition.

$$\frac{-\tau^{-2}}{-\tau^{-2}} \int_{\tau=0}^{\gamma} \tau^{k-1} G_{3,3}^{2,3} \left( \frac{(b_{\varsigma})^{2}}{(b_{\alpha})^{2} \tau} \Big|_{\{m_{s,\varsigma}, m_{m,\varsigma}\}, 1+k}^{\{1,1+k-m_{s},1+k-m_{m}\}, \{\}} \right) d_{\tau}$$

$$= -\int_{\tau=0}^{\gamma} \tau^{k+1} G_{3,3}^{2,3} \left( \frac{(b_{\varsigma})^{2}}{(b_{\alpha})^{2} \tau} \Big|_{\{m_{s,\varsigma}, m_{m,\varsigma}\}, 1+k}^{\{1,1+k-m_{s},1+k-m_{m}\}, \{\}} \right) (-\tau^{-2} d_{\tau}), \tag{5.11}$$

when integral in (5.11) is rearranged according to above variables, integral in (5.10) becomes as,

$$\int_{\tau=0}^{\gamma} \tau^{k-1} G_{3,3}^{2,3} \left( \frac{(b_{\varsigma})^{2}}{(b_{\alpha})^{2} \tau} \Big|_{\{m_{s,\varsigma}, m_{m,\varsigma}\}, 1+k}^{\{1,1+k-m_{s},1+k-m_{m}\}, \{\}} \right) d_{\tau}$$

$$= \int_{x=\frac{1}{\gamma}}^{\infty} x^{-k-1} G_{3,3}^{2,3} \left( \frac{(b_{\varsigma})^{2}}{(b_{\alpha})^{2}} x \Big|_{\{m_{s,\varsigma}, m_{m,\varsigma}\}, 1+k}^{\{1,1+k-m_{s},1+k-m_{m}\}, \{\}} \right) dx. \tag{5.12}$$

The definite integral in (5.12) and indefinite integral [127] are of the same form. Parameters in these formulas are matched by selecting  $\alpha = -k$ ,  $w = \frac{(b_s)^2}{(b_a)^2}$ ,  $a_1 = 1$ ,  $a_2 = 1 + k - m_s$ ,  $a_3 = 1 + k - m_m$ ,  $b_1 = m_{s,\varsigma}$ ,  $b_2 = m_{m,\varsigma}$ ,  $b_3 = 1 + k$ . Accordingly, (5.12)

can be simplified as follows,

$$F_{\gamma}(\gamma) = \frac{1}{\Gamma(m_{s})\Gamma(m_{m})\Gamma(m_{m,\varsigma})\Gamma(m_{s,\varsigma})} \times \left[ G_{4,4}^{2,4} \left( \frac{(b_{\varsigma})^{2}}{(b_{\alpha})^{2}} \infty \Big|_{\{m_{s,\varsigma}, m_{m,\varsigma}\}, \{1, 0\}}^{\{1,1,1-m_{s},1-m_{m}\}, \{\}\}} \right) - G_{4,4}^{2,4} \left( \frac{(b_{\varsigma})^{2}}{(b_{\alpha})^{2}} \frac{1}{\gamma} \Big|_{\{m_{s,\varsigma}, m_{m,\varsigma}\}, \{1, 0\}}^{\{1,1,1-m_{s},1-m_{m}\}, \{\}\}} \right) \right] - \frac{1}{\Gamma(m_{s})\Gamma(m_{m})\Gamma(m_{m,\varsigma})\Gamma(m_{s,\varsigma})} \times \left[ \sum_{k=1}^{\infty} \frac{(-(b_{\alpha})^{2}\kappa)^{k}}{k!} \left[ \gamma^{k} G_{4,4}^{2,4} \left( \frac{(b_{\varsigma})^{2}}{(b_{\alpha})^{2}} \frac{1}{\gamma} \Big|_{\{m_{s,\varsigma}, m_{m,\varsigma}\}, \{1+k, k\}}^{\{1+k, 1, 1+k-m_{s}, 1+k-m_{m}\}, \{\}\}} \right) \right].$$

$$(5.13)$$

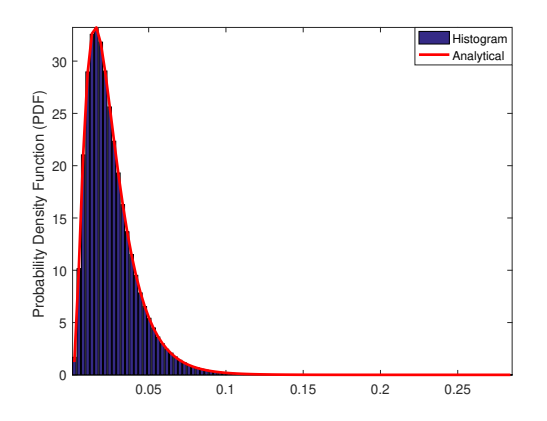
With the help of Matlab, the result of the following subtraction is determined as zero,

$$G_{4,4}^{2,4} \left( \frac{(b_{\varsigma})^2}{(b_{\alpha})^2} \infty \right|_{\{m_{s,\varsigma}, m_{m,\varsigma}\}, \{1, 0\}}^{\{1,1,1-m_{s},1-m_{m}\}, \{\}} - G_{4,4}^{2,4} \left( \frac{(b_{\varsigma})^2}{(b_{\alpha})^2} \frac{1}{\gamma} \right|_{\{m_{s,\varsigma}, m_{m,\varsigma}\}, \{1, 0\}}^{\{1,1,1-m_{s},1-m_{m}\}, \{\}} = 0$$
 (5.14)

Therefore, CDF of SINR in (5.9) is derived as follows,

$$F_{\gamma}(\gamma) = \frac{-1}{\Gamma(m_{s})\Gamma(m_{m})\Gamma(m_{m,\varsigma})\Gamma(m_{s,\varsigma})} \times \sum_{k=1}^{\infty} \frac{(-(b_{\alpha})^{2}\kappa)^{k}}{k!} \gamma^{k} G_{4,4}^{2,4} \left(\frac{(b_{\varsigma})^{2}}{(b_{\alpha})^{2}} \frac{1}{\gamma} \Big|_{\{m_{s,\varsigma}, m_{m,\varsigma}\}, \{1+k, k\}}^{\{1+k, 1, 1+k-m_{s}, 1+k-m_{m}\}, \{\}\}}\right).$$
(5.15)

In Figure 5.2 and Figure 5.3, analytical PDF and CDF expressions are compared with simulations in order to check their validity. In Figure 5.2 blue bars represent the histogram values and red lines represent approximate PDF. As can be observed, theoretical and simulation results perfectly match, thus the above distribution functions can be used to obtain performance metrics.



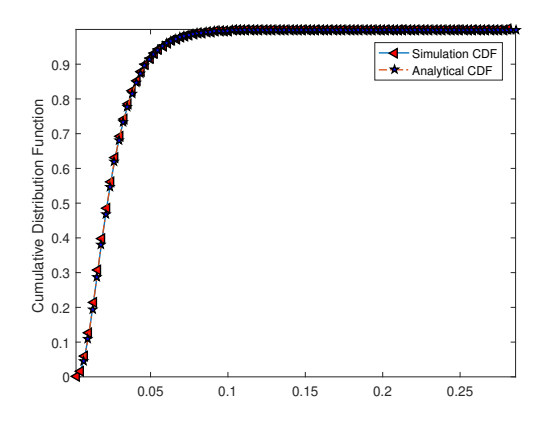


**Figure 5.2** Simulation and Theoretic PDF of SNR of Downlink-NOMA over  $K_G$  channel

Figure 5.3 Simulation and Theoretic CDFs of SNR of Downlink-NOMA over  $K_G$  channel

#### 5.3.2 Average Channel Capacity

By substituting (5.8) into (2.15),

$$\bar{C} = \frac{W}{\Gamma(m_{s})\Gamma(m_{m})\Gamma(m_{m,\varsigma})\Gamma(m_{s,\varsigma})ln(2)} \sum_{k=0}^{\infty} \frac{(-(b_{\alpha})^{2}\kappa)^{k}}{k!} \times \left[ \int_{\gamma=0}^{\infty} ln(1+\gamma)\gamma^{k-1} G_{3,3}^{2,3} \left( \frac{(b_{\varsigma})^{2}}{(b_{\alpha})^{2}\gamma} \Big|_{\{m_{s,\varsigma}, m_{m,\varsigma}\}, 1+k}^{\{1,1+k-m_{s},1+k-m_{m}\}, \{\}} \right) d\gamma \right].$$
(5.16)

Change of variables can be applied such that  $x = \frac{1}{\gamma}$ , then  $dx = -\gamma^{-2}d\gamma$  and  $\gamma = x^{-1}$ . Before all new values are substituted in integral (5.16), it is multiplied  $\frac{-\gamma^{-2}}{-\gamma^{-2}}$  as follows to provide equality  $dx = -\gamma^{-2}d\gamma$ ,

$$\frac{-\gamma^{-2}}{-\gamma^{-2}} \int_{\gamma=0}^{\infty} ln(1+\gamma)\gamma^{k-1} G_{3,3}^{2,3} \left(\frac{(b_{\varsigma})^{2}}{(b_{\alpha})^{2}\gamma}\Big|_{\{m_{s,\varsigma}, m_{m,\varsigma}\}, 1+k}^{\{1,1+k-m_{s},1+k-m_{m}\}, \{\}}\right) d\gamma$$

$$= -\int_{\gamma=0}^{\infty} ln(1+\gamma)\gamma^{k+1} G_{3,3}^{2,3} \left(\frac{(b_{\varsigma})^{2}}{(b_{\alpha})^{2}\gamma}\Big|_{\{m_{s,\varsigma}, m_{m,\varsigma}\}, 1+k}^{\{1,1+k-m_{s},1+k-m_{m}\}, \{\}}\right) (-\gamma^{-2}d\gamma). \tag{5.17}$$

After these processes, integral in (5.17) can be written as follows,

$$\int_{x=0}^{\infty} \ln(1+\frac{1}{x})x^{-k-1}G_{3,3}^{2,3} \left(\frac{(b_{\varsigma})^{2}}{(b_{\alpha})^{2}}x\right|_{\{m_{s,\varsigma}, m_{m,\varsigma}\}, 1+k}^{\{1,1+k-m_{s},1+k-m_{m}\}, \{\}} dx.$$
 (5.18)

When integration by parts is applied,  $u = ln\left(1+\frac{1}{x}\right)$ ,  $dv = x^{-k-1}G_{3,3}^{2,3}\left(\frac{(b_{\varsigma})^2}{(b_a)^2}x\Big|_{\{m_{s,\varsigma},\ m_{m,\varsigma}\},1+k \atop \{m_{s,\varsigma},\ m_{m,\varsigma},\$ 

$$\int_{x=0}^{\infty} \ln(1+\frac{1}{x})x^{-k-1}G_{3,3}^{2,3}\left(\frac{(b_{\varsigma})^{2}}{(b_{\alpha})^{2}}x\Big|_{\{m_{s,\varsigma}, m_{m,\varsigma}\}, 1+k}^{\{1,1+k-m_{s},1+k-m_{m}\}, \{\}}\right)dx$$

$$= \left[uv\right]_{x=0}^{\infty} - \int_{x=0}^{\infty} vdu$$

$$= \left[\ln\left(1+\frac{1}{x}\right)x^{-k}G_{4,4}^{2,4}\left(\frac{(b_{\varsigma})^{2}}{(b_{\alpha})^{2}}x\Big|_{\{m_{s,\varsigma}, m_{m,\varsigma}\}, \{1+k,k\}}^{\{1+k,1,1+k-m_{s},1+k-m_{m}\}, \{\}}\right)\right]_{x=0}^{\infty}$$

$$- \int_{x=0}^{\infty} x^{-k}G_{4,4}^{2,4}\left(\frac{(b_{\varsigma})^{2}}{(b_{\alpha})^{2}}x\Big|_{\{m_{s,\varsigma}, m_{m,\varsigma}\}, \{1+k,k\}}^{\{1+k,1,1+k-m_{s},1+k-m_{m}\}, \{\}}\right)\left(-\frac{1}{(1+x)x^{2}}\right)dx,$$
(5.19)

 $G_{4,4}^{2,4}\bigg(\infty\bigg|_{\{m_{s,\varsigma},\ m_{m,\varsigma}\},\{1+k,k\}}^{\{1+k,1,1+k-m_s,1+k-m_m\},\{\}}\bigg) \text{ is equal to a great number for } k=0 \text{ and it is }$  equal to zero for  $k\geq 0$ . Therefore,  $ln(1)0^kG_{4,4}^{2,4}\bigg(\infty\bigg|_{\{m_{s,\varsigma},\ m_{m,\varsigma}\},\{1+k,k\}}^{\{1+k,1,1+k-m_s,1+k-m_m\},\{\}}\bigg)=0$  and  $ln(\infty)\infty^kG_{4,4}^{2,4}\bigg(0\bigg|_{\{m_{s,\varsigma},\ m_{m,\varsigma}\},\{1+k,k\}}^{\{1+k,1,1+k-m_s,1+k-m_m\},\{\}}\bigg)=0.$  On the other hand,  $\bigg[ln\bigg(1+\frac{1}{x}\bigg)x^{-k}G_{4,4}^{2,4}\bigg(\frac{(b_\varsigma)^2}{(b_a)^2}x\bigg|_{\{m_{s,\varsigma},\ m_{m,\varsigma}\},\{1+k,k\}}^{\{1+k,1,1+k-m_s,1+k-m_m\},\{\}}\bigg)\bigg]_{x=0}^{\infty}=0,$ 

$$\int_{x=0}^{\infty} ln(1+\frac{1}{x})x^{-k-1}G_{3,3}^{2,3}\left(\frac{(b_{\varsigma})^{2}}{(b_{\alpha})^{2}}x\Big|_{\{m_{s,\varsigma}, m_{m,\varsigma}\}, 1+k}^{\{1,1+k-m_{s},1+k-m_{m}\}, \{\}}\right)dx$$

$$=\int_{x=0}^{\infty} x^{-k-2}(1+x)^{-1}G_{4,4}^{2,4}\left(\frac{(b_{\varsigma})^{2}}{(b_{\alpha})^{2}}x\Big|_{\{m_{s,\varsigma}, m_{m,\varsigma}\}, \{1+k,k\}}^{\{1+k,1,1+k-m_{s},1+k-m_{m}\}, \{\}}\right)dx, \tag{5.20}$$

integral in (2.16) and the formula in [65, Eq. 7.811/5] are of the same form,

$$\int_{x=0}^{\infty} x^{\rho-1} (x+\beta)^{-\sigma} G_{p,q}^{m,n} \left(\alpha x \Big|_{b_1,\dots,b_a}^{a_1,\dots,a_p}\right) dx = \frac{\beta^{\rho-\sigma}}{\Gamma(\sigma)} G_{p+1,q+1}^{m+1,n+1} \left(\alpha \beta \Big|_{\sigma-\rho,b_1,\dots,b_a}^{1-\rho,a_1,\dots,a_p}\right), \quad (5.21)$$

where  $\rho = -k - 1$ ,  $\beta = 1$ ,  $\sigma = 1$ , and  $\alpha = \frac{(b_{\varsigma})^2}{(b_{\alpha})^2}$ . Thus the integral in (5.16) can be obtained as follows,

$$\int_{x=0}^{\infty} x^{-k-2} (1+x)^{-1} G_{4,4}^{2,4} \left( \frac{(b_{\varsigma})^{2}}{(b_{\alpha})^{2}} x \Big|_{\{m_{s,\varsigma}, m_{m,\varsigma}\}, \{1+k,k\}}^{\{1+k,1,1+k-m_{s},1+k-m_{m}\}, \{\}\}} \right) dx$$

$$= G_{5,5}^{3,5} \left( \frac{(b_{\varsigma})^{2}}{(b_{\alpha})^{2}} \Big|_{\{2+k,m_{s,\varsigma}, m_{m,\varsigma}\}, \{1+k,k\}}^{\{2+k,m_{s,\varsigma}, m_{m,\varsigma}\}, \{1+k,k\}} \right), \tag{5.22}$$

Eventually, the AVC is obtained as below by substituting (5.22) into (5.16),

$$\bar{C} = \frac{W}{\Gamma(m_s)\Gamma(m_m)\Gamma(m_{m,\varsigma})\Gamma(m_{s,\varsigma})ln(2)} \times \\
\sum_{k=0}^{\infty} \frac{(-(b_{\alpha})^2 \kappa)^k}{k!} \left[ G_{5,5}^{3,5} \left( \frac{(b_{\varsigma})^2}{(b_{\alpha})^2} \Big|_{\{2+k, m_{s,\varsigma}, m_{m,\varsigma}\}, \{1+k,k\}}^{\{2+k, m_{s,\varsigma}, m_{m,\varsigma}\}, \{1+k,k\}} \right) \right].$$
(5.23)

#### 5.3.3 Symbol Error Rate

When integration by parts is applied in (2.16),  $u = erf c(\sqrt{B\gamma})$ ,  $dv = f_{\gamma}(\gamma)d_{\gamma}$ ,  $du = -\sqrt{\frac{B}{\pi\gamma}}e^{-B\gamma}d_{\gamma}$  and  $v = F_{\gamma}(\gamma)$ ,

$$\begin{split} \int_{\gamma=0}^{\infty} erf \, c(\sqrt{B\gamma}) f_{\gamma}(\gamma) d\gamma &= [uv]_{\gamma=0}^{\infty} - \int_{\gamma=0}^{\infty} v \, du \\ &= \left[ erf \, c(\sqrt{B\gamma}) F_{\gamma}(\gamma) \right]_{\gamma=0}^{\infty} - \int_{\gamma=0}^{\infty} F_{\gamma}(\gamma) \left( -\sqrt{\frac{B}{\pi\gamma}} e^{-B\gamma} \right) d_{\gamma}, \end{split} \tag{5.24}$$

First part of (5.24) is obtained as,

$$\left[erfc(\sqrt{B\gamma})F_{\gamma}(\gamma)\right]_{\gamma=0}^{\infty} = erfc(\sqrt{B\infty})F_{\gamma}(\infty) - erfc(\sqrt{B0})F_{\gamma}(0)$$
 (5.25)

$$erfc(\infty)=0,\ erfc(0)=1,\ F_{\gamma}(\infty)=1\ \text{and}\ F_{\gamma}(0)=0.$$
 Therefore, 
$$\left[erfc(\sqrt{B\gamma})F_{\gamma}(\gamma)\right]_{\gamma=0}^{\infty}=0,$$

$$-\int_{\gamma=0}^{\infty} v du = \int_{\gamma=0}^{\infty} \sqrt{\frac{B}{\pi \gamma}} e^{-B\gamma} F_{\gamma}(\gamma) d_{\gamma} = \frac{-\sqrt{B}}{\Gamma(m_{s}) \Gamma(m_{m}) \Gamma(m_{m,\varsigma}) \Gamma(m_{s,\varsigma}) \sqrt{\pi}} \times \\ \sum_{k=1}^{\infty} \frac{(-(b_{\alpha})^{2} \kappa)^{k}}{k!} \int_{\gamma=0}^{\infty} \gamma^{k-\frac{1}{2}} e^{-B\gamma} G_{4,4}^{2,4} \left(\frac{(b_{\varsigma})^{2}}{(b_{\alpha})^{2}} \frac{1}{\gamma} \Big|_{\{m_{s,\varsigma}, m_{m,\varsigma}\}, \{1+k, k\}}^{\{1+k, 1, 1+k-m_{s}, 1+k-m_{m}\}, \{\}\}} \right) d\gamma,$$
(5.26)

Meijer's G-function (5.26) can be converted into form [128] as follows,

$$G_{4,4}^{2,4}\left(\frac{(b_{\varsigma})^{2}}{(b_{\alpha})^{2}}\frac{1}{\gamma}\bigg|_{\{m_{s,\varsigma}, m_{m,\varsigma}\}, \{1+k, k\}}^{\{1+k, 1, 1+k-m_{s}, 1+k-m_{m}\}, \{\}}\right) = G_{4,4}^{4,2}\left(\frac{(b_{\alpha})^{2}\gamma}{(b_{\varsigma})^{2}}\bigg|_{\{-k, 0, m_{s}-k, m_{m}-k\}, \{\}}^{\{1-m_{s,\varsigma}, 1-m_{m,\varsigma}\}, \{-k, 1-k\}}\right), (5.27)$$

(5.26) can be written as follows,

$$\bar{P}_{se} = \frac{-A\sqrt{B}}{\Gamma(m_s)\Gamma(m_m)\Gamma(m_{m,\varsigma})\Gamma(m_{s,\varsigma})\sqrt{\pi}} \sum_{k=1}^{\infty} \frac{(-(b_{\alpha})^2 \kappa)^k}{k!} \times \int_{\gamma=0}^{\infty} \gamma^{k-\frac{1}{2}} e^{-B\gamma} G_{4,4}^{4,2} \left(\frac{(b_{\alpha})^2 \gamma}{(b_{\varsigma})^2} \Big|_{\{-k, 0, m_s-k, m_m-k\}, \{\}}^{\{1-m_{s,\varsigma}, 1-m_{m,\varsigma}\}, \{-k, 1-k\}}\right) d\gamma,$$
(5.28)

integral in (5.28) and [65, Eq. 7.813/1] are of the same form,

$$\int_{x=0}^{\infty} x^{-\rho} e^{-\beta x} G_{p,q}^{m,n} \left( \alpha x \Big|_{b_1,\dots,b_q}^{a_1,\dots,a_p} \right) dx = \beta^{\rho-1} G_{p+1,q}^{m,n+1} \left( \frac{\alpha}{\beta} \Big|_{b_1,\dots,b_q}^{\rho,a_1,\dots,a_p} \right), \tag{5.29}$$

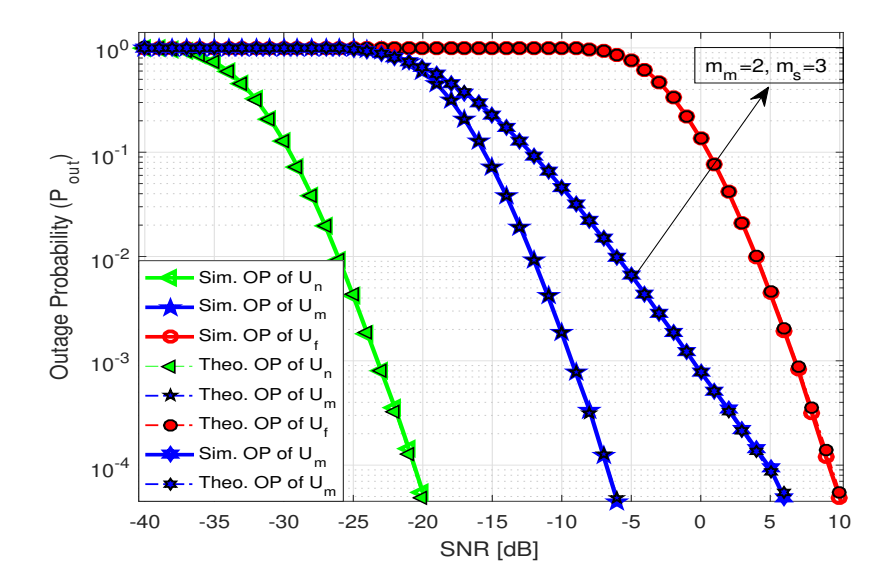


**Figure 5.4** Outage Probabilities of all users for Uplink-NOMA over  $K_G$  channels.

where  $\rho = \frac{1}{2} - k$ ,  $\beta = B$  and  $\alpha = \frac{(b_{\alpha})^2}{(b_{\epsilon})^2}$ . Therefore,

$$\int_{\gamma=0}^{\infty} \gamma^{k-\frac{1}{2}} e^{-B\gamma} G_{4,4}^{4,2} \left( \frac{(b_{\alpha})^{2} \gamma}{(b_{\zeta})^{2}} \Big|_{\{-k, 0, m_{s}-k, m_{m}-k\}, \{\}}^{\{1-m_{s,\zeta}, 1-m_{m,\zeta}\}, \{-k, 1-k\}} \right) d\gamma = B^{-k-\frac{1}{2}} G_{5,4}^{4,3} \left( \frac{(b_{\alpha})^{2}}{(b_{\zeta})^{2} B} \Big|_{\{-k, 0, m_{s}-k, m_{m}-k\}, \{\}}^{\{\frac{1}{2}-k, 1-m_{s,\zeta}, 1-m_{m,\zeta}\}, \{-k, 1-k\}} \right).$$
(5.30)

When the expression (5.30) is substituted in (5.26), SER is found as follows,

$$\bar{P}_{se} = \frac{-A}{\Gamma(m_s)\Gamma(m_m)\Gamma(m_{m,\varsigma})\Gamma(m_{s,\varsigma})\sqrt{\pi}} \times \sum_{k=1}^{\infty} \frac{(-(b_{\alpha})^2 \kappa B^{-1})^k}{k!} G_{5,4}^{4,3} \left(\frac{(b_{\alpha})^2}{(b_{\varsigma})^2 B}\right|_{\{-k, 0, m_s-k, m_m-k\}, \}\}}^{\{\frac{1}{2}-k, 1-m_{s,\varsigma}, 1-m_{m,\varsigma}\}, \{-k, 1-k\}}$$
(5.31)

#### 5.4 Simulation Results

In this section, simulation and analytical results are plotted and discussed for several cases. At least  $10^6$  symbols are randomly generated for all simulation curves and  $K_G$  coefficients  $m_m$  and  $m_s$  are selected as 5 and 6, respectively. In this scenario, BS and users have a single antenna. Users are referred to as nearest user  $(U_n)$ , a

median user  $(U_m)$ , and the farthest user  $(U_f)$  whose distances from BS are 1, 5, and 32, respectively. All simulations are carried out for BPSK modulation. Theoretical curves in the figures are obtained by considering the first 30 terms of the summations in the relevant equations.

OP results are illustrated in Figure 5.4 where theoretical results are plotted by using the expression (5.15). The SNR threshold is selected as  $4 \times 10^{-4}$  dB. As can be seen, theoretical and simulation results match perfectly. OP of  $U_n$  is lower than that of other users because its received power at BS is strongest.  $U_n$ ,  $U_m$  and  $U_f$  reach  $10^{-3}$  OP value at -23 dB, -9 dB, and 7 dB, respectively. On the other hand, theoretical and simulation results of  $U_m$  are also plotted by selecting multipath fading and shadowing parameters as 2 and 3, respectively. As expected, OP increases since channel distortions increase. It reach  $10^{-3}$  OP value at -1 dB.

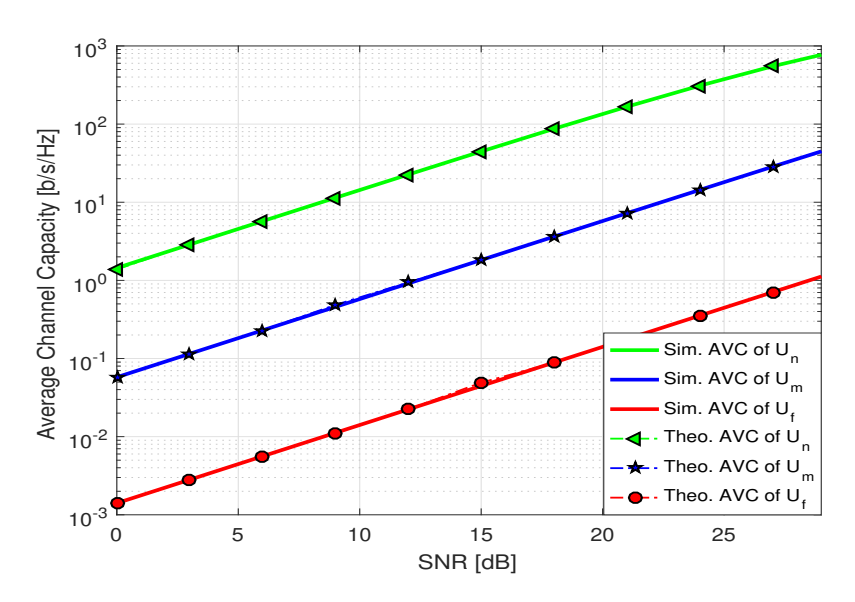


**Figure 5.5** Average Channel Capacities of each user in Uplink-NOMA over  $K_G$  channels.

The AVC curves are presented in Figure 5.5 where theoretical results from the expression (5.23) and simulation results match perfectly where the bandwidth is taken as 1 KHz. This figure shows that as the distance of the user from BS increases, the AVC also increases. For example, AVCs for  $U_n$ ,  $U_m$  and  $U_f$  are approximately 11.2 b/s/Hz,  $48.5 \times 10^{-2}$  b/s/Hz and  $11.2 \times 10^{-3}$  b/s/Hz, respectively at SNR=9 dB. Furthermore, when multipath and shadowing parameters increase, AVC also increases since the channel degradation is less.

Figure 5.6 depicts the SER performance where the theoretical results are plotted by using the expression (5.31). One can see that there is a little bit discrepancy between simulation and theoretical results. It stems from the truncation used in the summation

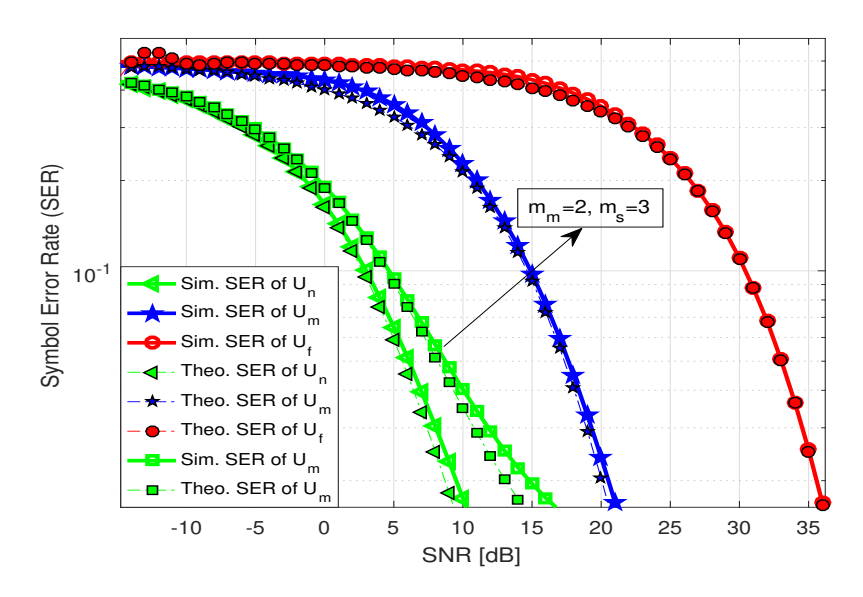


**Figure 5.6** SER of all users for Uplink-NOMA over  $K_G$  channels.

of the expression (5.31). As more terms are added, simulation results approach to theoretical ones.  $U_n$ ,  $U_m$  and  $U_f$  reach  $10^{-1}$  SER value at approximately 3 dB, 15 dB, and 30 dB, respectively. SER values of  $U_n$  are lower than the others since it is the nearest to the BS and its received power is the strongest. SER results of  $U_n$  for  $m_m = 2$  and  $m_s = 3$  are also shown where the SER reach  $10^{-1}$  value to 5 dB.

### 5.5 Chapter Summary

In this chapter, the uplink NOMA system consisting of a BS communicating with multiple users all equipped with a single antenna is analyzed when the realistic  $K_G$  channel model is considered to represent both shadowing and fading in practical wireless mediums. Theoretical analyses include detailed derivations of PDF and CDF of SINR, SER, OP, and AVC. With the help of extensive simulations, numerical examples validate the correctness of the mathematical findings for several channel parameters and also provide insights into the performance. As expected, being closer to the BS and decreasing shadowing impact result in better reliability and higher transmission rate. In order to benefit from the higher capacity of NOMA in practice, more sophisticated transmission approaches such as NOMA with physical layer security and energy harvesting, multiple antennas, and cooperative transmission with relaying can be incorporated. To this end, the comprehensive analysis presented in this chapter can be quite helpful and fundamental in deriving their analytical performance expressions over practical channel models.

# 6 RESULTS AND DISCUSSION

In this dissertation, performance analysis in vehicular  $K_G$  fading channels is carried out by applying the MRT technique which transfers the computational burden to the transmitter and hence, alleviates the complexity of the receiver. On the other hand, increasing network communication mandates the development of techniques decreasing latency and providing gain from the frequency spectrum. It is critical for vehicular communication because the data transmission rate must be higher due to high speed. Therefore, downlink and uplink-NOMA techniques for vehicular communication are investigated.

#### 6.1 Conclusions

MRT transferring the burden of the receiver to the transmitter is a beamforming technique. Although one or multiple antennas can be used in the receiver, multiple antennas have to been used in the transmitter in that technique. In this dissertation, MRT is firstly applied by using different modulation types and a different number of antennas in vehicular  $K_G$  fading channels, and performance metrics such as OP, AVC, and SER are derived. Furthermore, diversity and coding gains are obtained via asymptotic SNR PDF in high SNR values. All derivations are validated with simulations. Apart from these, in presence of channel estimation errors, it is detected with simulations that in which variance values, set floor emerges. On the set floor, increasing the SNR does not increase performance. Derivations of channel estimation errors can not be made due to channel and channel estimation errors have  $K_G$  and Gauss distributions, respectively. Because the closed-form of PDF emerging relationship with those distributions is not tractable.

Increasing data traffic requires gaining spectral efficiency and low latency. One of the most attractive techniques is NOMA envisioned used in 5G. In this technique, multiple users can communicate in the same resource blocks (in the same frequency band and time slot). Downlink and uplink NOMA are addressed in different chapters due to

different frequencies are used. Closed forms of OP, AVC, and SER are derived for those techniques and they are validated with simulations. On the other hand, asymptotic expressions of OP and SER are obtained in high SNR values. However, it is observed that asymptotic simulations and derivations for uplink-NOMA are not consistent due to its SNR PDF is much more complex.

#### 6.2 Future Works

- 1. MRT work performed in this dissertation is extended to investigating MRT and spatial modulation over  $K_G$  fading channels in the future. Spatial modulation increases the data transmission rate by not transmitting all data and it provides that channel is early to be free. But, the SER derivation of not transmitted bit especially in the  $K_G$  fading channel is fairly challenging compared to other techniques.
- 2. In downlink-NOMA, each user has to decode other users' stronger signals in order to achieve its signal. Therefore, it is a candidate for cooperative communication. In such a case, each user does not receive other user signals and decode stronger signals. Therefore, in the next work, we investigate the downlink-NOMA system by applying cooperative communication over the  $K_G$  fading channel.
- 3. Security vulnerabilities raise because each user receives signals of all other users in spite of NOMA provides gain from frequency spectrum and latency. We will consider outage secrecy in downlink-NOMA over the  $K_G$  fading channel to enable insights into this issue.
- 4. Recently, the other popular researching topic is free-space optics (FSO) communication in where the requirements of bandwidth are virtually unlimited and frequency bands are a license-free spectrum. It is attractive due to it yields the high transmission rate, low power consumption, and low interference. In this communication, distributions such as Negative Exponential/Gamma model (it is commonly known as K distribution.), I-K distribution, log-normal Rician channel (it is referred to as Beckman), Gamma-Gamma are used. Therefore, in the next works, we will investigate the performance of that communication by applying the MRT technique and gamma-gamma distribution.

- [1] R. Hult, G. R. Campos, E. Steinmetz, L. Hammarstrand, P. Falcone, H. Wymeersch, "Coordination of cooperative autonomous vehicles: Toward safer and more efficient road transportation," *IEEE Signal Processing Magazine*, vol. 33, no. 6, pp. 74–84, 2016. DOI: 10.1109/MSP.2016.2602005.
- [2] F. Qu, F.-Y. Wang, L. Yang, "Intelligent transportation spaces: Vehicles, traffic, communications, and beyond," *IEEE Communications Magazine*, vol. 48, no. 11, pp. 136–142, 2010. DOI: 10.1109/MCOM.2010.5621980.
- [3] L. Azpilicueta, C. Vargas-Rosales, F. Falcone, "Intelligent vehicle communication: Deterministic propagation prediction in transportation systems," *IEEE Vehicular Technology Magazine*, vol. 11, no. 3, pp. 29–37, 2016. DOI: 10.1109/MVT.2016.2549995.
- [4] M. Khodaei, P. Papadimitratos, "The key to intelligent transportation: Identity and credential management in vehicular communication systems," *IEEE Vehicular Technology Magazine*, vol. 10, no. 4, pp. 63–69, 2015. DOI: 10.1109/MVT.2015.2479367.
- [5] A. Cidronali, S. Maddio, M. Passafiume, G. Manes, "Car talk: Technologies for vehicle-to-roadside communications," *IEEE Microwave Magazine*, vol. 17, no. 11, pp. 40–60, 2016. DOI: 10.1109/MMM.2016.2600949.
- [6] M. Silva, F. Moita, U. Nunes, L. Garrote, H. Faria, J. Ruivo, "Isrobotcar: The autonomous electric vehicle project," in *2012 IEEE/RSJ International Conference on Intelligent Robots and Systems*, 2012, pp. 4233–4234. DOI: 10.1109/IROS.2012.6386292.
- [7] D. Jia, K. Lu, J. Wang, X. Zhang, X. Shen, "A survey on platoon-based vehicular cyber-physical systems," *IEEE Communications Surveys Tutorials*, vol. 18, no. 1, pp. 263–284, 2016. DOI: 10.1109/COMST.2015.2410831.
- [8] X. Ge, Z. Li, S. Li, "5g software defined vehicular networks," *IEEE Communications Magazine*, vol. 55, no. 7, pp. 87–93, 2017. DOI: 10.1109/MCOM.2017. 1601144.
- [9] A. F. Molisch, F. Tufvesson, J. Karedal, C. F. Mecklenbrauker, "A survey on vehicle-to-vehicle propagation channels," *IEEE Wireless Communications*, vol. 16, no. 6, pp. 12–22, 2009. DOI: 10.1109/MWC.2009.5361174.
- [10] A. Akki, F. Haber, "A statistical model of mobile-to-mobile land communication channel," *IEEE Transactions on Vehicular Technology*, vol. 35, no. 1, pp. 2–7, 1986. DOI: 10.1109/T-VT.1986.24062.
- [11] Y. Yang, "Inter-vehicle cooperative channel estimation for ieee802.11p systems," in 2016 IEEE 83rd Vehicular Technology Conference (VTC Spring), 2016, pp. 1–5. DOI: 10.1109/VTCSpring.2016.7504299.

- [12] G. Matz, "On non-wssus wireless fading channels," *IEEE Transactions on Wireless Communications*, vol. 4, no. 5, pp. 2465–2478, 2005. DOI: 10.1109/TWC. 2005.853905.
- [13] L. Bernado, T. Zemen, A. Paier, J. Karedal, B. H. Fleury, "Parametrization of the local scattering function estimator for vehicular-to-vehicular channels," in *2009 IEEE 70th Vehicular Technology Conference Fall*, 2009, pp. 1–5. DOI: 10.1109/VETECF.2009.5378762.
- [14] X. Cheng, C.-X. Wang, B. Ai, H. Aggoune, "Envelope level crossing rate and average fade duration of nonisotropic vehicle-to-vehicle ricean fading channels," *IEEE Transactions on Intelligent Transportation Systems*, vol. 15, no. 1, pp. 62–72, 2014. DOI: 10.1109/TITS.2013.2274618.
- [15] J. Karedal, F. Tufvesson, N. Czink, A. Paier, C. Dumard, T. Zemen, C. F. Mecklenbrauker, A. F. Molisch, "A geometry-based stochastic MIMO model for vehicle-to-vehicle communications," *IEEE Transactions on Wireless Communications*, vol. 8, no. 7, pp. 3646–3657, 2009. DOI: 10.1109/TWC.2009. 080753.
- [16] S. Herbert, I. Wassell, T.-H. Loh, J. Rigelsford, "Characterizing the spectral properties and time variation of the in-vehicle wireless communication channel," *IEEE Transactions on Communications*, vol. 62, no. 7, pp. 2390–2399, 2014. DOI: 10.1109/TCOMM.2014.2328635.
- [17] L. Cheng, B. E. Henty, D. D. Stancil, F. Bai, P. Mudalige, "Mobile vehicle-to-vehicle narrow-band channel measurement and characterization of the 5.9 ghz dedicated short range communication (dsrc) frequency band," *IEEE Journal on Selected Areas in Communications*, vol. 25, no. 8, pp. 1501–1516, 2007. DOI: 10.1109/JSAC.2007.071002.
- [18] L. Cheng, B. Henty, R. Cooper, D. D. Stancil, F. Bai, "Multi-path propagation measurements for vehicular networks at 5.9 ghz," in *2008 IEEE Wireless Communications and Networking Conference*, 2008, pp. 1239–1244. DOI: 10. 1109/WCNC.2008.223.
- [19] G. Acosta, K. Tokuda, M. Ingram, "Measured joint doppler-delay power profiles for vehicle-to-vehicle communications at 2.4 ghz," in *IEEE Global Telecommunications Conference*, 2004. GLOBECOM '04., vol. 6, 2004, 3813–3817 Vol.6. DOI: 10.1109/GLOCOM.2004.1379082.
- [20] Y. Li, R. He, S. Lin, K. Guan, D. He, Q. Wang, Z. Zhong, "Cluster-based nonstationary channel modeling for vehicle-to-vehicle communications," *IEEE Antennas and Wireless Propagation Letters*, vol. 16, pp. 1419–1422, 2017. DOI: 10.1109/LAWP.2016.2631633.
- [21] X. Zhao, Q. Han, S. Geng, J. Li, "V2v doppler spectra for geometry-based scattering models with moving scatterers," in 2015 IEEE 16th International Conference on Communication Technology (ICCT), 2015, pp. 752–756. DOI: 10.1109/ICCT.2015.7399941.
- [22] J. Maurer, T. Fugen, T. Schafer, W. Wiesbeck, "A new inter-vehicle communications (ivc) channel model," in *IEEE 60th Vehicular Technology Conference*, 2004. VTC2004-Fall. 2004, vol. 1, 2004, 9–13 Vol. 1. DOI: 10.1109/VETECF.2004.1399905.

- [23] J. Nuckelt, M. Schack, T. Kürner, "Geometry-based path interpolation for rapid ray-optical modeling of vehicular channels," in *2015 9th European Conference on Antennas and Propagation (EuCAP)*, 2015, pp. 1–5.
- [24] A. Borhani, "Modelling and analysis of non-stationary mobile fading channels using brownian random trajectory models," 2014.
- [25] Y. Yuan, C. Wang, X. Cheng, B. Ai, D. I. Laurenson, "Novel 3d geometry-based stochastic models for non-isotropic MIMO vehicle-to-vehicle channels," *IEEE Transactions on Wireless Communications*, vol. 13, no. 1, pp. 298–309, Jan. 2014.
- [26] S. Beygi, E. G. Ström, U. Mitra, "Geometry-based stochastic modeling and estimation of vehicle to vehicle channels," in 2014 IEEE International Conference on Acoustics, Speech and Signal Processing (ICASSP), May 2014, pp. 4289–4293.
- [27] X. Liang, X. Zhao, S. Li, Q. Wang, W. Lu, "A 3d geometry-based scattering model for vehicle-to-vehicle wideband MIMO relay-based cooperative channels," *China Communications*, vol. 13, no. 10, pp. 1–10, 2016. DOI: 10. 1109/CC.2016.7732007.
- [28] H. Ilhan, "The performance of MIMO system using MRT scheme in vehicular systems," *International Journal of Communication Systems*, vol. 30, no. 9, e3188, Sep. 2016. DOI: 10.1002/dac.3188. [Online]. Available: https://doi.org/10.1002%2Fdac.3188.
- [29] T. Abbas, J. Karedal, F. Tufvesson, "Measurement-based analysis: The effect of complementary antennas and diversity on vehicle-to-vehicle communication," *IEEE Antennas and Wireless Propagation Letters*, vol. 12, pp. 309–312, 2013. DOI: 10.1109/LAWP.2013.2250243.
- [30] G. Noh, J. Kim, S. Choi, N. Lee, H. Chung, I. Kim, "Feasibility validation of a 5g-enabled mmwave vehicular communication system on a highway," *IEEE Access*, vol. 9, pp. 36535–36546, 2021. DOI: 10.1109/ACCESS.2021.3062907.
- [31] M. Schack, D. Kornek, E. Slottke, T. Kürner, "Analysis of channel parameters for different antenna configurations in vehicular environments," in *2010 IEEE 72nd Vehicular Technology Conference Fall*, 2010, pp. 1–5. DOI: 10.1109/VETECF.2010.5594350.
- [32] J. M. Eckhardt, V. Petrov, D. Moltchanov, Y. Koucheryavy, T. Kürner, "Channel measurements and modeling for low terahertz band vehicular communications," *IEEE Journal on Selected Areas in Communications*, pp. 1–1, 2021. DOI: 10.1109/JSAC.2021.3071843.
- [33] P. Qi, Y. Zhang, Z. Yuan, L. Yu, P. Tang, J. Zhang, "Channel modeling based on 3d scenario information for v2i communications," in *2021 15th European Conference on Antennas and Propagation (EuCAP)*, 2021, pp. 1–5. DOI: 10. 23919/EuCAP51087.2021.9410931.
- [34] S. Ilarri, T. Delot, R. Trillo-Lado, "A data management perspective on vehicular networks," *IEEE Communications Surveys Tutorials*, vol. 17, no. 4, pp. 2420–2460, 2015. DOI: 10.1109/COMST.2015.2472395.

- [35] P. Alexander, D. Haley, A. Grant, "Cooperative intelligent transport systems: 5.9-ghz field trials," *Proceedings of the IEEE*, vol. 99, no. 7, pp. 1213–1235, 2011. DOI: 10.1109/JPROC.2011.2105230.
- [36] G. L. Stüber, G. L. Stèuber, *Principles of mobile communication*. Springer, 1996, vol. 2.
- [37] P. M. Shankar, *Fading and Shadowing in Wireless Systems*, 2nd. Springer Publishing Company, Incorporated, 2017, ISBN: 3319531972.
- [38] J. J. Egli, "Radio propagation above 40 mc over irregular terrain," *Proceedings of the IRE*, vol. 45, no. 10, pp. 1383–1391, Oct. 1957, ISSN: 0096-8390. DOI: 10.1109/JRPROC.1957.278224.
- [39] M. .-. Alouini, A. J. Goldsmith, "A unified approach for calculating error rates of linearly modulated signals over generalized fading channels," *IEEE Transactions on Communications*, vol. 47, no. 9, pp. 1324–1334, Sep. 1999, ISSN: 0090-6778. DOI: 10.1109/26.789668.
- [40] E. Al-Hussaini, A. Al-Bassiouni, "Performance of mrc diversity systems for the detection of signals with nakagami fading," *IEEE Transactions on Communications*, vol. 33, no. 12, pp. 1315–1319, Dec. 1985, ISSN: 0090-6778. DOI: 10.1109/TCOM.1985.1096243.
- [41] K. P. Peppas, "Performance evaluation of triple-branch gsc diversity receivers over generalized-k fading channels," *IEEE Communications Letters*, vol. 13, no. 11, pp. 829–831, Nov. 2009, ISSN: 1089-7798. DOI: 10.1109/LCOMM. 2009.091197.
- [42] Y. Karasawa, K. Kimura, K. Minamisono, "Analysis of availability improvement in lmss by means of satellite diversity based on three-state propagation channel model," *IEEE Transactions on Vehicular Technology*, vol. 46, no. 4, pp. 1047–1056, Nov. 1997, ISSN: 0018-9545. DOI: 10.1109/25.653078.
- [43] Weijun Cheng, "Performance analysis and comparison of dual-hop amplify-and-forward relaying over mixture gamma and generalized-k fading channels," in 2013 International Conference on Wireless Communications and Signal Processing, Oct. 2013, pp. 1–6.
- [44] N. I. Miridakis, "On the ergodic capacity of underlay cognitive dual-hop af relayed systems under non-identical generalized-*k*fading channels," *IEEE Communications Letters*, vol. 19, no. 11, pp. 1965–1968, Nov. 2015, ISSN: 1089-7798. DOI: 10.1109/LCOMM.2015.2475739.
- [45] A. Abdi, M. Kaveh, "On the utility of gamma pdf in modeling shadow fading (slow fading)," in 1999 IEEE 49th Vehicular Technology Conference (Cat. No.99CH36363), vol. 3, May 1999, 2308–2312 vol.3. DOI: 10.1109/VETEC. 1999.778479.
- [46] P. S. Bithas, P. T. Mathiopoulos, S. A. Kotsopoulos, "Diversity reception over generalized-k (kg) fading channels," *IEEE Transactions on Wireless Communications*, vol. 6, no. 12, pp. 4238–4243, Dec. 2007, ISSN: 1536-1276. DOI: 10.1109/TWC.2007.4400789.

- [47] S. Al-Ahmadi, H. Yanikomeroglu, "On the approximation of the pdf of the sum of independent generalized-k rvs by another generalized-k pdf with applications to distributed antenna systems," in *2010 IEEE Wireless Communication and Networking Conference*, Apr. 2010, pp. 1–6. DOI: 10.1109/WCNC. 2010.5506178.
- [48] G. Cooper, R. Nettleton, "A spread-spectrum technique for high-capacity mobile communications," *IEEE Transactions on Vehicular Technology*, vol. 27, no. 4, pp. 264–275, 1978. DOI: 10.1109/T-VT.1978.23758.
- [49] Y. Tokgoz, B. Rao, "Performance analysis of maximum ratio transmission based multi-cellular MIMO systems," *IEEE Transactions on Wireless Communications*, vol. 5, no. 1, pp. 83–89, 2006. DOI: 10.1109/TWC.2006.1576532.
- [50] C. He, G. Y. Li, F.-C. Zheng, X. You, "Energy-efficient resource allocation in ofdm systems with distributed antennas," *IEEE Transactions on Vehicular Technology*, vol. 63, no. 3, pp. 1223–1231, 2014. DOI: 10.1109/TVT.2013. 2282373.
- [51] E. Al-Hussaini, I. Sayed, "Performance of the decorrelator receiver for DS-CDMA mobile radio system employing RAKE and diversity through nakagami fading channel," *IEEE Transactions on Communications*, vol. 50, no. 10, pp. 1566–1570, Oct. 2002. DOI: 10.1109/tcomm.2002.803975. [Online]. Available: https://doi.org/10.1109%2Ftcomm.2002.803975.
- [52] V. K. Dwivedi, G. Singh, "Analysis of channel capacity of generalized -k fading with maximal-ratio combining diversity receivers," in 2011 International Conference on Communication Systems and Network Technologies, IEEE, Jun. 2011. DOI: 10.1109/csnt.2011.117. [Online]. Available: https://doi.org/10.1109%2Fcsnt.2011.117.
- [53] P. M. Shankar, "Performance analysis of diversity combining algorithms in shadowed fading channels," *Wireless Personal Communications*, vol. 37, pp. 61–72, Apr. 2006.
- [54] P. Shankar, "Error rates in generalized shadowed fading channels," *Wireless Personal Communications*, vol. 28, no. 3, pp. 233–238, Feb. 2004.
- [55] P. S. Bithas, V. Nikolaidis, A. G. Kanatas, G. K. Karagiannidis, "Uav-to-ground communications: Channel modeling and uav selection," *IEEE Transactions on Communications*, pp. 1–1, 2020.
- [56] H. Rasheed, F. Haroon, N. Rajatheva, "Energy detection with diversity combining over kg fading for cognitive vanet," ser. 2016 IEEE 84th Vehicular Technology Conference (VTC-Fall), Sep. 2016, pp. 1–5. DOI: 10.1109/VTCFall.2016.7880983.
- [57] H. Zhao, Z. Liu, L. Yang, M. Alouini, "Secrecy analysis in DF relay over generalized-*K* fading channels," *IEEE Transactions on Communications*, vol. 67, no. 10, pp. 7168–7182, Oct. 2019. DOI: 10.1109/tcomm.2019.2926719.
- [58] Z. Wang, H. Zhao, S. Wang, J. Zhang, M. Alouini, "Secrecy analysis in SWIPT systems over generalized-*K* fading channels," *IEEE Communications Letters*, vol. 23, no. 5, pp. 834–837, May 2019. DOI: 10 . 1109 / lcomm . 2019 . 2907490.

- [59] V. M. Blagojević, A. M. Cvetković, P. N. Ivaniš, "Performance analysis of energy harvesting DF relay system in generalized-K fading environment," *Physical Communication*, vol. 28, pp. 190–200, 2018.
- [60] G. P. Efthymoglou, N. Y. Ermolova, V. A. Aalo, "Channel capacity and average error rates in generalised-K fading channels," *IET Communications*, vol. 4, no. 11, pp. 1364–1372, Jul. 2010.
- [61] A. Dziri, M. Terre, N. Nasser, "Performance analysis of relay selection for IoT networks over generalized-K distribution," in 2019 15th International Wireless Communications Mobile Computing Conference (IWCMC), Tangier, Morocco, Jun. 2019, pp. 1411–1415. DOI: 10.1109/iwcmc.2019.8766438.
- [62] L. Zhang, H. Zhao, G. Pan, L. Yang, J. Chen, "Secure analysis over generalized-K channels," *Sciece China. Information Sciences*, vol. 63, May 2019. DOI: 10.1007/s11432-019-9892-y.
- [63] V. M. Blagojevic, A. M. Cvetkovic, "Outage probability of energy harvesting df relay systems in generalized-k fading," pp. 240–243, Oct. 2017.
- [64] P. S. Bithas, N. C. Sagias, P. T. Mathiopoulos, G. K. Karagiannidis, A. A. Rontogiannis, "On the performance analysis of digital communications over generalized-K fading channels," *IEEE Communications Letters*, vol. 10, no. 5, pp. 353–355, 2006. DOI: 10.1109/LCOMM.2006.1633320.
- [65] I. S. Gradshteyn, I. M. Ryzhik, *Table of integrals, series, and products*, Seventh. Elsevier/Academic Press, Amsterdam, 2007, pp. xlviii+1171, Translated from the Russian, Translation edited and with a preface by Alan Jeffrey and Daniel Zwillinger, With one CD-ROM (Windows, Macintosh and UNIX), ISBN: 978-0-12-373637-6; 0-12-373637-4.
- [66] A. Benjebbour, Y. Saito, Y. Kishiyama, A. Li, A. Harada, T. Nakamura, "Concept and practical considerations of non-orthogonal multiple access (NOMA) for future radio access," in *2013 International Symposium on Intelligent Signal Processing and Communication Systems*, Naha, Japan, 2013, pp. 770–774.
- [67] Y. Zhang, D. Kwan, "Energy-efficient user scheduling and power allocation for NOMA wireless networks," 2017.
- [68] A. Benjebbour, "An overview of non-orthogonal multiple access," *ZTE Communications*, vol. 15, no. S1, 21, pp. 21–30, 2017. DOI: 10.3969/j.issn.1673-5188.2017.S1.003.
- [69] G. Wunder, P. Jung, M. Kasparick, T. Wild, F. Schaich, Y. Chen, S. T. Brink, I. Gaspar, N. Michailow, A. Festag, L. Mendes, N. Cassiau, D. Ktenas, M. Dryjanski, S. Pietrzyk, B. Eged, P. Vago, F. Wiedmann, "5gnow: Non-orthogonal, asynchronous waveforms for future mobile applications," *IEEE Communications Magazine*, vol. 52, no. 2, pp. 97–105, 2014.
- [70] A. Benjebbour, "An overview of non-orthogonal multiple access," *NTT DO-COMO*, vol. 15, 2017. DOI: 10.3969/j..
- [71] R. C. Kizilirmak, "Non-orthogonal multiple access (NOMA) for 5g networks," in, ser. Towards 5G Wireless Networks, H. K. Bizaki, Ed., Rijeka: IntechOpen, 2016, ch. 4. DOI: 10.5772/66048. [Online]. Available: https://doi.org/10.5772/66048.

- [72] R. Duan, J. Wang, C. Jiang, H. Yao, Y. Ren, Y. Qian, "Resource allocation for multi-uav aided iot NOMA uplink transmission systems," *IEEE Internet of Things Journal*, vol. 6, no. 4, pp. 7025–7037, 2019. DOI: 10.1109/JIOT. 2019.2913473.
- [73] Y. Kwon, H. Baek, J. Lim, "Uplink NOMA using power allocation for uav-aided csma/ca networks," *IEEE Systems Journal*, pp. 1–4, 2020. DOI: 10.1109/JSYST.2020.3028884.
- [74] Y. Chen, L. Wang, Y. Ai, B. Jiao, L. Hanzo, "Performance analysis of NOMA-sm in vehicle-to-vehicle massive MIMO channels," *IEEE Journal on Selected Areas in Communications*, vol. 35, no. 12, pp. 2653–2666, 2017. DOI: 10.1109/JSAC.2017.2726006.
- [75] O. Badarneh, M. Aloqlah, "Performance analysis of digital communication systems over generalized  $\alpha-\eta-\mu$  fading channels," *IEEE Transactions on Vehicular Technology*, vol. 65, pp. 1–1, Jan. 2015. DOI: 10.1109/TVT.2015. 2504381.
- [76] Z. Wang, G. B. Giannakis, "A simple and general parameterization quantifying performance in fading channels," *IEEE Transactions on Communications*, vol. 51, no. 8, pp. 1389–1398, Aug. 2003.
- [77] K. Peppas, F. Lazarakis, A. Alexandridis, K. Dangakis, "Cascaded generalised-k fading channel," *IET Communications*, vol. 4, no. 1, pp. 116–124, Jan. 2010.
- [78] E. Salahat, H. Saleh, "Novel unified analysis of orthogonal space-time block codes over generalized-k and awgn MIMO networks," pp. 1–4, May 2015, ISSN: 1550-2252.
- [79] J. He, K. Xiao, "Performance analysis of ostbc-MIMO systems employing m-qam transmission over independent but not necessarily identical generalized-k fading channels," pp. 160–165, Jun. 2016, ISSN: null. DOI: 10.1109/ICCSN.2016.7586640.
- [80] X. Li, L. Li, X. Su, Z. Wang, P. Zhang, "Approximate capacity analysis for distributed MIMO system over generalized-k fading channels," pp. 235–240, Mar. 2015, ISSN: 1558-2612.
- [81] V. Dwivedi, G. Singh, "A novel mgf based analysis of channel capacity of generalized-k fading with maximal-ratio combining diversity," *Progress In Electromagnetics Research C*, vol. 26, pp. 153–165, Jan. 2012. DOI: 10.2528/PIERC11100103.
- [82] J. Jung, S. Lee, H. Park, S. Lee, I. Lee, "Capacity and error probability analysis of diversity reception schemes over generalized- *k* fading channels using a mixture gamma distribution," *IEEE Transactions on Wireless Communications*, vol. 13, no. 9, pp. 4721–4730, 2014.
- [83] T. K. Y. Lo, "Maximum ratio transmission," *IEEE Transactions on Communications*, vol. 47, no. 10, pp. 1458–1461, Oct. 1999.
- [84] K. Neupane, R. J. Haddad, D. L. Moore, "Secrecy analysis of massive MIMO systems with mrt precoding using normalization methods," pp. 1–6, Apr. 2018, ISSN: 1091-0050. DOI: 10.1109/SECON.2018.8478872.

- [85] F. Adachi, A. Boonkajay, "Analysis of maximal-ratio transmit and combining spatial diversity," *IEICE Communications Express*, vol. 8, no. 5, pp. 153–159, 2019.
- [86] S. S. Chauhan, S. Kumar, "Performance analysis of maximal ratio transmission with receiver antenna selection over correlated nakagami-m fading channels," *Wireless Networks*, vol. 26, Nov. 2019.
- [87] O. S. Badarneh, D. B. Da Costa, P. H. J. Nardelli, "Wireless-powered communication networks with random mobility," *IEEE Access*, vol. 7, pp. 166476–166492, 2019.
- [88] L. Yang, Q. T. Zhang, "Outage performance of MIMO relay channels with maximal ratio transmission," *Electronics Letters*, vol. 45, no. 5, pp. 273–274, Feb. 2009.
- [89] A. Aladwani, E. Erdoğan, T. Gucluoglu, "Impact of co-channel interference on two-way relaying networks with maximal ratio transmission," *Electronics*, vol. 8, p. 392, Apr. 2019. DOI: 10.3390/electronics8040392.
- [90] Y. Sahin, E. Erdoğan, T. Gucluoglu, "Performance analysis of two way decode and forward relay network with maximum ratio transmission," *Physical Communication*, vol. 32, Nov. 2018. DOI: 10.1016/j.phycom.2018.11.004.
- [91] A. Ibrahim, T. Gucluoglu, "Performance analysis of maximum ratio transmission based fso link over málaga turbulence channel," *Optics Communications*, Jun. 2019. DOI: 10.1016/j.optcom.2019.06.035.
- [92] A. M. Mathai, R. K. Saxena, Generalized Hypergeometric Functions with Applications in Statistics and Physical Sciences, Lecture Notes in Mathematics. 1973, vol. 348.
- [93] Indefinite integral of Meijer-G function. [Online]. Available: https://functions.wolfram.com/HypergeometricFunctions/MeijerG/21/01/01/(visited on 05/20/2020).
- [94] In function in terms of Meijer-G function. [Online]. Available: http://functions.wolfram.com/07.34.03.0456.01 (visited on 06/20/2020).
- [95] Besselk function in terms of Meijer-G function. [Online]. Available: http://functions.wolfram.com/03.04.26.0009.01 (visited on 08/20/2020).
- [96] Erfc function in terms of Meijer-G function. [Online]. Available: http://functions.wolfram.com/07.34.03.0619.01 (visited on 05/20/2020).
- [97] C. Wang, T. C. .-. Liu, X. Dong, "Impact of channel estimation error on the performance of amplify-and-forward two-way relaying," *IEEE Transactions on Vehicular Technology*, vol. 61, no. 3, pp. 1197–1207, Mar. 2012.
- [98] T. Hou, X. Sun, Z. Song, "Outage performance for non-orthogonal multiple access with fixed power allocation over nakagami-*m* fading channels," *IEEE Communications Letters*, vol. 22, no. 4, pp. 744–747, 2018.
- [99] J. Choi, "On multiple access using H-ARQ with SIC techniques for wireless ad hoc networks," *Wireless Personal Communications*, vol. 69, no. 1, pp. 187–212, Mar. 2012.

- [100] S. Arzykulov, T. A. Tsiftsis, G. Nauryzbayev, M. Abdallah, "Outage performance of cooperative underlay CR-NOMA with imperfect CSI," *IEEE Communications Letters*, vol. 23, no. 1, pp. 176–179, 2019. DOI: 10.1109/lcomm.2018.2878730.
- [101] Z. Ding, Z. Yang, P. Fan, H. V. Poor, "On the performance of non-orthogonal multiple access in 5G systems with randomly deployed users," *IEEE Signal Processing Letters*, vol. 21, no. 12, pp. 1501–1505, 2014.
- [102] I. Lee, J. Kim, "Average symbol error rate analysis for non-orthogonal multiple access with *M*-ary QAM signals in rayleigh fading channels," *IEEE Communications Letters*, vol. 23, no. 8, pp. 1328–1331, 2019. DOI: 10.1109/LCOMM. 2019.2921770.
- [103] F. Kara, H. Kaya, "BER performances of downlink and uplink NOMA in the presence of sic errors over fading channels," *IET Communications*, vol. 12, no. 15, pp. 1834–1844, 2018.
- [104] M. Sashiganth, S. Thiruvengadam, D. S. Kumar, "Outage analysis of SWIPT-based full-duplex cognitive NOMA downlink system over nakagami-m fading channels," *International Journal of Communication Systems*, vol. 33, no. 8, e4362, Feb. 2020. DOI: 10.1002/dac.4362.
- [105] M. Can, İ. Altunbaş, E. Basar, "NOMA-based downlink relaying with media-based modulation," *Physical Communication*, vol. 41, p. 101 116, Aug. 2020. DOI: 10.1016/j.phycom.2020.101116.
- [106] Y. Yu, H. Chen, Y. Li, Z. Ding, B. Vucetic, "On the performance of non-orthogonal multiple access in short-packet communications," *IEEE Communications Letters*, vol. 22, no. 3, pp. 590–593, 2018.
- [107] J. Choi, "NOMA: Principles and recent results," in 2017 International Symposium on Wireless Communication Systems (ISWCS), 2017, pp. 349–354.
- [108] A. Lozano, A. M. Tulino, S. Verdu, "High-SNR power offset in multiantenna communication," *IEEE Transactions on Information Theory*, vol. 51, no. 12, pp. 4134–4151, 2005. DOI: 10.1109/TIT.2005.858937.
- [109] P. Concus, D. Cassatt, G. Jaehnig, E. Melby, "Tables for the evaluation of  $\int x = 0^{\infty} x^{\beta} e^{-x} f(x) dx$  by gauss-laguerre quadrature," *Mathematics of Computation*, vol. 17, no. 83, pp. 245–256, 1963.
- [110] S. Atapattu, C. Tellambura, H. Jiang, "A mixture gamma distribution to model the SNR of wireless channels," *IEEE Transactions on Wireless Communications*, vol. 10, no. 12, pp. 4193–4203, 2011.
- [111] W. U. Khan, F. Jameel, T. Ristaniemi, B. M. Elhalawany, J. Liu, "Efficient power allocation for multi-cell uplink NOMA network," ser. 2019 IEEE 89th Vehicular Technology Conference (VTC2019-Spring), 2019, pp. 1–5. DOI: 10.1109/VTCSpring.2019.8746316.
- [112] R. Shen, X. Wang, Y. Xu, "Beamforming design for uplink multi-cell MIMO-NOMA systems," ser. 2019 IEEE 5th International Conference on Computer and Communications (ICCC), 2019, pp. 2039–2043. DOI: 10. 1109/ICCC47050.2019.9064165.

- [113] J. Dai, L. Sun, C. Yang, "On the average rate and power allocation of uplink multi-antenna NOMA systems," ser. 2017 IEEE 86th Vehicular Technology Conference (VTC-Fall), 2017, pp. 1–5. DOI: 10.1109/VTCFall.2017.8288076.
- [114] M. A. Sedaghat, R. R. Müller, "On user pairing in uplink NOMA," *IEEE Transactions on Wireless Communications*, vol. 17, no. 5, pp. 3474–3486, 2018. DOI: 10.1109/TWC.2018.2815005.
- [115] J. Seo, B. C. Jung, H. Jin, "Performance analysis of NOMA random access," *IEEE Communications Letters*, vol. 22, no. 11, pp. 2242–2245, 2018.
- [116] X. Xie, Y. Bi, X. Nie, "Performance analysis of uplink cooperative noma system with an af relay," in *2020 IEEE 20th International Conference on Communication Technology (ICCT)*, 2020, pp. 178–181. DOI: 10.1109/ICCT50939. 2020.9295870.
- [117] J. Wang, B. Xia, K. Xiao, Y. Gao, S. Ma, "Outage performance analysis for wireless non-orthogonal multiple access systems," *IEEE Access*, vol. 6, pp. 3611–3618, 2018. DOI: 10.1109/ACCESS.2018.2789581.
- [118] S. A. Tegos, P. D. Diamantoulakis, J. Xia, L. Fan, G. K. Karagiannidis, "Outage performance of uplink NOMA in land mobile satellite communications," *IEEE Wireless Communications Letters*, vol. 9, no. 10, pp. 1710–1714, 2020. DOI: 10.1109/LWC.2020.3001916.
- [119] B. Tahir, S. Schwarz, M. Rupp, "Outage analysis of uplink irs-assisted noma under elements splitting," Apr. 2021, pp. 1–5. DOI: 10.1109/VTC2021-Spring51267.2021.9449027.
- [120] S. Singh, M. Bansal, "Outage analysis of uplink noma based fd decode-and-forward cooperative relay system," in *2020 IEEE 4th Conference on Information Communication Technology (CICT)*, 2020, pp. 1–6. DOI: 10.1109/CICT51604.2020.9312108.
- [121] P. Xu, J. Quan, Z. Yang, G. Chen, Z. Ding, "Performance analysis of buffer-aided hybrid noma/oma in cooperative uplink system," *IEEE Access*, vol. 7, pp. 168759–168773, 2019. DOI: 10.1109/ACCESS.2019.2955118.
- [122] N. P. Le, L. C. Tran, X. Huang, J. Choi, E. Dutkiewicz, S. L. Phung, A. Bouzerdoum, "Performance analysis of uplink noma systems with imperfect sic detection and delay constraints over composite fading channels," *IEEE Transactions on Vehicular Technology*, pp. 1–1, 2021. DOI: 10.1109/TVT. 2021.3086045.
- [123] S. Sharma, S. D. Roy, S. Kundu, "Secrecy performance of uplink-downlink noma network at physical layer," in *2021 Sixth International Conference on Wireless Communications, Signal Processing and Networking (WiSPNET)*, 2021, pp. 57–61. DOI: 10.1109/WiSPNET51692.2021.9419364.
- [124] F. T. A. Rabee, R. D. Gitlin, "Performance of uplink non-orthogonal multiple access (NOMA) in the presence of channel estimation errors," ser. IEEE Wireless Telecommunications Symposium (WTS2019), April 9- 12, New York City, USA, Apr. 2019.

- [125] X. Wang, F. Labeau, L. Mei, "Closed-form ber expressions of qpsk constellation for uplink non-orthogonal multiple access," *IEEE Communications Letters*, vol. 21, no. 10, pp. 2242–2245, 2017.
- [126] J. Bae, K.-H. Lee, J. M. Kim, B. C. Jung, J. Joung, "Performance analysis of uplink noma-iot networks with space-time line code," in *2019 IEEE 90th Vehicular Technology Conference (VTC2019-Fall)*, 2019, pp. 1–5. DOI: 10.1109/VTCFall.2019.8891160.
- [127] Indefinite integral of combination of Meijer-G and elementary functions. [Online]. Available: https://functions.wolfram.com/HypergeometricFunctions/MeijerG/21/01/02/01/0002/(visited on 12/23/2020).
- [128] Transform of Meijer-G function to other form of Meijer-G function. [Online]. Available: https://functions.wolfram.com/HypergeometricFunctions/MeijerG/17/02/03/0002/(visited on 12/20/2020).
- [129] P. M. Shankar, *Fading and Shadowing in Wireless Systems*. Springer International Publishing, Apr. 2014, pp. 1–464.

# ADERIVATIONS OF (3.11) AND (3.12)

In this section, derivation of the parameters t in (3.11) and a in (3.12) which are needed to determine coding and diversity gain, is presented. As aforementioned in section (3.3.1), there is a relationship like  $\gamma_{\varsigma} = \beta \Omega_{0,\varsigma}$  between  $\gamma_{\varsigma}$  and  $\beta$ . Therefore, there is not any difference in their PDFs excluding their averages so that while the average of  $\gamma_{\varsigma}$  is equal to  $\gamma_{0,\varsigma}$ , the average of  $\gamma_{\varsigma}$  is equal to  $\gamma_{0,\varsigma}$ . In that case, the PDF in (3.5) for  $\gamma_{\varsigma}$  can be rewritten as

$$f(\beta) = \frac{2^{(3-m_{s,\varsigma}-m_{m,\varsigma})} b_{\varsigma}^{2} \left(2(b_{\varsigma}^{2}\beta)^{\frac{1}{2}}\right)^{(m_{s,\varsigma}+m_{m,\varsigma}-2)}}{\Gamma(m_{m,\varsigma})\Gamma(m_{s,\varsigma})} K_{m_{s,\varsigma}-m_{m,\varsigma}} \left[2(b_{\varsigma}^{2}\beta)^{\frac{1}{2}}\right], \qquad \beta > 0$$
(A.1)

where  $b_{\varsigma} = \sqrt{\frac{m_{s,\varsigma}m_{m,\varsigma}}{\tau}} = \sqrt{m_{s,\varsigma}m_{m,\varsigma}}$  since  $\mathbb{E}[\beta] = \tau = 1$ . The relationship between the modified Bessel function of the second kind and Meijer-G [92, Section 2.6] is

$$r^{a}K_{a}(r) = 2^{a-1}G_{0,2}^{2,0}\left(\frac{r^{2}}{4}\Big|_{\frac{a+\alpha}{2}, \frac{a-\alpha}{2}}\right),$$
 (A.2)

in such case, the term  $\left(2(b_{\varsigma}^2\beta)^{\frac{1}{2}}\right)^{(m_{s,\varsigma}+m_{m,\varsigma}-2)} K_{m_{s,\varsigma}-m_{m,\varsigma}}[2(b_{\varsigma}^2\beta)^{\frac{1}{2}}]$  in (A.1) can be written in terms of Meijer-G function where  $r=2(b_{\varsigma}^2\beta)^{\frac{1}{2}},\ a=m_{s,\varsigma}+m_{m,\varsigma}-2$  and  $\alpha=m_{s,\varsigma}-m_{m,\varsigma}$ . According to (A.2), (A.1) can be rewritten as,

$$f(\beta) = \frac{2^{(3-m_{s,\varsigma}-m_{m,\varsigma})}b_{\varsigma}^{2}}{\Gamma(m_{m,\varsigma})\Gamma(m_{s,\varsigma})}2^{a-1}G_{0,2}^{2,0}\left(\frac{r^{2}}{4}\Big|_{\frac{a+\nu}{2}, \frac{a-\nu}{2}}\right), \qquad \beta > 0$$
 (A.3)

when r, a and  $\alpha$  are substituted into (A.3), it can be written as,

$$f(\beta) = \frac{b_{\varsigma}^{2}}{\Gamma(m_{m,\varsigma})\Gamma(m_{\varsigma,\varsigma})} G_{0,2}^{2,0}(b_{\varsigma}^{2}\beta|_{m_{s,\varsigma}-1, m_{m,\varsigma}-1}). \tag{A.4}$$

The asymptotic expansion of Meijer-G function  $G_{0,2}^{2,0}(b_{\varsigma}^2\beta|_{m_{s,\varsigma}-1, m_{m,\varsigma}-1})$  in (A.4) is given as follows ([92, Theorem 1.4.3, (1.4.14)]) where z, q, p,  $a_p$  and  $b_q$  correspond to  $b_{\varsigma}^2\beta$ , 2, 0, (-, -) and  $(m_{s,\varsigma}-1, m_{m,\varsigma}-1)$ , respectively,

$$G_{p,q}^{q,0}(z|_{b_q}^{a_p}) \sim H_{p,q}(z) = \left[e^{(p-q)z^{\frac{1}{q-p}}}\right] z^{\rho^*} \left[\frac{(2\pi)^{\frac{q-p-1}{2}}}{(q-p)^{\frac{1}{2}}} + \frac{M_1}{z^{\frac{1}{q-p}}} + \frac{M_2}{z^{\frac{1}{q-p}}} + \dots\right], \tag{A.5}$$

$$\rho^* = \frac{1}{q-p} \left[ \sum_{j=1}^q b_j - \sum_{j=1}^p a_j + \frac{p-q+1}{2} \right], \tag{A.6}$$

When p = 0 and q = 2 are substituted into (A.5) and (A.6), they become,

$$G_{0,2}^{2,0}(z|_{b_q}^{a_p}) \sim \left[e^{-2\sqrt{z}}\right] z^{\rho^*} \left[\pi^{\frac{1}{2}} + \frac{M_1}{z^{\frac{1}{2}}} + \frac{M_2}{z^{\frac{1}{2}}} + \dots\right],\tag{A.7}$$

and

$$\rho^* = \frac{1}{2} [m_{s,\varsigma} + m_{m,\varsigma} - \frac{5}{2}]. \tag{A.8}$$

Moreover, Maclaurin series expansion of  $e^{-2\sqrt{z}}$  can be used to get,

$$G_{0,2}^{2,0}(z|_{b_q}^{a_p}) \sim \left[1 + \sum_{i=1}^{\infty} \frac{(-2\sqrt{z})^i}{i!}\right] z^{\rho^*} \left[\pi^{\frac{1}{2}} + \frac{M_1}{z^{\frac{1}{2}}} + \frac{M_2}{z^{\frac{1}{2}}} + \dots\right], \tag{A.9}$$

$$G_{0,2}^{2,0}(z|_{b_q}^{a_p}) \sim z^{\rho^*} \pi^{\frac{1}{2}} + z^{\rho^*} \left[ \frac{M_1}{z^{\frac{1}{2}}} + \frac{M_2}{z^{\frac{1}{2}}} + \dots \right] + z^{\rho^*} \sum_{i=1}^{\infty} \frac{(-2\sqrt{z})^i}{i!} \left[ \pi^{\frac{1}{2}} + \frac{M_1}{z^{\frac{1}{2}}} + \frac{M_2}{z^{\frac{1}{2}}} + \dots \right]. \quad (A.10)$$

This result can be used in (2.17) to obtain,

$$f(\beta) = a\beta^{t} + o(\beta^{t}) \sim \frac{b_{\varsigma}^{2}}{\Gamma(m_{m,\varsigma})\Gamma(m_{s,\varsigma})} \left[ z^{\rho^{*}} \pi^{\frac{1}{2}} + z^{\rho^{*}} \left[ \frac{M_{1}}{z^{\frac{1}{2}}} + \frac{M_{2}}{z^{\frac{1}{2}}} + \dots \right] + z^{\rho^{*}} \sum_{i=1}^{\infty} \frac{(-2\sqrt{z})^{i}}{i!} \left[ \pi^{\frac{1}{2}} + \frac{M_{1}}{z^{\frac{1}{2}}} + \frac{M_{2}}{z^{\frac{1}{2}}} + \dots \right] \right],$$
(A.11)

where

$$o(\beta^{t}) = \frac{b_{\varsigma}^{2}}{\Gamma(m_{m,\varsigma})\Gamma(m_{s,\varsigma})} \left[ z^{\rho^{*}} \left[ \frac{M_{1}}{z^{\frac{1}{2}}} + \frac{M_{2}}{z^{\frac{1}{2}}} + \dots \right] + z^{\rho^{*}} \sum_{i=1}^{\infty} \frac{(-2\sqrt{z})^{i}}{i!} \left[ \pi^{\frac{1}{2}} + \frac{M_{1}}{z^{\frac{1}{2}}} + \frac{M_{2}}{z^{\frac{1}{2}}} + \dots \right] \right],$$
(A.12)

and

$$a\beta^{t} = \frac{b_{\varsigma}^{2}}{\Gamma(m_{m,\varsigma})\Gamma(m_{s,\varsigma})} z^{\rho^{*}} \pi^{\frac{1}{2}} = \frac{b_{\varsigma}^{2}}{\Gamma(m_{m,\varsigma})\Gamma(m_{s,\varsigma})} (b_{\varsigma}^{2}\beta)^{\frac{1}{2}[m_{s,\varsigma}+m_{m,\varsigma}-\frac{5}{2}]} \pi^{\frac{1}{2}}$$

$$= \frac{(b_{\varsigma})^{(m_{s,\varsigma}+m_{m,\varsigma}-\frac{1}{2})} \pi^{\frac{1}{2}}}{\Gamma(m_{m,\varsigma})\Gamma(m_{s,\varsigma})} \beta^{\frac{1}{2}[m_{s,\varsigma}+m_{m,\varsigma}-\frac{5}{2}]},$$
(A.13)

which finally allows us to obtain,

$$a = \frac{(\sqrt{m_{s,\varsigma}m_{m,\varsigma}})^{(m_{s,\varsigma}+m_{m,\varsigma}-\frac{1}{2})}\pi^{\frac{1}{2}}}{\Gamma(m_{m,\varsigma})\Gamma(m_{s,\varsigma})}.$$
(A.14)

and

$$t = \frac{1}{2} [m_{s,\varsigma} + m_{m,\varsigma} - \frac{5}{2}]. \tag{A.15}$$

# DERIVATION OF (3.24)

In this section, the solution of the integral in (3.24) for SER computation is presented. Firstly, it can be written in the following form,

$$\bar{P}_{se} = \frac{2A}{\sqrt{\pi}\Gamma(m_{m,\varsigma})\Gamma(m_{s,\varsigma})} (b_{\varsigma})^{m_{m,\varsigma}+m_{s,\varsigma}-2} (b_{\varsigma})^{2} \times \\
\int_{\gamma_{\varsigma}=0}^{\infty} (\gamma_{\varsigma})^{(m_{m,\varsigma}+m_{s,\varsigma})/2-1} K_{m_{s,\varsigma}-m_{m,\varsigma}} \left(2\sqrt{\gamma_{\varsigma}(b_{\varsigma})^{2}}\right) G_{1,2}^{2,0} \left(B\gamma_{\varsigma}\Big|_{0,\frac{1}{2}}^{1}\right) d\gamma_{\varsigma}.$$
(B.1)

When the term  $(b_c)^2$  is taken inside of integral in (B.1)

$$\bar{P}_{se} = \frac{2A}{\sqrt{\pi}\Gamma(m_{m,\varsigma})\Gamma(m_{s,\varsigma})} (b_{\varsigma})^{m_{m,\varsigma}+m_{s,\varsigma}-2} \times \int_{\gamma_{\varsigma}=0}^{\infty} (\gamma_{\varsigma})^{(m_{m,\varsigma}+m_{s,\varsigma})/2-1} K_{m_{s,\varsigma}-m_{m,\varsigma}} \left(2\sqrt{\gamma_{\varsigma}(b_{\varsigma})^{2}}\right) G_{1,2}^{2,0} \left(B\gamma_{\varsigma}\right|_{0,\frac{1}{2}}^{1} (b_{\varsigma})^{2} d\gamma_{\varsigma},$$
(B.2)

The integral in (B.2) can be put into the form of [65, pp. 7.821/3] by applying the change of variable as  $x=(b_\varsigma)^2\gamma_\varsigma$ . Thus,  $\frac{d}{dx}x=\frac{d}{dx}b_\varsigma^2\gamma_\varsigma\implies dx=(b_\varsigma)^2d\gamma_\varsigma$  and  $\gamma_\varsigma=\frac{x}{(b_\varsigma)^2}$ . By rearranging (B.2), one can obtain

$$\bar{P}_{se} = \frac{2A}{\sqrt{\pi}\Gamma(m_{m,\varsigma})\Gamma(m_{s,\varsigma})} (b_{\varsigma})^{m_{m,\varsigma}+m_{s,\varsigma}-2} \times \int_{x=0}^{\infty} \left(\frac{x}{(b_{\varsigma})^{2}}\right)^{(m_{m,\varsigma}+m_{s,\varsigma})/2-1} K_{m_{s,\varsigma}-m_{m,\varsigma}} (2\sqrt{x}) G_{1,2}^{2,0} \left(\frac{Bx}{(b_{\varsigma})^{2}}\Big|_{0,\frac{1}{2}}^{1}\right) dx,$$
(B.3)

when term  $\left(\frac{1}{(b_{\varsigma})^2}\right)^{(m_{m,\varsigma}+m_{s,\varsigma})/2-1}$  is taken outside of the integral in (B.3), then SER

becomes,

$$\bar{P}_{se} = \frac{2A}{\sqrt{\pi}\Gamma(m_{m,\varsigma})\Gamma(m_{s,\varsigma})} \int_{x=0}^{\infty} x^{(m_{m,\varsigma}+m_{s,\varsigma})/2-1} \times K_{m_{s,\varsigma}-m_{m,\varsigma}} (2\sqrt{x}) G_{1,2}^{2,0} \left(\frac{Bx}{(b_{\varsigma})^{2}}\Big|_{0,\frac{1}{2}}^{1}\right) dx,$$
(B.4)

The solution for this type of integrals is given in [65, pp. 7.821/3] as follows,

$$\int_{x=0}^{\infty} x^{-\rho} K_{\nu}(2\sqrt{x}) G_{pq}^{mn} \left(\alpha x \Big|_{b1,\dots,bq}^{a_1,\dots,a_p}\right) dx = \frac{1}{2} G_{p+2,q}^{m,n+2} \left(\alpha \Big|_{b1,\dots,bq}^{\rho-\frac{1}{2}\nu,\rho+\frac{1}{2}\nu,a_1,\dots,a_p}\right), \tag{B.5}$$

The integral in (B.3) can be put into the form of the integral in (B.4) by using change of variable as  $\rho=1-(m_{m,\varsigma}+m_{s,\varsigma})/2$ ,  $\nu=m_{s,\varsigma}-m_{m,\varsigma}$ , m=2, n=0, p=1, q=2,  $\alpha=\frac{B}{(b_\varsigma)^2}$ ,  $a_1=1$ ,  $b_1=0$  and  $b_2=\frac{1}{2}$ . When all these parameters are substituted into (B.4) and by using the Meijer-G function with new parameters in (B.3), the (3.25) can be obtained.

### DERIVATION OF (4.5)

In this section, PDF of  $\gamma$  in (4.5) is derived in three steps by finding PDFs of  $\frac{\delta}{\lambda}$ ,  $\frac{\delta}{\lambda} + \rho$  and  $\frac{\kappa}{\frac{\delta}{\lambda} + \rho}$ . In the first step, PDF of  $\frac{\delta}{\lambda}$  needs to be evaluated to obtain PDF of  $\gamma$ . The PDF of  $\tau = \frac{\delta}{\lambda}$  can be found via CDF of  $\lambda$  in (2.11). The CDF of  $\tau$  is  $F_{\tau}(\tau) = 1 - Pr(0 \le \lambda \le \frac{\delta}{\tau})$ , then

$$F_{\tau}(\tau) = 1 - \int_{\lambda=0}^{\frac{\delta}{\tau}} f_{\lambda}(\lambda) d\lambda = 1 - F_{\lambda}\left(\frac{\delta}{\tau}\right). \tag{C.1}$$

When derivative process is applied to both side of (C.1), then  $f_{\tau}(\tau) = \frac{\delta}{\tau^2} f_{\lambda}(\frac{\delta}{\tau})$ . By substituting  $\frac{\delta}{\tau}$  in (2.11),  $f_{\tau}(\tau)$  is found as,

$$f_{\tau}(\tau) = \frac{2\delta \Xi^{\frac{m_s + m_m}{2}}}{\Gamma(m_s)\Gamma(m_m)\tau^2} \left(\frac{\delta}{\tau}\right)^{\frac{m_s + m_m - 2}{2}} K_{m_s - m_m} \left(2\sqrt{\frac{\delta}{\tau}}\Xi\right), \quad \tau \ge 0.$$
 (C.2)

(4.4) can be written as  $\gamma = \frac{\kappa}{\tau + \rho}$ . To obtain PDF of  $\gamma$ , it is required to evaluate PDF of  $\varsigma = \tau + \rho$  in the second step. It can be obtained by utilizing CDF in such a way that  $F_{\varsigma}(\varsigma) = Pr(\tau + \rho \leq \varsigma) \Longrightarrow F_{\varsigma}(\varsigma) = Pr(0 \leq \tau \leq \varsigma - \rho) = F_{\tau}(\varsigma - \rho)$ . It is evident that after derivative of  $F_{\tau}(\varsigma - \rho)$  is determined and the chain rule is applied  $f_{\varsigma}(\varsigma)$  is obtained as,

$$f_{\varsigma}(\varsigma) = \frac{2\delta \Xi^{\frac{m_s + m_m}{2}}}{\Gamma(m_s)\Gamma(m_m)(\varsigma - \rho)^2} \left(\frac{\delta}{\varsigma - \rho}\right)^{\frac{m_s + m_m - 2}{2}} K_{m_s - m_m} \left(2\sqrt{\frac{\delta}{\varsigma - \rho}}\Xi\right). \tag{C.3}$$

(4.4) becomes  $\gamma = \frac{\kappa}{\varsigma}$ . In third step, PDF of  $\gamma$  can be evaluated by using CDF in such a way that  $F_{\gamma}(\gamma) = Pr(\frac{\kappa}{\varsigma} \leq \gamma) \Longrightarrow F_{\gamma}(\gamma) = 1 - Pr(\rho \leq \varsigma \leq \frac{\kappa}{\gamma})$ . Then, by repeating processes in the first step,  $f_{\gamma}(\gamma)$  can be given as follows,

$$f_{\gamma}(\gamma) = \frac{\kappa}{\gamma^2} \frac{2\delta \Xi^{\frac{m_s + m_m}{2}}}{\Gamma(m_s)\Gamma(m_m)(\frac{\kappa}{\gamma} - \rho)^2} \left(\frac{\delta}{\frac{\kappa}{\gamma} - \rho}\right)^{\frac{m_s + m_m - 2}{2}} K_{m_s - m_m} \left(2\sqrt{\frac{\delta}{\frac{\kappa}{\gamma} - \rho}}\Xi\right). \tag{C.4}$$

Boundary values of  $\gamma$  are determined as  $0 \le \gamma \le \frac{\kappa}{\rho}$ . When (C.4) is arranged, (4.5) is obtained.

# DERIVATIONS OF (4.13) AND (4.14)

In this section, derivation of the parameters a and t which are needed to determine coding and diversity gain, is presented. The term  $\left(2\sqrt{\beta\Psi}\right)^{m_s+m_m-2}K_{m_s-m_m}\left[2\sqrt{\beta\Psi}\right]$  in (4.13) can be written in terms of Meijer's G-function [92, Section 2.6] as follows,

$$\left(2\sqrt{\beta\Psi}\right)^{m_s+m_m-2} K_{m_s-m_m} \left(2\sqrt{\beta\Psi}\right) = 2^{m_s+m_m-3} G_{0,2}^{2,0} \left(\beta\Psi|_{m_s-1, m_m-1}\right). \tag{D.1}$$

When (D.1) is substituted into (4.13), it can be written as follows,

$$f(\beta) = \frac{\Psi}{\Gamma(m_m)\Gamma(m_s)} G_{0,2}^{2,0} \left(\beta \Psi|_{m_s - 1, m_m - 1}\right). \qquad \beta > 0 \qquad (D.2)$$

The asymptotic expansion of Meijer's G-function

 $G_{0,2}^{2,0}(\beta\Psi|_{m_s-1, m_m-1})$  in (D.2) is given as follows ([92, Theorem 1.4.3, Eq. (1.4.14)]) where z, q, p,  $a_p$  and  $b_q$  correspond to  $\beta\Psi$ , 2, 0, (-, -) and  $(m_s-1, m_m-1)$ , respectively.

$$G_{p,q}^{q,0}(z|_{b_q}^{a_p}) \sim H_{p,q}(z) = \left[e^{(p-q)z^{\frac{1}{q-p}}}\right] z^{\rho^*} \left[\frac{(2\pi)^{\frac{q-p-1}{2}}}{(q-p)^{\frac{1}{2}}} + \frac{M_1}{z^{\frac{1}{q-p}}} + \frac{M_2}{z^{\frac{1}{q-p}}} + \dots\right], \tag{D.3}$$

$$\rho^* = \frac{1}{q-p} \left[ \sum_{j=1}^q b_j - \sum_{j=1}^p a_j + \frac{p-q+1}{2} \right]. \tag{D.4}$$

When p=0 and q=2 are substituted into (D.3) and (D.4), they become  $G_{0,2}^{2,0}(z|_{b_q}^{a_p}) \sim [e^{-2\sqrt{z}}]z^{\rho^*} \left[\pi^{\frac{1}{2}} + \frac{M_1}{z^{\frac{1}{2}}} + \frac{M_2}{z^{\frac{1}{2}}} + \dots\right]$  and  $\rho^* = \frac{1}{2}[m_s + m_m - \frac{5}{2}]$ .

Moreover, Maclaurin series expansion of  $e^{-2\sqrt{z}}$  can be used to get,

$$G_{0,2}^{2,0}(z|_{b_q}^{a_p}) \sim \left[1 + \sum_{i=1}^{\infty} \frac{(-2\sqrt{z})^i}{i!}\right] z^{\rho^*} \left[\pi^{\frac{1}{2}} + \frac{M_1}{z^{\frac{1}{2}}} + \frac{M_2}{z^{\frac{1}{2}}} + \ldots\right], \tag{D.5}$$

$$G_{0,2}^{2,0}(z|_{b_q}^{a_p}) \sim z^{\rho^*} \pi^{\frac{1}{2}} + z^{\rho^*} \left[ \frac{M_1}{z^{\frac{1}{2}}} + \frac{M_2}{z^{\frac{1}{2}}} + \dots \right] +$$

$$z^{\rho^*} \sum_{i=1}^{\infty} \frac{(-2\sqrt{z})^i}{i!} \left[ \pi^{\frac{1}{2}} + \frac{M_1}{z^{\frac{1}{2}}} + \frac{M_2}{z^{\frac{1}{2}}} + \dots \right].$$
(D.6)

This result can be used in (2.17) to obtain,

$$f(\beta) = a\beta^{t} + o(\beta^{t}) \sim \frac{\Psi}{\Gamma(m_{m})\Gamma(m_{s})} \left[ z^{\rho^{*}} \pi^{\frac{1}{2}} + z^{\rho^{*}} \left[ \frac{M_{1}}{z^{\frac{1}{2}}} + \frac{M_{2}}{z^{\frac{1}{2}}} + \dots \right] + z^{\rho^{*}} \sum_{i=1}^{\infty} \frac{(-2\sqrt{z})^{i}}{i!} \left[ \pi^{\frac{1}{2}} + \frac{M_{1}}{z^{\frac{1}{2}}} + \frac{M_{2}}{z^{\frac{1}{2}}} + \dots \right] \right],$$
(D.7)

where

$$o(\beta^{t}) = \frac{\Psi}{\Gamma(m_{m})\Gamma(m_{s})} \left[ z^{\rho^{*}} \left[ \frac{M_{1}}{z^{\frac{1}{2}}} + \frac{M_{2}}{z^{\frac{1}{2}}} + \dots \right] + z^{\rho^{*}} \sum_{i=1}^{\infty} \frac{(-2\sqrt{z})^{i}}{i!} \left[ \pi^{\frac{1}{2}} + \frac{M_{1}}{z^{\frac{1}{2}}} + \frac{M_{2}}{z^{\frac{1}{2}}} + \dots \right] \right],$$
(D.8)

and

$$a\beta^{t} = \frac{\Psi}{\Gamma(m_{m})\Gamma(m_{s})} z^{\rho^{*}} \pi^{\frac{1}{2}} = \frac{\Psi}{\Gamma(m_{m})\Gamma(m_{s})\delta} (\beta\Psi)^{\frac{1}{2}[m_{s}+m_{m}-\frac{5}{2}]} \pi^{\frac{1}{2}}$$

$$= \frac{\Psi^{\frac{1}{2}(m_{s}+m_{m}-\frac{1}{2})} \pi^{\frac{1}{2}}}{\Gamma(m_{m})\Gamma(m_{s})\delta} \beta^{\frac{1}{2}[m_{s}+m_{m}-\frac{5}{2}]},$$
(D.9)

which eventually offers to obtain (4.14) and (4.15).

# DERIVATION OF (5.8)

In this section, PDF of  $\gamma$  in (5.8) is obtained. (5.8) can be rewritten as  $\gamma = \frac{\alpha}{\kappa + \beta}$ , PDF of  $\tau = \kappa + \beta$  firstly can be evaluated by utilizing CDF such that  $F_{\tau}(\tau) = Pr(\tau \le \tau) = Pr(\kappa + \beta \le \tau) \Longrightarrow F_{\tau}(\tau) = Pr(0 \le \beta \le \tau - \kappa)$ ,

$$F_{\tau}(\tau) = \int_{\beta=0}^{\tau-\kappa} f_{\beta}(\beta) d\beta, \tag{E.1}$$

When integral in (E.1) is solved  $f_{\tau}(\tau) = f_{\beta}(\tau - \kappa)$  is obtained,

$$f_{\tau}(\tau) = \frac{2(b_{\varsigma})^{m_{m,\varsigma}+m_{s,\varsigma}}}{\Gamma(m_{m,\varsigma})\Gamma(m_{s,\varsigma})} (\tau - \kappa)^{(m_{m,\varsigma}+m_{s,\varsigma})/2-1} K_{m_{s,\varsigma}-m_{m,\varsigma}} (2b_{\varsigma}\sqrt{(\tau - \kappa)}), \tag{E.2}$$

Boundary values of  $\tau$  are evaluated as  $\kappa \leq \tau \leq \infty$ ,

$$f_{\tau}(\tau) = \begin{cases} \frac{2(b_{\varsigma})^{m_{m,\varsigma}+m_{s,\varsigma}}}{\Gamma(m_{m,\varsigma})\Gamma(m_{s,\varsigma})} (\tau - \kappa)^{\frac{m_{m,\varsigma}+m_{s,\varsigma}-2}{2}} K_{m_{s,\varsigma}-m_{m,\varsigma}} (2b_{\varsigma}\sqrt{(\tau - \kappa)}), & \kappa \leq \tau \\ 0, & \text{otherwise.} \end{cases}$$
(E.3)

(5.8) becomes  $\gamma = \frac{\alpha}{\tau}$  and PDF of  $\gamma$  can be evaluated. Eq. 2.265 [129] leads that PDF of division of two random variables  $\alpha$  and  $\tau$  is found as,

$$f_{\gamma}(\gamma) = \int_{\tau=\kappa}^{\infty} \tau f_{\alpha,\tau}(\gamma\tau,\tau) d\tau = \int_{\tau=\kappa}^{\infty} \tau f_{\alpha}(\gamma\tau) f_{\tau}(\tau) d\tau, \tag{E.4}$$

where  $f_{\alpha}(\gamma\tau) = \frac{2(b_{\alpha})^{m_s+m_m}}{\Gamma(m_s)\Gamma(m_m)}(\gamma\tau)^{\frac{m_s+m_m-2}{2}}K_{m_s-m_m}(2b_{\alpha}\sqrt{\gamma\tau})$ . When  $f_{\alpha}(\gamma\tau)$  is substituted in

(E.4), it can be rewritten as follows,

$$f_{\gamma}(\gamma) = \int_{\tau=\kappa}^{\infty} \tau \frac{2(b_{\alpha})^{m_{s}+m_{m}}}{\Gamma(m_{s})\Gamma(m_{m})} (\gamma \tau)^{\frac{m_{s}+m_{m}-2}{2}} K_{m_{s}-m_{m}} (2b_{\alpha}\sqrt{\gamma \tau}) \frac{2(b_{\varsigma})^{m_{m,\varsigma}+m_{s,\varsigma}}}{\Gamma(m_{m,\varsigma})\Gamma(m_{s,\varsigma})} \times (\tau-\kappa)^{\frac{m_{m,\varsigma}+m_{s,\varsigma}-2}{2}} K_{m_{s,\varsigma}-m_{m,\varsigma}} (2b_{\varsigma}\sqrt{(\tau-\kappa)}) d\tau,$$
(E.5)

After performing some mathematical manipulations, (E.5) becomes as below,

$$f_{\gamma}(\gamma) = \frac{2^{1-m_{s}-m_{m}}\gamma^{-1}}{\Gamma(m_{s})\Gamma(m_{m})} \frac{2^{1-m_{m,\varsigma}-m_{s,\varsigma}}}{\Gamma(m_{m,\varsigma})\Gamma(m_{s,\varsigma})} \int_{\tau=\kappa}^{\infty} (2b_{\alpha}\sqrt{\gamma\tau})^{m_{s}+m_{m}} K_{m_{s}-m_{m}} (2b_{\alpha}\sqrt{\gamma\tau}) \times$$

$$(2b_{\varsigma}\sqrt{\tau-\kappa})^{m_{m,\varsigma}+m_{s,\varsigma}} (\tau-\kappa)^{-1} K_{m_{s,\varsigma}-m_{m,\varsigma}} (2b_{\varsigma}\sqrt{(\tau-\kappa)}) d\tau,$$
(E.6)

Bessel-k functions in (E.6) can be written by terms of Meijer's G-function [92, Section 2.6],

$$(2b_{\alpha}\sqrt{\gamma\tau})^{m_s+m_m}K_{m_s-m_m}(2b_{\alpha}\sqrt{\gamma\tau}) = 2^{m_s+m_m-1}G_{0,2}^{2,0}\left((b_{\alpha})^2\gamma\tau\Big|_{m_s,m_m}\right), \tag{E.7}$$

Likewise,

$$(2b_{\varsigma}\sqrt{\tau-\kappa})^{m_{m,\varsigma}+m_{s,\varsigma}}K_{m_{s,\varsigma}-m_{m,\varsigma}}(2b_{\varsigma}\sqrt{(\tau-\kappa)})$$

$$=2^{m_{m,\varsigma}+m_{s,\varsigma}-1}G_{0,2}^{2,0}\Big((b_{\varsigma})^{2}(\tau-\kappa)\bigg|_{m_{s,\varsigma}, m_{m,\varsigma}}\Big),$$
(E.8)

Meijer's G-functions in (E.7) and (E.8) can be used in (E.6) to obtain,

$$f_{\gamma}(\gamma) = \frac{1}{\Gamma(m_s)\Gamma(m_m)\Gamma(m_{m,\varsigma})\Gamma(m_{s,\varsigma})\gamma} \times \int_{\tau=\kappa}^{\infty} (\tau - \kappa)^{-1} G_{0,2}^{2,0} \left( (b_{\alpha})^2 \gamma \tau \Big|_{m_s, m_m} \right) G_{0,2}^{2,0} \left( (b_{\varsigma})^2 (\tau - \kappa) \Big|_{m_{s,\varsigma}, m_{m,\varsigma}} \right) d\tau,$$
(E.9)

when change of variable with  $x = \tau - \kappa$  is applied, then  $dx = d\tau$  and new parameters

are substituted in (E.9), then it can be rewritten as follows,

$$f_{\gamma}(\gamma) = \frac{1}{\Gamma(m_{s})\Gamma(m_{m})\Gamma(m_{m,\varsigma})\Gamma(m_{s,\varsigma})\gamma} \times \int_{x=0}^{\infty} x^{-1} G_{0,2}^{2,0} \left( (b_{\alpha})^{2} \gamma(x+\kappa) \Big|_{m_{s}, m_{m}} \right) G_{0,2}^{2,0} \left( (b_{\varsigma})^{2} x \Big|_{m_{s,\varsigma}, m_{m,\varsigma}} \right) dx,$$
(E.10)

When variable is changed such that  $t=(b_{\alpha})^{2}\gamma x$ , then  $\frac{d}{dx}t=\frac{d}{dx}[(b_{\alpha})^{2}\gamma x] \implies dt=(b_{\alpha})^{2}\gamma dx$  and furthermore,  $x=\frac{t}{(b_{\alpha})^{2}\gamma}$ . Before all new values are substituted in integral (E.10), it is multiplied  $\frac{(b_{\alpha})^{2}\gamma}{(b_{\alpha})^{2}\gamma}$  as follows to provide equality  $dt=(b_{\alpha})^{2}\gamma dx$ .

$$\frac{(b_{\alpha})^{2}\gamma}{(b_{\alpha})^{2}\gamma} \int_{x=0}^{\infty} x^{-1} G_{0,2}^{2,0} \left( (b_{\alpha})^{2} \gamma(x+\kappa) \Big|_{m_{s}, m_{m}} \right) G_{0,2}^{2,0} \left( (b_{\varsigma})^{2} x \Big|_{m_{s,\varsigma}, m_{m,\varsigma}} \right) dx$$

$$= \frac{1}{(b_{\alpha})^{2}\gamma} \int_{x=0}^{\infty} x^{-1} G_{0,2}^{2,0} \left( (b_{\alpha})^{2} \gamma(x+\kappa) \Big|_{m_{s}, m_{m}} \right) G_{0,2}^{2,0} \left( (b_{\varsigma})^{2} x \Big|_{m_{s,\varsigma}, m_{m,\varsigma}} \right) \left[ (b_{\alpha})^{2} \gamma dx \right]. \tag{E.11}$$

When all above parameters are substituted in (E.11), it becomes,

$$f_{\gamma}(\gamma) = \frac{1}{\Gamma(m_s)\Gamma(m_m)\Gamma(m_{m,\varsigma})\Gamma(m_{s,\varsigma})\gamma} \times \int_{t=0}^{\infty} t^{-1} G_{0,2}^{2,0} \left(\frac{(b_{\varsigma})^2}{(b_{\alpha})^2 \gamma} t \Big|_{m_{\varsigma,\varsigma}, m_{m}}\right) G_{0,2}^{2,0} \left((b_{\alpha})^2 \gamma \kappa + t \Big|_{m_{\varsigma,\varsigma}, m_{m}}\right) dt,$$
(E.12)

[92, Eq.3.2.12] is as follows,

$$\int_{0}^{\infty} t^{\sigma-1} G_{p,q}^{m,n} \left( \lambda t \Big|_{b_{q}}^{a_{p}} \right) G_{\Upsilon,\delta}^{\alpha,\beta} \left( b + t \Big|_{d_{\delta}}^{c_{\Upsilon}} \right) dt$$

$$= \sum_{k=0}^{\infty} \frac{(-b)^{k}}{k!} G_{\delta+p+1,\Upsilon+q+1}^{\beta+m,\alpha+n+1} \left( \lambda \Big|_{b_{q},1+k-\sigma-c_{\Upsilon},1+k-\sigma}^{1-\sigma,a_{p},1+k-\sigma-c_{\Upsilon},1+k-\sigma} \right), \tag{E.13}$$

The integral in (E.12) can be put into the form of the integral in (E.13) by using change of variable as  $\sigma=0$ , m=2, n=0, p=0, q=2,  $\lambda=\frac{(b_\varsigma)^2}{(b_\alpha)^2\gamma}$ ,  $a_p=\{\}$ ,  $b_q=\{m_{s,\varsigma},\ m_{m,\varsigma}\}$ ,  $\alpha=2$ ,  $\beta=0$ ,  $\gamma=0$ ,  $\delta=2$ ,  $b=(b_\alpha)^2\gamma\kappa$ ,  $c_\gamma=\{\}$  and  $d_\delta=\{m_s,\ m_m\}$ . When all these parameters are substituted into (E.13) and by using the Meijer's G-function with new

parameters in (E.12), the (E.4) can be obtained.

$$\int_{t=0}^{\infty} t^{-1} G_{0,2}^{2,0} \left( \frac{(b_{\varsigma})^{2}}{(b_{\alpha})^{2} \gamma} t \Big|_{m_{s,\varsigma}, m_{m,\varsigma}} \right) G_{0,2}^{2,0} \left( (b_{\alpha})^{2} \gamma \kappa + t \Big|_{m_{s}, m_{m}} \right) dt$$

$$= \sum_{k=0}^{\infty} \frac{(-(b_{\alpha})^{2} \gamma \kappa)^{k}}{k!} G_{3,3}^{2,3} \left( \frac{(b_{\varsigma})^{2}}{(b_{\alpha})^{2} \gamma} \Big|_{\{m_{s,\varsigma}, m_{m,\varsigma}\}, 1+k}^{\{1,1+k-m_{s},1+k-m_{m}\}, \{\}} \right). \tag{E.14}$$

Finally, when the result in (E.14) is substituted in (E.12), the SINR PDF can be obtained as shown in expression (5.8).

### **PUBLICATIONS FROM THE THESIS**

### **Papers**

- 1. K. Aslan and T. Gucluoglu, "Performance of maximal ratio transmission over generalised-K fading channels," IET Communications, vol. 14, no. 19, pp. 3440–3447, Oct. 2020.
- 2. K. Aslan and T. Gucluoglu, "Performance Analysis of Downlink-NOMA over Generalized-k Fading Channels," Physical Communication, vol. 48, pp. 101414, Oct. 2021.
- 3. K. Aslan and T. Gucluoglu, "Performance Analysis of NOMA Uplink Transmission over Generalized-k Fading Channels," Wiley, vol. xx, no. xx, pp. xxxx–xxxx, xxx. 2021.